Department of Physics and Astronomy

University of Heidelberg

Master thesis in Physics
submitted by

Konstantinos Sfairopoulos

born in Thessaloniki, Greece
2021

Black-Hole Laser Instabilities

in Bose-Einstein Condensates

This Master thesis has been carried out by

Konstantinos Sfairopoulos

at the

Kirchhoff-Institute for Physics, Heidelberg

under the supervision of

Prof. Dr. Thomas Gasenzer

Black-Hole-Laser-Instabilitäten in Bose-Einstein Kondensaten:

Die vorliegenden Arbeit befasst sich mit der Realisierung von zu gravitativen Phänomenen analogen Prozessen in Bose-Einstein-Kondensaten. Die Grundlage hierfür bildet die Realisierung des Ereignishorizonts eines Schwarzen Lochs mit Hilfe stufenartiger Diskontinuitäten der Parameter des Kondensats, speziell der Flußgeschwindigkeit des Suprafluids. Solche Diskontinuitäten der Geschwindigkeit werden sowohl in einem ein- wie auch einem zweikomponentigen Bose-Einstein Kondensat zu einer Black-Hole-Laser-Konfiguration kombiniert, welche jeweils auf ihre linearen Anregungen hin untersucht wird. In der für das Zweikomponentengas betrachteten Konfiguration wird ein entgegengesetzt gerichteter Fluß in den beiden Komponenten angenommen, mit einer die Schallgeschwindigkeit jeweils übersteigenden Flußgeschwindigkeit. Durch Lösen der Bogoliubov-de Gennes-Gleichungen werden die stabilen sowie instabilen linearen Anregungen des gekoppelten Systems auf dem Hintergrund eines zirkulär geschlossenen suprafluiden Flusses bestimmt und mit denen des einkomponentigen Black-Hole-Lasers verglichen.

Black-Hole Laser Instabilities in Bose-Einstein Condensates:

In this thesis, a broad, generic and concise introduction to the field of Analogue Gravity is developed. It is followed by a description of the simplest nontrivial example of an analogue black hole with steplike discontinuities of the background parameters, a configuration which is treated analytically, and a treatment of a one-component and a two-component black-hole laser. For the subsequent analysis and results, the platform of Bose Einstein Condensates (BECs) is used. Furthermore, the existence and characteristics of a realistic configuration for subsequent experiments on Analogue Gravity based on BECs is theoretically investigated, through the creation of a black hole laser for two-component one-dimensional BECs. The specific configuration possesses a counterflow between the two superfluid components. A simplification of the generic model is dealt with, consisting of steplike velocity profiles, through asymptotic analysis. For this reason,the stability of the simpler one-component black-hole laser is first examined,by taking into account linear quantum fluctuations from the Bogoliubov-de Gennes equations. Consequently,the theory of linear instabilities for BECs is thoroughly described and then applied to both configurations in hand. The onset of complex modes is tracked, thus concluding their linear instability.

Contents

1 Introduction

"Black holes are like sharks. Elegant, simple, probably scary (more than what they deserve) and possibly lurking in deep, dark places all around us", as Joshua Sokol once phrased in the Quanta Magazine in 2020 [1]. Black holes fascinated and revolutionized physics from the very first moment. Their nature remained hidden and has proven harder to understand than most of the concepts that General Relativity has given birth to. Their existence provides a fundamental test-field of strong gravitational fields, beyond the point of Newtonian approximations. They are encountered in astrophysics and stellar-evolution physics, but also in a variety of different fields [2]. Their very blackness makes it hard to estimate their number or their size. In the framework of General Relativity, black holes can naturally emerge as the last stage of the stellar evolution for supermassive stars, as the core of galaxies, etc. After the observation of gravitational waves, the arguments against their existence have nearly completely disappeared. Black holes are also valuable in the insight that can provide onto the connection between Quantum Physics and gravity. The field of Quantum Field Theory of Curved Spacetime has flourished parallel to black hole physics [3, 4]. When we describe them quantum-field theoretically, we find that black holes behave as real objects with a non-zero temperature and entropy: they behave like black bodies. Due to the attribution of a temperature, thermodynamics do not just emerge accidentally but black holes follow, not just formally,thermodynamic laws. Black holes fall into a crossroad where thermodynamics, Quantum Physics and General Relativity approach each other. They constitute one of the best tools for the description of a possible theory of Quantum Gravity, a theory that could harmonically merge Quantum Physics and General Relativity into one entity, one 'theory of everything' [5–8].

Although the concept of black holes emerged in the second half of the twentieth century, originally found in David Finkelstein's writings in 1958 [9], the arguments behind its existence where known to Newtonian physicists, like Mitchell or Laplace, much earlier. Newtonian dynamics do not treat the effects of gravity on light. However, we can find a prototypical measure of their interaction, if it really exists. Light is characterized by its speed, c. The obvious measure would be the escape velocity from an object of mass M and radius R, $v_{esc} = \left(\frac{2GM}{R}\right)^{1/2}$. In this case, if the speed of light was $c < |V_{esc}|$, a distant observer would be unable to detect any light source. Equally well, this bound can be expressed as $M \sim \left(\frac{c^2}{G}\right)^{3/2} \rho^{-1/2}$, where spherical symmetry was assumed. Before the discovery of white dwarfs and the revolutionization of the physical understanding brought by General Relativity, the densest matter had approximately $\rho = 5000\, kgm^{-3}$ and the smallest object having this normal density would have a mass of

$$M_\star \sim 10^8 \left(\frac{\rho_\star}{\rho}\right)^{1/2} M_\odot, \tag{1.1}$$

where $M_\odot$ corresponds to the solar mass. The mass $M_\star$, being much greater than any other known star's mass, would be invisible from any observer.

However, in the twentieth century, the discovery of heavy matter of orders 10^9 – $10^{17}\ kg\ m^{-3}$ and the unambiguous description of the interaction of light with gravity changed the Newtonian picture. The existence of such heavy and high density stellar objects made the concept of black holes feasible. The formulation of General Relativity made black holes, at least crudely, describable. Indeed, the theory of General Relativity predicted the existence of supermassive astrophysical objects that would deform spacetime.

Black holes are regarded as objects in a region of spacetime where gravity is so strong that nothing can escape from it. Primarily, spacetime can have a black hole, if it can be divided into two mutually exclusive and exhaustive regions, the interior and the exterior of the black hole. The exterior of the black hole being the region of spacetime causally connected with a region infinitely far away from the interior of the black hole and the interior as the region of spacetime from where nothing, not even in principle, can escape, regardless of how long it tries. The boundary of the region from which no escape is possible is defined as the event horizon. Even if the event horizon is of utmost significance for the black hole, General Relativity does not provide it with any locally detectable features [5, 7, 8, 10].

It is important to note that the development of General Relativity did not alter the relation that was earlier found between mass and density in Newtonian gravity. It does however alter its conceptual consequences. Now, the density characterizes the black hole itself. Furthermore the black hole's mass has collapsed into a singularity; it does not possess a material limit-surface (see Figure 1.1). This is now being played by the event horizon.

In the eighties, Hawking came to some remarkable conclusions regarding black holes [11, 12]. He stated that, when quantum effects are taken into account, black holes should emit blackbody radiation. Following Hawking's analysis and the attribution of thermodynamic properties to black holes, we can define a temperature, which was found to be inversely proportional with the black hole's mass [5, 13],

$$k_B T = \frac{\hbar \kappa}{2\pi c} = \frac{\hbar c^2}{8\pi G M}. \tag{1.2}$$

In astrophysics, this amazing result of Hawking, in which an unprecedented exhibition of physical constants from otherwise disparate areas of physics, like Quantum Mechanics, Relativity and Thermodynamics, coexist is encountered, has few practical significance with regard to nowadays experimental infrastructure. For a solar-mass black hole, Hawking's equation, Equation 1.2, gives a temperature six orders of magnitude smaller than the Cosmic Microwave Background, meaning that the existence of black holes would be hidden from human detection for many more years to come, unless a different and indirect method is found. Otherwise, we would need to find 'micro' black holes that have possibly formed in the early stages of universe, which would be good candidates for the detection of Hawking radiation. However, they have not been found until now, if they exist.

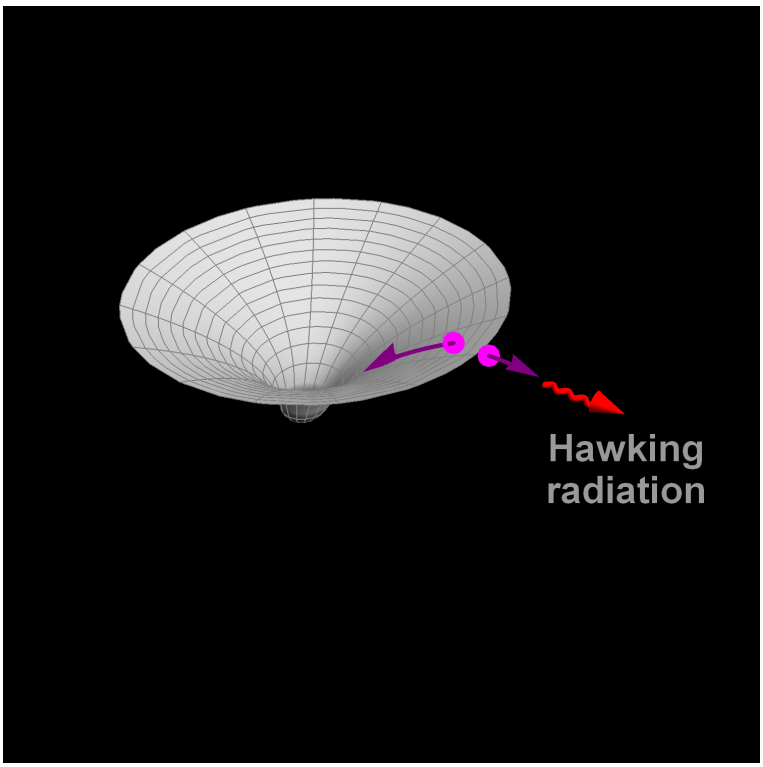

Figure 1.1: An illustration of the emission of Hawking radiation from a black hole.

From a more philosophical point of view, the treatment of black holes as being eternal or global objects or perfect absorbers needs to be used with care, as we nowadays accept the semiclassical picture of black holes evaporating as they emit Hawking radiation [11, 12]. Hawking's work initialized a 'merging' of the fields of Gravity, Quantum Theory and Thermodynamics. However, this 'merging' is not quite true as General Relativity and Quantum Theory are in conceptual and physical tension in a variety of aspects with each other. Even now, it is far from clear what it means to attribute thermodynamic properties to black holes or even the necessity of this attribution. The problem is even amplified when one realizes that black holes themselves suffer from necessity [14].

Analogue Models of Gravity could possibly give an answer to some of these problems [13, 15]. These models attempt to describe gravitational effects through the use of other physical systems, like acoustics in a moving fluid or Bose-Einstein Condensates (BECs) [13, 16–20]. Physical phenomena studied in an analogue model could otherwise be hidden into the complexity of real world and, thus, their nature would be hidden from human detection and study. As a result, analogue models open a new world of 'artificial' systems where we can model real world gravitational phenomena and extract useful information in our quest of exploring universe. After many years of intense research, last decade has also shown the first experimental realizations of Analogue Gravity models based on BECs [21–25].

There is indeed another area where analogue models could possibly help with the explanation of Hawking radiation. In astrophysics, a black hole could be the last evolutionary

stage after the collapse of a star. Those quantum vacuum modes which are incident from infinity, propagate through the collapsing spacetime and go again towards infinity, as they experience a gravitational redshift because of the gravitational collapse. The modes of the quantum vacuum which just managed to escape from the black hole are responsible for the steady thermal flux seen at late times. These modes are slowed down and redshifted to greater and greater scales. Any low-frequency mode can be traced back to those modes with ever-increasing frequency, but these frequencies can easily exceed the Planck scale. In these scales, Quantum Field Theory is not justified, but Hawking radiation seems to be dependent crucially on these frequencies in order to generate the low-frequency late-time modes [26–28].

What can analogue models say about this *Transplanckian problem*? An analogue model with an artificial event horizon is subject to the same restrictions as the astrophysical one, but analogue models *with* dispersion can *avoid* it. The behaviour of waves in different scales is now governed by dispersion. The mechanisms that now describe the system are much better understood than the Quantum Theory of Gravity that would describe the Transplanckian frequencies. Analogue models are also predicted with the same temperature as the astrophysical ones. As a result, it is obvious that analogue models provide a very nice platform where problems of different nature can be tackled, being based on the restless nature of the quantum vacuum instead of gravitation. Regarding the Transplanckian problem, analogue models with dispersion conclude that Hawking radiation exists independently of the high frequency regime, something clearly in favour of the existence of Hawking radiation [29, 30].

Initially, the field of Analogue Gravity focused on improving our understanding of Quantum Gravity applications. After years of enormous progress, it has evolved as an autonomous field. In this process, Analogue-Gravity techniques have been used in condensed matter or optical systems, but generally in many more fields in different contexts, shining new light on a variety of questions, improving our understanding of Gravity but also of the test-fields themselves. The initial motivation for having a test-field where questions regarding Quantum Gravity will be tested remains, but other directions of research have flourished as well. Analogue Gravity initiated a quest for the detection of Hawking radiation in analogue systems; this time, however, in a context very different to the original. The description of Hawking radiation and its implications in ultracold bosonic systems, a well-established field by now, will be the topic of research for the rest of this work.

The description of analogue effects in gravity will be first introduced through the example of the wave equation without dispersion [26]. This will be the topic of Chapter 2, together with a general introduction to the terminology used in the field. Quantum Field Theory for moving media can generally provide the bosonic nature for the quantization of the field in presence of a moving background [3, 4]. Different representations can be used for dealing with problems of varying background parameters across the analogue event horizon [20, 31]. The steplike or flat profile, where the background velocity and the speed of sound change across the horizon abruptly through 'steps', will be mainly used, as it stands out for its simplicity and accuracy [32, 33]. Then, the link with Unruh and Hawking effects will be provided, based on a more *kinematic* viewpoint.

Analogue gravity models are deeply connected to the specific model where the implementation takes place. As a result, a widely-used, thoroughly described, easily implemented and highly controllable system needs to be used for better results. BECs constitute one of these systems [34, 35]. From their first experimental realization, BECs have revolutionized ultracold physics contributing to the second Quantum Revolution [36]. What about trying to combine BECs with gravity, two otherwise quite successfully explained fields in order to deal with their remaining conceptual and practical problems? This will be the topic of Chapter 3.

In next chapters, systems based on BECs where the speed of sound crosses twice the velocity of the background flow, forming a supersonic region of finite length, called black-hole laser will be described [37–40]. Having in mind their description, the general theory of instabilities in BECs will be exposed in Chapter 5. Then, the description of the lasing effect of the black-hole laser will smoothly follow in Chapter 4. The emergence of the lasing effect for background velocity profiles that crosses twice the speed of sound indicates the linear instability of the black-hole laser, as described by the Bogoliubov-de Gennes equations. Black-hole lasers will be analysed in stages, giving first a brief classical description of the lasing effect, before describing it with the inclusion of quantum effects in a semiclassical approximation. The treatment of modes describing instabilities through the Bogoliubov-de Gennes equations for the quantum fluctuations of the respective Gross-Pitaevskii equations will be gradually and thoroughly exposed in order to contain the most general framework.

Chapter 6 will be concerned with an introductory analysis for the constituent regions of the black-hole laser emerging from a two-component Rabi-coupled BEC. The Rabi-coupled condensates will be initially described in detail for no background velocity. This analysis will be useful for the numerical results of Chapter 7, as the outer regions of the black-hole laser from the general countersuperflow of two-component Rabi-coupled BECs will be treated through an asymptotic analysis. Note that the supersonic cavity for the two-component BEC system will assume no Rabi or intraspecies coupling, in a first, simplified picture. Although the most general configuration will be deduced and explained, only the asymptotic modes for steplike velocity profiles will be analysed. Finally, we will discuss the instability properties of the black-hole laser formed from this two-component model.

In conclusion, a general summary and further perspectives for study regarding black-hole lasers will be given in Chapter 8.

2 An Introduction to Analogue Gravity

A spherically symmetric vacuum solution of Einstein's equations is determined by one essential constant, the mass M, and is described by the Schwarzschild metric,

$$\mathrm{d}s^2 = \left(1 - \frac{r_s}{r}\right) c^2\, \mathrm{d}t_S^2 - \left(1 - \frac{r_S}{r}\right)^{-1} \mathrm{d}r^2 - r^2\, \mathrm{d}\omega^2\,, \tag{2.1}$$

where $\mathrm{d}\omega^2 = \mathrm{d}\theta^2 + \sin^2\theta\, \mathrm{d}\phi^2$ is the angular line element, t_S the Schwarzschild time and $r_S = 2GM/c^2$ the Schwarzschild radius. The corresponding Schwarzschild metric is asymptotically flat. Near infinity, this metric can be approximated by the linearised gravity solution with the Newtonian potential $\phi = -M/r$. This allows one to conclude that the mass, M, is the mass of the gravitating object. The Schwarzschild metric describes the spacetime exterior of a star or planet with slow rotation, as well as, more generally, every spacetime of spherically distributed static matter with radial motion, thus preserving spherical symmetry. According to Birkhoff's theorem, the external metric does not depend on such motion [5, 8]. As $r_S/r \to 0$, the Schwarzschild metric approaches the flat Minkowski metric, so the coordinates (t_S, r, θ, ϕ) correspond to the usual spherical coordinates of flat spacetime for an observer at infinity. Indeed, the metric equation, Equation 2.1, contains two singularities, one at r = 0 and another at $r = r_S$. At the centre of the black hole, at $r = 0$, the curvature is infinite. Near this *singularity*, the tidal forces grow infinitely (physical singularity) and cannot be removed by any coordinate transformation. In contrast, the singularity on the surface $r = r_S$ gives a vanishing Killing vector. Outside the surface $r = r_S$, the coordinate t is the timelike coordinate. Inside the Schwarzschild radius, we observe that t and r interchange their character; r becomes the timelike coordinate and t the spacelike one. The null surface $r = r_S$ separating the exterior from the interior of the star (or the black hole) is, in fact, a regular surface of the spacetime manifold. This can be tested by calculating curvature invariants and, in Painlevé-Gullstrand coordinates, it can be seen that it indeed vanishes [5–8]. By defining a new time coordinate

$$t = t_S + 2\frac{\sqrt{r_S\, r}}{c} + \frac{r_S}{c} \ln\left(\frac{\sqrt{\frac{r}{r_S}} - 1}{\sqrt{\frac{r}{r_S}} + 1}\right), \tag{2.2}$$

the Schwarzschild-metric equation, Equation (2.1), can be transformed into

$$\mathrm{d}s^2 = c^2\, \mathrm{d}t^2 - \left(\mathrm{d}r + \sqrt{\frac{r_S}{r}} c\, \mathrm{d}t\right)^2 - r^2\, \mathrm{d}\omega^2\,. \tag{2.3}$$

In these coordinates, (t, r, θ, ϕ), the metric possesses no singularity at $r = r_S$.

Returning to the Schwarzschild metric, by approximating to the near horizon region, one can arrive to a Rindler metric. This has some clear consequences. It means that a particle or light ray falling into the black hole needs only a finite proper time to reach the event horizon, while the time t_S measured by an external observer for the same process would be infinite. Lastly, a distant observer would detect a redshift for the free falling observer analogous to $e^{-\kappa t}$, with the infinite redshift surface being the event horizon. It can be seen that the spacetime, described in the Schwarzschild coordinates, is geodesically incomplete, as there exists a continuation of the geometry beyond the Schwarzschild horizon. A black hole interior is a mysterious region of the Schwarzschild spacetime from where nothing can escape, unless there is a mechanism for causality violation. However, the interior of the black hole does not affect classical calculations conducted in its exterior.

In order to explicitly view the behaviour of light trajectories and how they are affected by the two different metrics previously defined, consider only radial curves for simplicity. This will lead to

$$\mathrm{d}s^2 = 0 \Rightarrow \frac{\mathrm{d}t_S}{\mathrm{d}r} = \pm\frac{1}{c}\left(1 - \frac{r_S}{r}\right)^{-1}, \tag{2.4}$$

meaning that light behaves as it does in flat spacetime. Far from the Schwarzschild radius, it behaves as

$$\frac{\mathrm{d}t_S}{\mathrm{d}r} = \pm\frac{1}{c}. \tag{2.5}$$

It can be seen that, as the Schwarzschild radius is approached, light travels progressively slower, approaching the horizon at an infinite time t_S. Now, considering the Painlevé-Gullstrand metric and by focusing once more on only the radial trajectories, equation

$$\frac{\mathrm{d}r}{\mathrm{d}t} = -c\sqrt{\frac{r_S}{r}} \tag{2.6}$$

is obtained. Then, the metric becomes

$$\mathrm{d}s^2 = c^2\,\mathrm{d}t^2 \rightarrow \mathrm{d}s^2_{max}\,. \tag{2.7}$$

As a result, these trajectories are geodesics and t measures proper time. This geometry could equally describe an inwards fluid flow with velocity $-c\sqrt{\frac{r_S}{r}}$ that tends to converge to the point $r = 0$. This represents the *comoving frame* of the fluid. At the Schwarzschild radius, the fluid flows inwards with speed c. Anything that falls beneath this radius, is being dragged by the black hole towards $r = 0$. By briefly discussing the radial curves,

$$\frac{\mathrm{d}t}{\mathrm{d}r} = \pm\frac{1}{c}\left(1 \mp \sqrt{\frac{r_S}{r}}\right)^{-1}, \tag{2.8}$$

it can be inferred from the velocity of the propagation on top of the 'fluid' that light can propagate in two distinctive ways; *with* the fluid (negative and positive signs, respectively)

or *against* it. This velocity of propagation is $\mp c - c\sqrt{\frac{r_S}{r}}$, consisting of the sum (difference) of the light's and fluid's velocity. Trajectories with velocity $-c - c\sqrt{\frac{r_S}{r}}$ are regular as they travel across the horizon with increasing velocity as they reach smaller radii. However, light rays that are propagating against the fluid are not regular at the horizon, meaning that rays with positive total velocity will escape to infinity and rays with negative velocity will be dragged by the fluid towards $r = 0$.

This analogy with a moving medium forms the basic concept of Analogue Gravity [13]. As a result, it is obviously needed to reformulate the corresponding metric, in order to be able to express all analogue models that are using general velocity profiles, $V(\mathbf{x})$. Furthermore, 1 + 1 dimensional space will be considered from now on and all the results will be formulated in this setting.

The metric for general moving media is

$$\mathrm{d}s^2 = c^2\,\mathrm{d}t^2 - (\mathrm{d}x - V(x)\,\mathrm{d}t)^2\,. \tag{2.9}$$

It is of fundamental importance to stress that in the analysis above, c indicated the speed of light, but this restriction does not apply from this point onwards. Thus, the velocity c will now indicate any velocity with respect to the medium. The comoving frame will then be the frame in which the wave speed is exactly c (medium at rest). The coordinates x and t will indicate the *lab frame*. Thus far, a discussion of the Schwarzschild metric had been pursued and, in the process, an analogy for the description of other moving media of generic background (not relativistic in any sense) was found. The metric for a moving medium with respect to the relativistic case was found as well and, in order to fully relate the new analogue system with the relativistic one, an analogue version of the black hole itself needs to be found. As a result, one can, for clarity reasons, speak of a waterfall configuration [26, 41]. The speed of the flow will increase with the direction of travel, something that is indicated in Figure 2.1. At some point, the observers (the fish in this framework) moving with maximum speed, c, will not be able to propagate any more against the fluid, giving rise to the concept of the analogue black hole. All fish that pass this point, the analogue event horizon, will be dragged towards the interior of the analogue black hole, without any chance of escaping, irrespective of how much or how long they try. In analogue models of gravity, there is no problem in defining the time-symmetric version of an analogue black hole, the analogue white hole, without any reference to its questionable gravitational existence. One can again consider the waterfall configuration, but now with the water flowing *from* the waterfall. Water flows very fast for the fish to be able to swim against the flow, but as the flow becomes progressively slower, fish will be able to propagate against the water flow at some point, which again indicates the event horizon. Previously, fish could not escape from the analogue black hole. Now, they cannot enter the analogue white hole. As it can be seen, the analogue white hole forms the time reversed version of the analogue black hole. This can be indicated by a change of sign in Equation 2.9, as $V \to -V$ [26, 42].

For the astrophysical situation, white holes are of limited use. They are encoded into the solutions of Schwarzschild metric, but are valid for $t_S \to -\infty$. However, in analogue

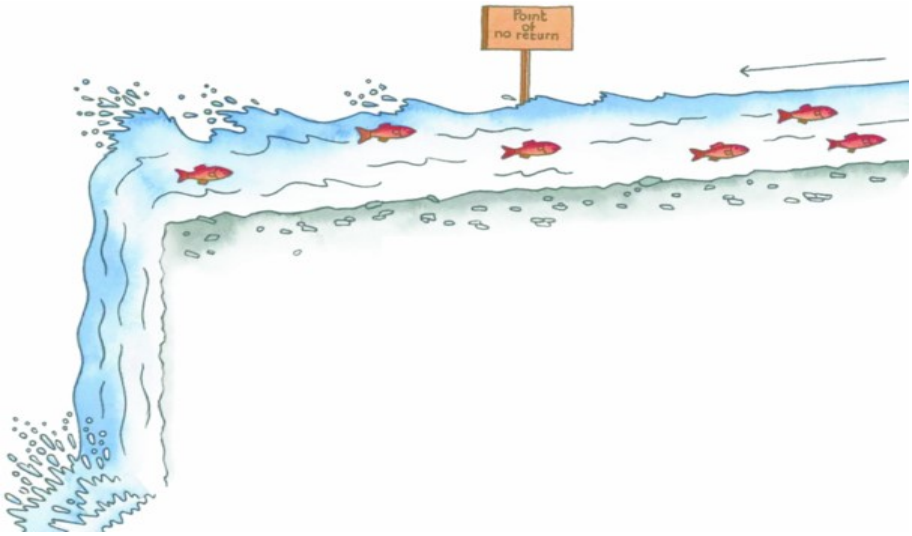

Figure 2.1: Illustration of an analogue black hole in an analogue spacetime [43]. A river (the moving frame) and the fish (the observers) can equally play the role of the moving particles in the vicinity of a gravitational black hole. The subsonic region is upstream and the supersonic downstream. Fish are dragged towards the waterfall (horizon) and the supersonic region. Everything enters the supersonic region (the interior of the black hole).

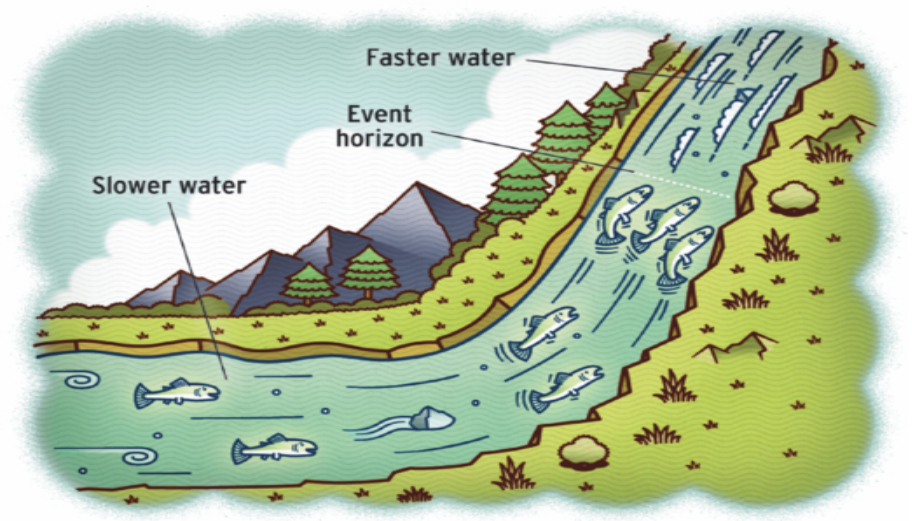

Figure 2.2: Illustration of the analogue white hole in an analogue spacetime [44]. In this case, the supersonic region is upstream and the subsonic downstream. The analogue black and white holes are symmetric with respect to the change in sign of the velocity of the moving frame. Fish cannot enter the analogue white hole, irrespective of how much or how long they try.

models there is no restriction in obtaining, using or interpreting them. More complex situations can form as well, where two event horizons are formed into a system, the *black-hole laser* [37, 38]. Most of the analysis in the rest of this work will be concerned with black-hole laser configuration (see Chapters 5-7).

2.1 A role model. The wave equation

In this section, the basic concepts of Quantum Field Theory in Curved Spacetime will be introduced, with an emphasis on analogue models. The prototypical example explored is the massless scalar field. This section takes its inspiration from [20, 26, 31].

Starting from the action formulation for the massless scalar field, one can define the action

$$S = \iint \mathrm{d}x\,\mathrm{d}t\, L\left(\phi, \phi^*, \partial_t\phi, \partial_t\phi^*, \partial_x\phi, \partial_x\phi^*\right) \tag{2.10}$$

with

$$L = \frac{1}{2}\sqrt{-g}g^{\mu\nu}\partial_\mu\phi^*\partial_\nu\phi, \tag{2.11}$$

where the Lagrangian of flat space has been expressed in covariant form. The metric tensor, $g_{\mu\nu}$, is used, with a determinant g. Then, Euler-Lagrange equations

$$\frac{\partial L}{\partial\phi^*} - \frac{\partial}{\partial t}\left(\frac{\partial L}{\partial\left(\partial_t\phi^*\right)}\right) - \frac{\partial}{\partial x}\left(\frac{\partial L}{\partial\left(\partial_x\phi^*\right)}\right) = 0 \tag{2.12}$$

give, for the Lagrangian density

$$L = \frac{1}{2c}\left(\left|\left(\partial_t + V\partial_x\right)\phi\right|^2 - c^2\left|\partial_x\phi\right|^2\right), \tag{2.13}$$

the following dispersionless wave equation:

$$\left(\partial_t + \partial_x V\right)\left(\partial_t + V\partial_x\right)\phi - c^2\partial_x^2\phi = 0. \tag{2.14}$$

It is obvious that partial derivatives are considered as operators, acting on everything to their right.

Attempting to transform the solution of the wave equation into a form which will be useful for our subsequent analysis in analogue gravity phenomenology, one can define the new fields:

$$u = t - \int^x \frac{\mathrm{d}x'}{c + V\left(x'\right)} \tag{2.15}$$

$$v = t + \int^x \frac{\mathrm{d}x'}{c - V\left(x'\right)}. \tag{2.16}$$

These fields transform the metric equation, Equation 2.9, into

$$\mathrm{d}s^2 = \left(c^2 - V^2(x)\right)\mathrm{d}u\,\mathrm{d}v\,, \tag{2.17}$$

which results to the transformed wave equation

$$\partial_u\partial_v\phi = 0. \tag{2.18}$$

The wave equation, Equation 2.18, is now in a form which has the solution

$$\phi = \phi_u(u) + \phi_v(v) = \phi_u\left(t - \int^x \frac{\mathrm{d}x'}{c + V(x')}\right) + \phi_v\left(t + \int^x \frac{\mathrm{d}x'}{c - V(x')}\right). \tag{2.19}$$

In order to specify the model, one can assume that $V < 0$. Then, ϕ_u is right-moving, counterpropagating to the background flow, and ϕ_v is propagating with the fluid. If it is assumed that the spacetime possesses a horizon, then it is necessary that $V = -c$. As a result, the u-mode diverges at the horizon, while the v-mode is defined in the infinite space. The important concept here is that the u-mode does not cover both the interior and the exterior of the black hole. Thus another u-mode needs to be introduced, in order to cover the other half of spacetime left uncovered. The v-mode does not have any divergence and, as a result, needs no new inclusion. The u-mode can come arbitrarily close to the horizon but cannot cross it. One can equally well use the concept of a wavepacket which can propagate in only one half of the spacetime and approach the horizon after infinite time. Now, suppose that a wavepacket is formed close to the horizon and starts to propagate further away. In the *asymptotic future*, the wavepacket will pick up speed and move further away from the horizon. In the *asymptotic past*, however, the wavepacket approaches as close as possible to the horizon. Each wavepacket has its own trajectory and, as electric or magnetic field lines, different wavepacket trajectories cannot cross each other. Many wavepackets which appear far away from each other in the asymptotic future will come closer to each other as the time of their formation is approached in the asymptotic past. Equally, lines of constant u bunch together as they approach the horizon in the asymptotic past. Note that the Transplanckian problem states this exact conclusion; that as we trace back the wavepackets, they should have originated from arbitrarily close to the horizon.

Summing up, he existence of the horizon has, until now, lead to the definition of two u-modes, the u_r and the u_l mode, across the horizon. Equally well, the existence of a horizon gives rise to one subsonic and one supersonic region, meaning a region where $|V| < c$ and one with $|V| > c$.

Moving on to the description of the modes of the system, it can be seen that, as the Lagrangian 2.13 is translationally invariant, the existence of stationary modes (energy eigenstates)

$$\phi(t, x) = e^{-i\omega t}\phi_\omega(x) \tag{2.20}$$

is guaranteed. Making use of the coordinates 2.15-2.16, the solution of the wave equation can be expressed in the form

$$\phi_\omega(x) = C_u e^{i\omega\int^x \frac{\mathrm{d}x'}{c+V(x')}} + C_v e^{-i\omega\int^x \frac{\mathrm{d}x'}{c-V(x')}} = C_u\phi^u_\omega(x) + C_v\phi^v_\omega(x) \tag{2.21}$$

and, if there is a spacetime possessing a horizon,

$$\begin{aligned}\phi_\omega(x) &= C_{u_r} e^{i\omega \int_{x_r}^{x} \frac{\mathrm{d}x'}{c+V(x')}} \Theta(x - x_H) \\ &\quad + C_{u_l} e^{i\omega \int_{x_l}^{x} \frac{\mathrm{d}x'}{c+V(x')}} \Theta(x_H - x) + C_v e^{-i\omega \int^{x} \frac{\mathrm{d}x'}{c-V(x')}} \\ &= C_{u_r} \phi_\omega^{u_r}(x)\Theta(x - x_H) + C_{u_l} \phi_\omega^{u_l}(x)\Theta(x_H - x) + C_v \phi_\omega^{v}(x). \end{aligned} \tag{2.22}$$

In this process, the Heaviside step function has been used, in order to distinguish between the interior and the exterior of the black hole. In both definitions of the field, one can discern the modes that propagate with the fluid and those that propagate against it; the u-modes constitute the counterpropagating modes (with u_r the counterpropagating mode in the subsonic right region and u_l the counterpropagating mode in the supersonic left region, respectively) and the v-modes constitute the copropagating modes in the whole spacetime.

The wavevectors of these solutions can now be defined as

$$k_\omega^{u/v}(x) = \pm \frac{\omega}{c \pm V(x)}. \tag{2.23}$$

In this way, the mode solution becomes

$$\phi_\omega^{u/v}(x) = e^{i \int^{x} \mathrm{d}x' k_\omega^{u/v}(x')} \tag{2.24}$$

and the dispersion relation can found to be

$$\omega_{cm}^2 = (\omega - Vk)^2 = c^2 k^2, \tag{2.25}$$

where it has been used that, due to the Doppler shift, the wavefrequency in the comoving frame is related with the wavefrequency in the laboratory frame via this simple form. The decomposition of the modes will give the dispersion profiles

$$\omega_{cm} = \omega - Vk = \begin{cases} ck & \text{for } u\text{-modes} \\ -ck & \text{for } v\text{-modes} \end{cases}. \tag{2.26}$$

This equation indicates that the comoving frequency is related with the lab-frame's frequency and with the dispersion relation itself. As a result, it can be used for the graphical solution of the dispersion diagrams, as shown in Figures 2.3 and 2.4.

Furthermore, the Lagrangian 2.13 is invariant under phase rotations, thus giving another conserved quantity, the scalar product. This can now be defined as

$$(\phi_1, \phi_2) = i \int_{-\infty}^{\infty} \mathrm{d}x \left(\phi_1^* \left(\partial_t + V\partial_x\right)\phi_2 - \phi_2((\partial_t + V\partial_x)\,\phi_1^*\right) \tag{2.27}$$

$$= i \int_{-\infty}^{+\infty} \mathrm{d}x \left(\phi_1^* \pi_2 - \phi_2 \pi_1^*\right), \tag{2.28}$$

with the conjugate momentum[1]

$$\pi = \frac{\partial L}{\partial\left(\partial_t \phi^*\right)} = \left(\partial_t + V\partial_x\right)\phi. \tag{2.29}$$

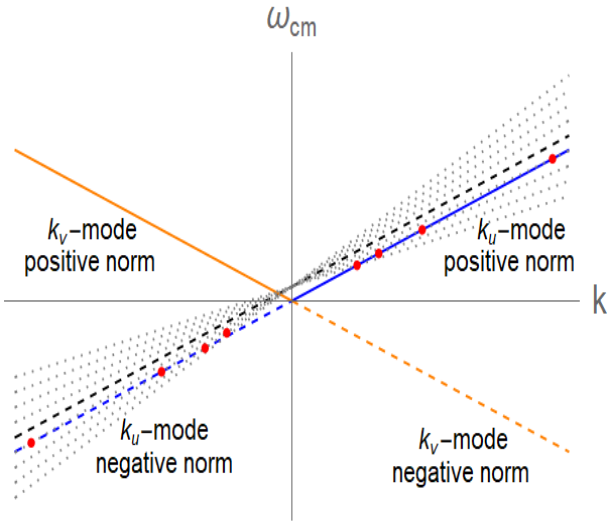

Figure 2.3: Dispersion relation in the comoving frame. The blue and orange dotted lines represent the negative-norm branches. This dispersion profile can be divided into the positive u- and v- and the negative u- and v- branches, consisting of these four sectors in total. The black line crossing the dispersion relation corresponds to the relation $\omega_{cm} = \omega - Vk$ for a given laboratory frequency, ω. The point of intersection of this equation with the dispersion profile gives the values of the wavevectors for the given energy. The only slope which gives no intersection point is for $V = -c$, or differently, when the intersection points has moved to infinity. This precisely indicates the existence of the Transplanckian problem. For the v-branch, the existence of the Transplanckian problem can again be inferred when the intersection point moves to infinity.

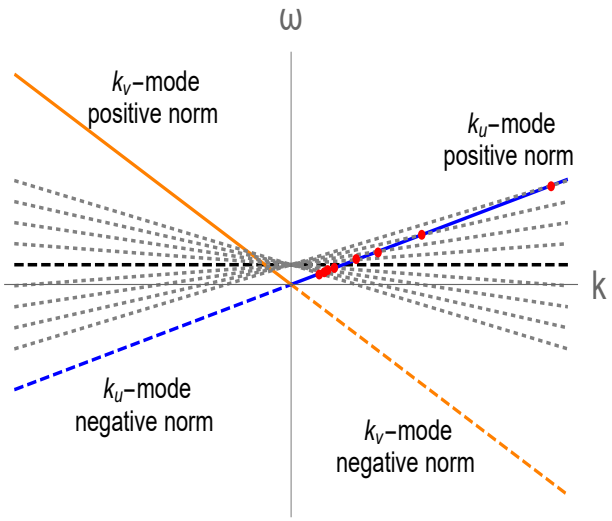

Figure 2.4: Dispersion relation in the laboratory frame. The blue and orange dotted lines represent the negative-norm branches. Now, the two branches of u and v character are not symmetric. This time, the Transplanckian problem can be visualized as follows: when $V = -c$ the frequency of the u-branch, for example, will be a line parallel to the constant ω solution. As a result, there will be no k-solution as before. The same reasoning holds for the v-branch as well.

From the definition of the scalar product, one can further define the scalar product of a field with itself, its *norm*. For the subsequent analysis, it is crucial to mention that the scalar product defined in Equation 2.27 is *not* positive definite, seen from the relation

$$(\phi_1^*, \phi_2^*) = -(\phi_1, \phi_2)^* \,. \tag{2.30}$$

This means that if ϕ solves the real wave equation with positive norm, then ϕ^* solves it as well, but with negative norm.

2.1.1 Different field decompositions: The k- and ω-representations

Both the k- and the ω-representations serve well for the decomposition of the field into components in the process of its quantization [20, 26, 31]. The k-representation takes into account the special case (which is not so special after all), where k is a conserved quantity. This happens to be the case in spacetimes with background velocity V constant in space. Then, the Lagrangian will be invariant under spatial translations and the constancy of the wavevector will follow as well. States of constant wavevector, k, are momentum eigenstates. By assuming constant background velocity, there is no horizon formed in the spacetime and no splitting of the u-mode occurs.

[1] Note that this scalar product is sensible only for complex fields. Nevertheless, even real fields can be decomposed into complex components that will respectively obey this scalar product rule.

By investigating the scalar product of the two modes in this setting, one obtains

$$\left(e^{i(k_1 x-\omega^u(k_1)t)}, e^{i(k_2 x-\omega^u(k_2)t)}\right) = 4\pi c k_1 \delta(k_1 - k_2) \tag{2.31}$$

$$\left(e^{i(k_1 x-\omega^v(k_1)t)}, e^{i(k_2 x-\omega^v(k_2)t)}\right) = -4\pi c k_1 \delta(k_1 - k_2) \tag{2.32}$$

$$\left(e^{i(k_1 x-\omega^u(k_1)t)}, e^{i(k_2 x-\omega^v(k_2)t)}\right) = 0. \tag{2.33}$$

In this process, the key relation used is that, when acting on a stationary mode, the operator $\partial_t + V\partial_x$ becomes $(\partial_t + V\partial_x) \rightarrow -i\omega_{cm} = \mp ick$, where the $\mp$ sign refers to the u- and v- modes, respectively.

From this result, the first conclusion can be inferred: plane waves of different nature are mutually orthogonal and the sign of their norm is equal to the sign of their comoving frequency. Thus, the dispersion profile can be decomposed as

$$\omega_{cm} = \omega - Vk = \begin{cases} |ck| & \text{for positive-norm modes} \\ -|ck| & \text{for negative-norm modes} \end{cases}. \tag{2.34}$$

Until now, two different classifications for the modes have been used. Regarding the norm, positive and negative-norm branches can be distinguished. Furthermore, modes can be described as copropagating (the v-branch) or counterpropagating to the fluid flow (the u-branch). These two classifications can be combined (see Figures 2.3 and 2.4), into one classification scheme

- $k > 0$, $ck > 0$ means $k > 0$, $c > 0 \xrightarrow{V_{gr}>0}$ *positive* u-mode
- $k < 0$, $ck < 0$ means $k < 0$, $c > 0 \xrightarrow{V_{gr}>0}$ *negative* u-mode
- $k > 0$, $ck < 0$ means $k > 0$, $c < 0 \xrightarrow{V_{gr}<0}$ *positive* v-mode
- $k < 0$, $ck > 0$ means $k < 0$, $c < 0 \xrightarrow{V_{gr}<0}$ *negative* v-mode,

where $V_{gr} = \frac{\mathrm{d}\omega}{\mathrm{d}k}$ is the group velocity, defined as the tangent of the dispersion profile in any specific point.

As a result, the sign of the wavevector defines the direction of travel on top of the fluid (comoving frame) for positive-norm modes, while the opposite is true for negative-norm modes. From the inner product equations, Equations 2.32, the orthonormal k-basis, normalized to $\pm\delta(k - k')$, can be defined as

$$\phi^u_k(x,t) = \frac{1}{\sqrt{4\pi\,|ck|}} e^{i(kx-\omega^u(k)t)} \equiv \phi^u_k(x) e^{-i\omega^u(k)t} \tag{2.35}$$

$$\phi^v_k(x,t) = \frac{1}{\sqrt{4\pi\,|ck|}} e^{i(kx-\omega^v(k)t)} \equiv \phi^v_k(x) e^{-i\omega^v(k)t} \tag{2.36}$$

with $\omega^{u/v}(k) = (V \pm c)\,k$.

Proceeding by using Fourier analysis and decomposing the total field into positive (first terms in the integrals) and negative-norm modes (complex conjugated terms in the integrals), one obtains:

$$\begin{aligned}\phi(x,t) &= \int_{-\infty}^{+\infty} \mathrm{d}k \left(\alpha^u(k)\phi_k^u(x)e^{-i\omega^u(k)t} + \alpha^v(k)\phi_k^v(x)e^{-i\omega^v(k)t}\right) \\ &= \int_{-\infty}^{0} \mathrm{d}k \left(\alpha^v(k)\phi_k^v(x)e^{-i\omega^v(k)t} + \alpha^{v*}(k)\phi_k^{v*}(x)e^{i\omega^v(k)t}\right) \\ &\quad + \int_{0}^{+\infty} \mathrm{d}k \left(\alpha^u(k)\phi_k^u(x)e^{-i\omega^u(k)t} + \alpha^{u*}(k)\phi_k^{u*}(x)e^{i\omega^u(k)t}\right) \end{aligned} \tag{2.37}$$

with orthonormality conditions

$$\alpha^u(k) = (\phi_k^u, \phi)\,, \tag{2.38}$$
$$\alpha^v(k) = (\phi_k^v, \phi)\,, \tag{2.39}$$
$$\alpha^{u*}(k) = -(\phi_k^{u*}, \phi)\,, \tag{2.40}$$
$$\alpha^{v*}(k) = -(\phi_k^{v*}, \phi)\,. \tag{2.41}$$

The quantization procedure further assumes that the generally complex-valued functions $\alpha^{u/v}(k)$ are promoted to operators[2]. As a result, with the real-valued field, $\phi \to \hat{\phi}$, the field equation, Equation 2.37, can be quantized as

$$\begin{aligned}\hat{\phi}(x,t) &= \int_{-\infty}^{0} \mathrm{d}k \left(\hat{\alpha}^v(k)\phi_k^v(x)e^{-i\omega^v(k)t} + \hat{\alpha}^{v\dagger}(k)\phi_k^{v*}(x)e^{i\omega^v(k)t}\right) \\ &\quad + \int_{0}^{+\infty} \mathrm{d}k \left(\hat{\alpha}^u(k)\phi_k^u(x)e^{-i\omega^u(k)t} + \hat{\alpha}^{u\dagger}(k)\phi_k^{u*}(x)e^{i\omega^u(k)t}\right). \end{aligned} \tag{2.42}$$

Now that the crucial step of quantizing the field is complete, the process can be continued in order to find the field's canonical momentum, the mode operators 2.41 and finally their canonical commutation relations. Then, the conjugate momentum is

$$\begin{aligned}\hat{\pi}(x,t) &= \int_{-\infty}^{0} \mathrm{d}k \left(\hat{\alpha}^v(k)\pi_k^v(x)e^{-i\omega^v(k)t} + \hat{\alpha}^{v\dagger}(k)\pi_k^{v*}(x)e^{i\omega^v(k)t}\right) \\ &\quad + \int_{0}^{+\infty} \mathrm{d}k \left(\hat{\alpha}^u(k)\pi_k^u(x)e^{-i\omega^u(k)t} + \hat{\alpha}^{u\dagger}(k)\pi_k^{u*}(x)e^{i\omega^u(k)t}\right) \end{aligned} \tag{2.43}$$

and the mode operators can be found to be

$$\hat{\alpha}_k^u = i \int_{-\infty}^{\infty} \mathrm{d}x \left(\phi_k^{u*}(x)e^{i\omega^u(k)t}\hat{\pi}(x,t) - \pi_k^{u*}(x)e^{i\omega^u(k)t}\hat{\phi}(x,t)\right) \tag{2.44}$$
$$\hat{\alpha}_k^v = i \int_{-\infty}^{\infty} \mathrm{d}x \left(\phi_k^{v*}(x)e^{i\omega^v(k)t}\hat{\pi}(x,t) - \pi_k^{v*}(x)e^{i\omega^v(k)t}\hat{\phi}(x,t)\right) \tag{2.45}$$

[2]In the previous analysis, the coefficients of the complex-conjugate modes have been written as complex-conjugated as well, in order to preserve the real character of the total field

$$\hat{\alpha}_k^{u\dagger} = -i \int_{-\infty}^{\infty} \mathrm{d}x \left(\phi_k^u(x) e^{-i\omega^u(k)t} \hat{\pi}(x,t) - \pi_k^u(x) e^{-i\omega^u(k)t} \hat{\phi}(x,t) \right) \tag{2.46}$$

$$\hat{\alpha}_k^{v\dagger} = -i \int_{-\infty}^{\infty} \mathrm{d}x \left(\phi_k^v(x) e^{-i\omega^v(k)t} \hat{\pi}(x,t) - \pi_k^v(x) e^{-i\omega^v(k)t} \hat{\phi}(x,t) \right) \tag{2.47}$$

with commutation relations

$$\left[\hat{\phi}(x,t), \hat{\pi}(x',t) \right] = i\delta(x - x') \tag{2.48}$$

$$\left[\hat{\phi}(x,t), \hat{\phi}(x',t) \right] = 0 \tag{2.49}$$

$$\left[\hat{\pi}(x,t), \hat{\pi}(x',t) \right] = 0. \tag{2.50}$$

These commutation relations can be used to find the respective commutation relations for the mode operators, $\hat{\alpha}_k^u, \hat{\alpha}_k^{u\dagger}, \hat{\alpha}_k^v, \hat{\alpha}_k^{v\dagger}$. By using simple algebra, the desired result is achieved,

$$\left[\hat{\alpha}_k^u, \hat{\alpha}_{k'}^{u\dagger} \right] = \left[\hat{\alpha}_k^v, \hat{\alpha}_{k'}^{v\dagger} \right] = \delta(k - k'), \tag{2.51}$$

where all other commutators vanish.

The meaning of these results is of paramount importance. The procedure followed indicates that the mode operators $\hat{\alpha}_k^u, \hat{\alpha}_k^{u\dagger}, \hat{\alpha}_k^v, \hat{\alpha}_k^{v\dagger}$ are of bosonic nature. Operators of positive norm correspond to annihilation operators and operators of negative norm to creation ones in a generalization of quantum-field-theoretic techniques in flat space [3, 4, 45]. As a result, the sign of the norm determines, not only the sign of the frequency in the comoving frame, but also the nature of the bosonic operators.

Now that the nature of the modes has been found and the quantization of the field in the k-representation has been explained, the ω-representation and its relative differences with the previous procedure will be presented.

Firstly, the k-representation is only valid for a constant background velocity profile, V. In the presence of a spacetime with horizons, this representation is no longer applicable if the velocity changes in different regions of space. However, there is one exception in this rule that deals with steplike (or flat) velocity profiles. The k representation in that case gives valid results as it corresponds to measurable quasiparticles at infinity. Now, for the inhomogeneous velocity profiles, exact solutions will be given as sums over eigenfrequencies and these can be subsequently grouped into groups of equal frequency, ω.

The resulting k-representation for a homogeneous flow is transformed into the ω-representation as

$$\begin{aligned} \hat{\phi}(x,t) &= \int_{-\infty}^{+\infty} \mathrm{d}k \left(\hat{\alpha}_k^v \phi_k^v(x) e^{-i\omega^v(k)t} + \hat{\alpha}_k^u \phi_k^u(x) e^{-i\omega^u(k)t} \right) \\ &\to \int_{-\infty}^{+\infty} \mathrm{d}\omega \left(\hat{\alpha}_\omega^v \phi_\omega^v(x) e^{-i\omega t} + \hat{\alpha}_\omega^u \phi_\omega^u(x) e^{-i\omega t} \right), \end{aligned} \tag{2.52}$$

where the following commutation relations

$$\left[\phi^u_\omega, \phi^u_{\omega'}\right] = \delta(\omega - \omega') \tag{2.53}$$

$$\left[\hat{\alpha}^u_\omega, \hat{\alpha}^{u\dagger}_{\omega'}\right] = \delta(\omega - \omega') \tag{2.54}$$

$$\left[\hat{\alpha}^v_\omega, \hat{\alpha}^{v\dagger}_{\omega'}\right] = \delta(\omega - \omega') \tag{2.55}$$

are assumed.

With the use of the algebraic relations

$$\delta(\omega - \omega') = \left|\frac{\mathrm{d}k}{\mathrm{d}\omega}\right| \delta(k - k') \tag{2.56}$$

and

$$\mathrm{d}\omega = \left|\frac{\mathrm{d}\omega}{\mathrm{d}k}\right| \mathrm{d}k\,, \tag{2.57}$$

one obtains

$$\phi^u_\omega = \sqrt{\left|\frac{\mathrm{d}k^u}{\mathrm{d}\omega}\right|}\phi_{k^u(\omega)} \tag{2.58}$$

$$\phi^v_\omega = \sqrt{\left|\frac{\mathrm{d}k^v}{\mathrm{d}\omega}\right|}\phi_{k^v(\omega)} \tag{2.59}$$

$$\hat{\alpha}^u_\omega = \sqrt{\left|\frac{\mathrm{d}k^u}{\mathrm{d}\omega}\right|}\hat{\alpha}_{k^u(\omega)} \tag{2.60}$$

$$\hat{\alpha}^v_\omega = \sqrt{\left|\frac{\mathrm{d}k^v}{\mathrm{d}\omega}\right|}\hat{\alpha}_{k^v(\omega)}. \tag{2.61}$$

With these transformations, the desired mapping onto Equation 2.52 with the needed commutation relations for the ω-representation, Equation 2.58, is achieved. Indeed, the new orthonormal basis will be

$$\phi^u_\omega(x,t) = \frac{1}{\sqrt{4\pi\left|ck^u(\omega)v_g(k^u(\omega))\right|}} e^{i(k^u(\omega)x - \omega t)} \equiv \phi^u_\omega(x)e^{-i\omega t} \tag{2.62}$$

$$\phi^v_\omega(x,t) = \frac{1}{\sqrt{4\pi\left|ck^v(\omega)v_g(k^v(\omega))\right|}} e^{i(k^v(\omega)x - \omega t)} \equiv \phi^v_\omega(x)e^{-i\omega t}. \tag{2.63}$$

It is stressed that these modes are again normalized as those in the k-representation to $\pm\delta(\omega - \omega')$ depending on the sign of their norm.

Now that the field decomposition in the ω-representation is found, we would like to express it in terms of annihilation and creation operators for its quantization. In contrast to the k-representation case, here the decomposition works differently; for $\omega > 0$, the v-branch has always positive norm, but the u-branch has positive norm for the flow being

subsonic and negative for the flow being supersonic. The u-part of the field is decomposed as

$$\hat{\phi}^u(x,t) = \begin{cases} \int_0^{+\infty} \mathrm{d}\omega \left(\hat{\alpha}^u_\omega \phi^u_\omega(x) e^{-i\omega t} + \hat{\alpha}^{u\dagger}_\omega \phi^{u*}_\omega(x) e^{i\omega t} \right) & \text{for } |V| < c \\ \int_0^{+\infty} \mathrm{d}\omega \left(\hat{\alpha}^u_{-\omega} \phi^u_{-\omega}(x) e^{-i\omega t} + \hat{\alpha}^{u\dagger}_{-\omega} \phi^{u*}_{-\omega}(x) e^{i\omega t} \right) & \text{for } |V| > c \end{cases} \tag{2.64}$$

with the positive-norm modes represented by the first terms in both relations and the negative-norm ones (their complex conjugates) following.

Until now, the quantized field has only partly transformed to the ω-representation, as only the homogeneous case in the ω-representation was dealt with. The following analysis will concern the general inhomogeneous analysis.

In the inhomogeneous case, there is a reference frame where the flow profile is time independent, something that did not hold true for the homogeneous case. There, due to the translational invariance we could shift between subsonic and supersonic flows, with no mode mixing. Then, the definition of the modes in this non-uniform-velocity background will be derived and the expression for the positive-norm u-modes will be written down

$$\phi^u_{\omega,R}(x,t) = \Theta(x) \frac{1}{\sqrt{4\pi c\omega}} e^{-i\omega u_r} \tag{2.65}$$

$$\phi^u_{-\omega,L}(x,t) = \Theta(-x) \frac{1}{\sqrt{4\pi c\omega}} e^{i\omega u_l}. \tag{2.66}$$

Modes with the same frequency can mix, meaning that linear combinations of the modes of the form

$$\begin{aligned} &\left(\alpha\phi^u_{\omega_1,r} + \beta\phi^{u*}_{-\omega_1,l}, \alpha\phi^u_{\omega_2,r} + \beta\phi^{u*}_{-\omega_2,l} \right) \\ &\qquad = \alpha^*\alpha \left(\phi^u_{\omega_1,r}, \phi^u_{\omega_2,r} \right) + \alpha^*\beta \left(\phi^u_{\omega_1,r}, \phi^{u,*}_{-\omega_2,l} \right) \\ &\qquad\quad + \beta^*\alpha \left(\phi^{u*}_{-\omega_1,l}, \phi^u_{\omega_2,r} \right) + \beta^*\beta \left(\phi^{u*}_{-\omega_1,l}, \phi^{u,*}_{-\omega_2,l} \right) \\ &\qquad = \left(|\alpha|^2 - |\beta|^2 \right) \delta(\omega_1 - \omega_2) \end{aligned} \tag{2.67}$$

can be constructed with $|\alpha|^2 - |\beta|^2 = \pm 1$. Modes are normalized with positive or negative norm, respectively. Lastly, these linear combinations are also orthogonal to any combination involving the modes $\phi^u_{-\omega,l}$ and $\phi^{u*}_{\omega,r}$. As a result, any set of modes of this form can be regarded as a complete and orthonormal set of positive or negative-norm modes, depending on the assigned sign, with

$$\phi^u_{\omega,1} = \alpha_{\omega,1}\phi^u_{\omega,r} + \beta_{\omega,1}\phi^{u,*}_{-\omega,l} \tag{2.68}$$

$$\phi^u_{\omega,2} = \alpha_{\omega,2}\phi^u_{-\omega,l} + \beta_{\omega,2}\phi^{u,*}_{\omega,r} \tag{2.69}$$

and

$$|\alpha_{\omega,j}|^2 - |\beta_{\omega,j}|^2 = 1. \tag{2.70}$$

Equation 2.68 gives infinite possibilities for linear combinations of modes. However, the physically interesting ones reduce to the *ingoing* and the *outgoing* modes. Outgoing modes can be defined from Equation 2.68 with $\alpha_{\omega,j} = 1$ and $\beta_{\omega,j} = 0$. These modes can be regarded as single outgoing wavepackets, indicating wavepackets that have formed at the horizon and propagate to the right with frequency ω, being excitations of the mode $\phi^u_{\omega,r}$, or to the left with frequency $-\omega$, being excitations of the $\phi^u_{-\omega,l}$. These modes propagate towards infinity in the *asymptotic* future. Equally we can define the ingoing modes, as those wavepackets of ingoing character in the *asymptotic* past. The modes ϕ^v_ω are definitely of ingoing character in the asymptotic past, but u-modes are always outgoing. Is it possible that u-modes be defined with ingoing character? There are two ways of resolving this problem. The simplest one is to consider a black hole from the earliest stage in each evolution [46]. Before the formation of the black hole, u-modes can be of ingoing character. There is no point where these u-modes can diverge, as it happens across the horizon, before the black hole's formation. Furthermore, the sign of the wavevector of each mode can never change and, thus, positive-norm modes are made up of positive wavevectors and similarly for the negative-norm ones. After the evolution of the initial ingoing modes through the different stages of the history of the black hole, we are only interested in their final form, as the intermediate stages will not alter states in later times. As discussed in Appendix B and in [47–49], the relation between α and β coefficients of Equation 2.68 can be inferred. They can be normalized and written as a sum of the form

$$\phi^{u,in}_{\omega,r} = \frac{1}{\sqrt{2\sinh\left(\frac{\pi\omega}{\alpha}\right)}}\left(e^{\frac{\pi\omega}{2\alpha}}\phi^{u,out}_{\omega,r} + e^{\frac{-\pi\omega}{2\alpha}}\phi^{u,out*}_{-\omega,l}\right) \tag{2.71}$$

$$\phi^{u,in}_{-\omega,l} = \frac{1}{\sqrt{2\sinh\left(\frac{\pi\omega}{\alpha}\right)}}\left(e^{\frac{\pi\omega}{2\alpha}}\phi^{u,out}_{-\omega,l} + e^{\frac{-\pi\omega}{2\alpha}}\phi^{u,out*}_{\omega,r}\right), \tag{2.72}$$

where the modes $\phi^{u,out}_{\omega,r}$ and $\phi^{u,out}_{-\omega,l}$ are those defined in Equation 2.65. Negative-norm modes can be formed by taking the complex conjugate of the modes $\phi^{u,in*}_{-\omega,l}$ and $\phi^{u,in*}_{\omega,r}$.

Let us now give a *kinematic* description of the nature of ingoing modes and, subsequently, of the Hawking effect. How can the appearance of stationary ingoing modes, like in Equation 2.71, be described in a spacetime with a horizon? Modes that are located at points far away from the horizon stay unaffected during its creation. The worst scenario would mean that they possibly change their direction of travel, while their region becomes from subsonic supersonic. Now what happens to those modes that originate exactly at the point where the horizon appears? These modes, as shown in Equation 2.71, are expressed with respect to outgoing modes and thus, at the moment of the creation of the black hole, one outgoing mode will propagate in the interior of the black hole and the other in its exterior, with direction towards infinity. These two pieces of the initial ingoing mode are seemingly disconnected, but they are in fact strongly entangled.

The total field can be decomposed into modes in the ingoing or the outgoing basis as

$$\hat{\phi}(t,x) = \int_0^\infty \mathrm{d}\omega\left(\hat{\alpha}^{u,in}_{\omega,r}\phi^{u,in}_{\omega,r}(t,x) + \hat{\alpha}^{u,in}_{-\omega,l}\phi^{u,in}_{-\omega,l}(t,x) + \hat{\alpha}^{v}_{\omega}\phi^{v}_{\omega}(t,x) + h.c.\right) \tag{2.73}$$

or

$$\hat{\phi}(t,x) = \int_0^\infty \mathrm{d}\omega \left(\hat{\alpha}^{u,out}_{\omega,r} \phi^{u,out}_{\omega,r}(t,x) + \hat{\alpha}^{u,out}_{-\omega,l} \phi^{u,out}_{-\omega,l}(t,x) + \hat{\alpha}^{v}_{\omega} \phi^{v}_{\omega}(t,x) + h.c. \right), \tag{2.74}$$

respectively, with h.c. denoting hermitian conjugates. From this equation it is now obvious that, in the presence of horizons, there is always some mode mixing in the description of the quantized field; incoming and outgoing bases are inequivalent. In this conversion process, incoming particles are converted into outgoing ones, following conservation of energy and momentum. If all the wavepackets had the same norm and there was no mixing of opposite norm wavepackets, then, if we decreased the rate of outgoing particles to zero, the same would have happened for the ingoing ones. Now that we have mode mixing, decreasing the ingoing modes does not necessarily mean that the rate of conversion for outgoing modes will decrease as well. The only constraint that remains is the condition $|\alpha|^2 - |\beta|^2 = 1$. This relation is solely responsible for the mixing of modes, meaning that annihilation and creation operators mix even in the absence of ingoing modes. This means that the presence of ingoing modes is no more a prerequisite for the existence of outgoing ones! This is the effect of spontaneous emission [26, 50].

Let us now define the vacuum state, which will be different for ingoing and outgoing modes when mode mixing occurs. The vacuum state is the state where no excited modes can ne encountered and it is an eigenstate of all annihilation operators,

$$\hat{\alpha} \left|0\right\rangle = 0, \quad \forall\, \hat{\alpha}. \tag{2.75}$$

This state can be an *in*-vacuum or an *out*-vacuum state, according to the type of modes used.

Finally, using Equations 2.71 and 2.73, the expressions for the mode operators,

$$\hat{\alpha}^{u,out}_{\omega,r} = \frac{1}{\sqrt{2\sinh\left(\frac{\pi\omega}{\alpha}\right)}} \left(e^{\frac{\pi\omega}{2\alpha}} \hat{\alpha}^{u,in}_{\omega,r} + e^{\frac{-\pi\omega}{2\alpha}} \hat{\alpha}^{u,in\dagger}_{-\omega,l} \right) \tag{2.76}$$

$$\hat{\alpha}^{u,out}_{-\omega,l} = \frac{1}{\sqrt{2\sinh\left(\frac{\pi\omega}{\alpha}\right)}} \left(e^{\frac{\pi\omega}{2\alpha}} \hat{\alpha}^{u,in}_{-\omega,l} + e^{\frac{-\pi\omega}{2\alpha}} \hat{\alpha}^{u,in\dagger}_{\omega,r} \right), \tag{2.77}$$

can be found.

2.2 Unruh and Hawking Radiation

The Unruh effect deals with uniformly accelerating noninertial observers in Minkowski spacetime, or equivalently said, with Quantum Field Theory in Rindler space. Rindler space represents part of Minkowski space. Then, a uniformly accelerating particle in its uniformly accelerating reference frame, in which it is at rest, undergoes hyperbolic motion [4, 5, 51]. One can always choose a Rindler frame (rest frame, see figure 2.5) for an observer's noninertial uniformly accelerating trajectory, $x^\mu(\tau)$, where τ is the proper time, such that $\ddot{x}^\mu \ddot{x}_\mu = -\alpha^2$, where α is the proper acceleration and the dots denote derivatives

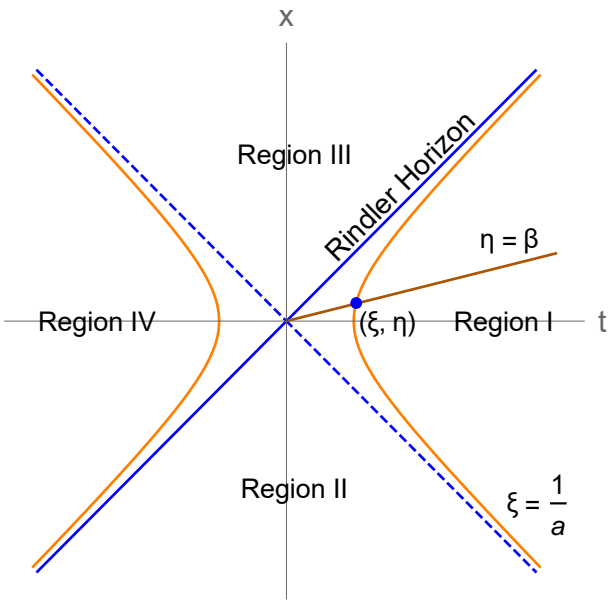

Figure 2.5: Minkowski diagram with the Rindler chart. Regions I and IV correspond to the right and left Rindler wedges and Regions II and III to the past future Rindler wedges. Lines of constant ξ correspond to the trajectories of accelerated (in Minkowski space) observers.

with respect to time. An example solution of this equation in a 1 + 1 dimensional space would be

$$t = \frac{1}{\alpha} sinh(\alpha\tau) \tag{2.78}$$

$$x = \frac{1}{\alpha} cosh(\alpha\tau). \tag{2.79}$$

The acceleration, α, is being treated here as a constant parameter. By taking the second proper time derivatives of $t(\tau)$ and $x(\tau)$, this parametrization can be simply verified.

Furthermore, it can be seen that $x^2 - t^2 = \frac{1}{\alpha^2}$ and that the particle indeed follows a hyperbolic motion. The lines $x = t$ represent the horizon for our observer and the region $x \leq t$ is forbidden to the Rindler observer. The observers can lie in one of the 4 regions of Minkowski spacetime, called 'wedges', depending on the sign of their acceleration. These 4 regions are disconnected with each other and observers in different regions cannot communicate with each other. Now, Equations 2.78 and 2.79 can be transformed into the right Ringler wedge coordinates, (η, ξ), as

$$t = \frac{1}{\alpha} e^{\alpha\xi} sinh(\alpha\eta), \tag{2.80}$$

$$x = \frac{1}{\alpha} e^{\alpha\xi} cosh(\alpha\eta). \tag{2.81}$$

The metric in these coordinates becomes

$$ds^2 = e^{2\alpha\xi}(d\eta^2 - d\xi^2), \tag{2.82}$$

which is independent of η. Thus, $\frac{\partial}{\partial \eta}$ is a Killing field. Analogously, one could have used a set of coordinates for the left Rindler wedge by taking the opposite signs in the previous calculation.

After a lengthy calculation, which can be viewed in Appendix B, it can be proven that an observer in Rindler space sees a thermal distribution. One can equally say that this observer is immersed in a thermal bath of particles. The thermal distribution will be of the form (see Equation B.23)

$$|B|^2 = \frac{1}{e^{2\pi\omega/\alpha - 1}} \tag{2.83}$$

with a temperature (see Equation B.24),

$$k_B T = \frac{\hbar \alpha}{2\pi c}. \tag{2.84}$$

At this point, it is of interest to mention that, for a parametric amplifier, there indeed exists a temperature of the same kind as above, but each amplified mode has a temperature of its own. Here, the whole electromagnetic spectrum has the same temperature. The temperature equation, Equation B.24, is universal and depends only on the acceleration of the observer and on natural constants. It is incredibly small, as in order to achieve room temperature, an acceleration of the order of 10^{22} times the gravitational acceleration on Earth needs to be imposed. With this result, the derivation of the Unruh effect is concluded, as the relation between accelerating observers and the number of particles observed in Minkowski vacuum has been established. Thus, the Unruh effect is defined by the fact that the usual vacuum state for Quantum Field Theory in Minkowski spacetime, restricted to the right Rindler wedge, is a thermal state with τ playing the role of time and similarly for the left Rindler wedge [46, 52]. As a result, creation of radiation out of 'nothing' is not just a possibility, but a necessity in uniformly accelerating systems.

After obtaining the results concerning Unruh radiation, its interpretation can now be explored. The major question concerns the nature of the quantum vacuum and how an accelerated object emits thermal radiation. For this, one can consider an inertial frame of empty Minkowski spacetime, where the accelerated observer seems to be emitting photon pairs. In this inertial frame, the momenta of the photons are of opposite value, something which is no longer true for the accelerating frame (Rindler frame), due to the Doppler effect. The reason for the emitted radiation is the quantum friction that is produced due to the momentum imbalance. This is an outstanding result, as the quantum friction obviously depends only on the acceleration and not on the velocity. Another important application of this effect deals with two accelerating observers having opposite accelerations. Being on conjugate Rindler wedges (in the positive and negative one, respectively), they independently feel the Minkowski vacuum as thermal radiation. But the most astonishing fact comes from the nature of the photons that the two accelerating observers detect; they always find them correlated with each other. Apparent random events caused by the quantum vacuum have been correlated across space, signalling their entanglement [50]. The two partner-photons that appear to be correlated are in two different Rindler wedges, being separated by a horizon.

Let us now move to the description of Hawking radiation in the simplest possible relativistic framework, the spherically symmetric black hole. In this approach, the black hole's spacetime will be described like a moving medium and a strict and heavy mathematical formulation will be avoided. It is also important to notice that the derivation of the Hawking effect does not rely on Einstein's equations [11, 12]. It is a purely kinematic effect that was derived before the proliferation of Quantum Field Theory in Curved Spacetime. It only requires the existence of a Lorentzian metric and a horizon. No more details relevant to dynamical effects are necessary.

By conveying the kinematic nature of Hawking effect and by using Equation 2.76, one obtains

$$\left\langle n^{u,out}_{\omega,r} \right\rangle = \langle 0_{in}|\hat{\alpha}^{u,out\dagger}_{\omega,r}\hat{\alpha}^{u,out}_{\omega',r}|0_{in}\rangle\,, \tag{2.85}$$

which after substitution from Equation 2.76,

$$\langle 0_{in}|\frac{1}{\sqrt{2\sinh\left(\frac{\pi\omega}{\alpha}\right)2\sinh\left(\frac{\pi\omega'}{\alpha}\right)}}\left(e^{\frac{\pi\omega}{2\alpha}}\hat{\alpha}^{u,in\dagger}_{\omega,r}+e^{\frac{-\pi\omega}{2\alpha}}\hat{\alpha}^{u,in}_{\omega,l}\right)\left(e^{\frac{\pi\omega'}{2\alpha}}\hat{\alpha}^{u,in}_{\omega',r}+e^{\frac{-\pi\omega}{2\alpha}}\hat{\alpha}^{u,in\dagger}_{\omega',l}\right)|0_{in}\rangle\,, \tag{2.86}$$

becomes

$$\frac{1}{e^{\frac{2\pi\omega}{\alpha}}-1}\delta(\omega-\omega') \tag{2.87}$$

with α denoting the surface gravity. This form of thermal radiation is of a similar nature to Unruh radiation with spectral flux density (meaning the number of quasiparticles emitted per unit time per unit bandwidth) [26, 53, 54] found to be

$$\frac{\partial^2 N}{\partial t\partial\omega} = \frac{1}{2\pi}\frac{1}{e^{\frac{2\pi\omega}{\alpha}}-1}. \tag{2.88}$$

As emphasized in the previous section, outgoing creation operators come into $r-l$ pairs, signalling the strong correlation between the emitted particles on both sides of the horizon. In next chapters, we will reformulate this results, in its Analogue-Gravity version; vacuum excitations (quasiparticles) come into pairs, one is emitted in the subsonic and the other in the supersonic regime. Furthermore, the number of quasiparticles emitted on both sides is equal and the two regions are maximally entangled.

3 Bose-Einstein Condensation and Analogue Gravity

3.1 Bose-Einstein Condensates of dilute gases

Bose-Einstein Condensation (BEC), a phenomenon that was predicted by Einstein nearly a century ago, was experimentally observed in 1995. Bose gases, when cooled down near the absolute zero temperature, tend to condense to their ground state and form a new state of matter. The major boost in the field of Bose gases happened after their experimental realization. In the past twenty five years there has been an incredible increase in research related to them. Novel phenomena and experimental infrastructure, as well as specific techniques have improved, with new ones even being invented, in an unprecedented explosion of research related to cold gases [34, 35, 55].

In dealing with the weakly interacting Bose gas, one requires a description of the interactions of bosons in low temperatures. In this case, the dynamics of the single particle states are not going to fully define the general Hamiltonian problem. Their mean-field description will be derived, meaning that their interactions are mediated by a classical field with Gaussian fluctuations.

Consider normal-ordered bosonic field operators which interact via an instantaneous two-body potential $V(|\mathbf{x}-\mathbf{y}|)$, where x and y are the positions of the two bosons in the spherically symmetric potential term. The Hamiltonian that describes the system then reads

$$H = \int \mathrm{d}\mathbf{x}\, \hat{\Phi}^\dagger(\mathbf{x},t)\left(\frac{-\boldsymbol{\nabla}^2}{2m}\right)\hat{\Phi}(\mathbf{x},t) + \frac{1}{2}\int \mathrm{d}\mathbf{x}\,\mathrm{d}\mathbf{x}\, \hat{\Phi}^\dagger(\mathbf{x},t)\hat{\Phi}^\dagger(\mathbf{y},t)V(|\mathbf{x}-\mathbf{y}|)\,\hat{\Phi}(\mathbf{y},t)\hat{\Phi}(\mathbf{x},t) \tag{3.1}$$

with the bosonic commutation relation

$$\left[\hat{\Phi}(\mathbf{x},t), \hat{\Phi}^\dagger(\mathbf{x}',t)\right] = \delta(\mathbf{x}-\mathbf{x}'). \tag{3.2}$$

The integrations are taking place in 3 spatial dimensions and the quartic interaction term represents a density interaction term $\sim n(\mathbf{x})V(|\mathbf{x}-\mathbf{y}|)\,n(\mathbf{y})$, giving their mutual interaction energy contribution, with the factor of $1/2$ introduced to avoid double-counting.

In mean-field, $\hat{\Phi} \to \Phi$. In this case, the equation of motion would be

$$\left(i\partial_t + \frac{\boldsymbol{\nabla}^2}{2m} - \int \mathrm{d}\mathbf{y}\, V(|\mathbf{x}-\mathbf{y}|)\,\Phi^*(\mathbf{y},t)\Phi(\mathbf{y},t)\right)\Phi(\mathbf{x},t) = 0. \tag{3.3}$$

This is a non-linear Schrödinger equation, which can be solved for a given potential and initial and boundary conditions in any time and space domain. For a contact interaction potential type, the time-evolution of the macroscopic wavefunction in response to some excitation can be reduced to the Gross-Pitaevskii equation

$$\left(i\partial_t + \frac{\boldsymbol{\nabla}^2}{2m} - V_{ext} - g\left|\Phi(\mathbf{x},t)\right|^2\right)\Phi(\mathbf{x},t) = 0, \tag{3.4}$$

where $g = \frac{4\pi\hbar^2\alpha}{m}$ is the effective coupling constant of the contact interaction potential $V(\mathbf{x}-\mathbf{x}') = g\delta^{(3)}(\mathbf{x}-\mathbf{x}')$, which is spherically symmetric (s-wave scattering). Also included is the effect of an external potential, which is indispensable for systems in traps (where ultracold Bose gases are usually produced and studied)[1].

Returning to the operator problem, the total particle number conservation is now taken into account in the Hamiltonian formulation. Concurrently, moving to the momentum space using a Fourier transform gives[2]

$$\hat{\alpha}_{\mathbf{x}} = \frac{1}{V}\int \mathrm{d}\mathbf{x}\,\hat{\Phi}(\mathbf{x},t)e^{i\mathbf{x}\cdot\mathbf{x}} \tag{3.5}$$

$$V_{\mathbf{k}} = \int \mathrm{d}\mathbf{x}\,e^{i\mathbf{k}\cdot\mathbf{x}}V(\mathbf{x}). \tag{3.6}$$

The Hamiltonian, after some algebraic manipulations, becomes

$$\hat{K} = \hat{H} - \mu\hat{N} = \sum_{\mathbf{k}}\left(\epsilon_{\mathbf{k}} - \mu'\right)\hat{\alpha}^{\dagger}_{\mathbf{k}}\hat{\alpha}_{\mathbf{k}} + \frac{1}{2V}\sum_{\mathbf{k},\mathbf{k}',\mathbf{q}}\hat{\alpha}^{\dagger}_{\mathbf{k}-\mathbf{q}}\hat{\alpha}^{\dagger}_{\mathbf{k}'+\mathbf{q}}V_{\mathbf{q}}\hat{\alpha}_{\mathbf{k}}\hat{\alpha}_{\mathbf{k}'}, \tag{3.7}$$

where $\mu' = \mu - V(0)$ and V denotes the volume of the periodic box where the normalisation takes place.

The process that follows identifies quantum operators with mean-field values, with the addition of some weak quantum fluctuations. The aim is to describe the zero-temperature ground state of an interacting Bose gas. At sufficiently low temperatures, well below the BEC temperature, a macroscopic fraction of the atoms are accumulated into the single particle lowest energy state, described by the macroscopic wavefunction $|\Phi\rangle$. Assuming that the ground state will be occupied by N_0 bosons and that $N - N_0 \ll N$, where N is the total number of atoms and N_0 is the fraction of them which occupy the ground state of the system, one can assume that

$$\langle\Phi|\hat{\alpha}^{\dagger}_0\hat{\alpha}_0|\Phi\rangle = N_0 \tag{3.8}$$

and that the ground state is a coherent state

$$\hat{\alpha}_0\left|\Phi\right\rangle = \sqrt{N_0}\left|\Phi\right\rangle. \tag{3.9}$$

[1] In free space, one can set $V_{ext} = 0$

[2] Note that in this section, the symbol V denotes the volume normalization, the symbol V_{ext} denotes the external potential and the symbol $V(\mathbf{x})$ denotes the (contact) potential. In Section 3.2, the same symbol V will be encountered, indicating the background flow of superfluids. Furthermore, the lower-case letters u and v will be used in order to indicate the modes of the system, sometimes with an extra index for further specification.

This is a reasonable approximation for a weakly interacting Bose gas[3]. In this approach, it is assumed that the total particle number must be conserved.

Thus, in this coherent-state representation, $\hat{\alpha}_0$ can be replaced with $\hat{\alpha}_0 \to \sqrt{N_0}$. Next, one can assume all other occupation numbers to be small (for all higher energy states) and approximate the Hamiltonian 3.7 to $O\left(\hat{\alpha}^3_{\mathbf{x}\neq 0}\right)$. The resulting grand canonical Hamiltonian reads

$$K = K_{MF} + O\left(\hat{\alpha}^3_{\mathbf{x}\neq 0}\right) \tag{3.10}$$

with

$$\begin{aligned} K_{MF} = &\frac{1}{2}V_0 n_0 N_0 - \frac{1}{2}\sum_{\mathbf{k}\neq 0}(\epsilon_{\mathbf{k}} - \mu'_{\mathbf{k}}) - \mu N_0 \\ &+ \frac{1}{2}\sum_{\mathbf{k}\neq 0,\mathbf{k}'\neq 0}\begin{pmatrix}\hat{\alpha}^\dagger_{\mathbf{k}} & \hat{\alpha}_{-\mathbf{k}}\end{pmatrix}\begin{pmatrix}\mathcal{P}_{\mathbf{k},\mathbf{k}'} & \mathcal{M}_{\mathbf{k},-\mathbf{k}'} \\ -\mathcal{M}_{-\mathbf{k},\mathbf{k}'} & -\mathcal{P}_{-\mathbf{k},-\mathbf{k}'}\end{pmatrix}\begin{pmatrix}\hat{\alpha}_{\mathbf{k}'} \\ -\hat{\alpha}^\dagger_{\mathbf{k}'}\end{pmatrix}, \end{aligned} \tag{3.11}$$

where n is the number operator and

$$\mathcal{P}_{\mathbf{k},\mathbf{k}'} = (\epsilon_{\mathbf{k}} - \mu_{\mathbf{k}'})\,\delta_{\mathbf{k},\mathbf{k}'} \tag{3.12}$$

$$\mathcal{M}_{\mathbf{k},\mathbf{k}'} = -n_0 V_{\mathbf{k}} \delta_{\mathbf{k},-\mathbf{k}'} \tag{3.13}$$

with $\mu_{\mathbf{k}'} = \mu - n_0 V_0 - \frac{1}{2}n_0\,(V_{\mathbf{k}} + V_{-\mathbf{k}})$ and $n_0 = N_0/V$. It has also been assumed that the potential term is spherically symmetric, $V_{\mathbf{k}} = V_{-\mathbf{k}}$.

The goal is then to diagonalize the relation 3.11 for K_{MF}. For this reason, one can choose a linear transformation of the field operators, which preserves its bosonic-nature commutator and is usually called a *Bogoliubov transformation*.

Thus, a new set of bosonic operators is introduced, as well as the following notation

$$A_{\mathbf{k}} = \begin{pmatrix}\hat{\alpha}_{\mathbf{k}} \\ -\hat{\alpha}^\dagger_{\mathbf{k}}\end{pmatrix} \tag{3.14}$$

$$B_{\mathbf{k}} = \begin{pmatrix}\hat{b}_{\mathbf{k}} \\ -\hat{b}^\dagger_{\mathbf{k}}\end{pmatrix} \tag{3.15}$$

$$U_{\pm,\mathbf{k}} = \begin{pmatrix}u^*_{\mathbf{k}} & \pm v_{\mathbf{k}} \\ \pm v^*_{\mathbf{k}} & u_{\mathbf{k}}\end{pmatrix} \tag{3.16}$$

with

$$A_{\mathbf{k}} = U_{+,\mathbf{k}} B_{\mathbf{k}} \tag{3.17}$$

and the Pauli σ_3-matrix, $\sigma_3 = \begin{pmatrix}1 & 0 \\ 0 & -1\end{pmatrix}$ and $u_{\mathbf{k}}$ and $v_{\mathbf{k}}$ are in general complex functions. Due to the assumptions that the new basis functions need to obey bosonic commutation relations, similarly to the previous ones, the functions $u_{\mathbf{k}}$ and $v_{\mathbf{k}}$ then obey

$$|u_{\mathbf{k}}|^2 - |v_{\mathbf{k}}|^2 = 1. \tag{3.18}$$

[3]Although the assumption of a coherent state strictly constrains the phase and particle number operators.

In the new quasiparticle basis, the mean-field Hamiltonian can be rewritten as

$$K_{MF}^{(2)} = \frac{1}{2} \sum_{\mathbf{k}\neq 0, \mathbf{k}'\neq 0} \omega_{\mathbf{k}} \left(\hat{b}_{\mathbf{k}}^{\dagger} \hat{b}_{\mathbf{k}} + \hat{b}_{\mathbf{k}} \hat{b}_{\mathbf{k}}^{\dagger} \right), \tag{3.19}$$

if the *Bogoliubov-de Gennes equations*

$$\left(\begin{pmatrix} \mathcal{P}_{\mathbf{k},\mathbf{k}} & \mathcal{M}_{\mathbf{k},-\mathbf{k}} \\ -\mathcal{M}_{-\mathbf{k},\mathbf{k}} & -\mathcal{P}_{\mathbf{k},-\mathbf{k}} \end{pmatrix} - \omega_{\mathbf{k}} I \right) \begin{pmatrix} u_{\mathbf{k}}^{*} \\ v_{\mathbf{k}}^{*} \end{pmatrix} = 0, \tag{3.20}$$

are satisfied.

Returning to Equation 3.11 for the mean-field Hamiltonian, its final form can be written in the new basis as

$$K_{MF} = E_0 + \sum_{\mathbf{k}\neq 0} \omega_{\mathbf{k}} b_{\mathbf{k}}^{\dagger} b_{\mathbf{k}} \tag{3.21}$$

with ground state energy

$$E_0 = \left(-\mu + \frac{1}{2} n_0 V_0 \right) N_0 + \frac{1}{2} \sum_{\mathbf{k}\neq 0} \left(\omega_{\mathbf{k}} + \mu - n_0 \left(V_0 + V_{\mathbf{k}} \right) - \epsilon_{\mathbf{k}} \right). \tag{3.22}$$

The eigenvalue problem 3.20 leads to the dispersion profile of the excitations of the weakly interacting Bose gas, the *Bogoliubov dispersion relation*,

$$\omega_{\mathbf{k}} = \sqrt{\epsilon_{\mathbf{k}} \left(\epsilon_{\mathbf{k}} + 2 n_0 V_{\mathbf{k}} \right)}, \tag{3.23}$$

where $\epsilon_{\mathbf{k}} = \frac{\mathbf{k}^2}{2m}$. Then, the dispersion relation for $k \to 0$ and $k \to \infty$ approaches the limits

$$\omega_{\mathbf{x}} = \begin{cases} c|\mathbf{k}| & \text{when } k \to 0 \\ \frac{\mathbf{k}^2}{2m} & \text{when } k \to \infty \end{cases} \tag{3.24}$$

with $c = \sqrt{\frac{n_0 V_0}{m}}$ being the *speed of sound* which characterizes the propagation of low-lying excitations of the Bogoliubov spectrum (sound waves) and $\hbar = 1$. Note that the potential V for $V_{k=0}$ is $V_{k=0} = g$, notation that will be adopted from now on, indicating that particles interact only via s-wave scattering [34].

The vanishing of the gap for the weakly interacting Bose gas is a revelation of Goldstone's theorem, as the original $U(1)$ symmetry is spontaneously broken and a gapless mode appears in the spectrum [55].

3.2 An application of Analogue Gravity in atomic Bose-Einstein Condensates

This section will focus on the applications of weakly interacting Bose gases within the framework of Analogue Gravity. It will attempt to give a first application of the model example studied in the previous chapter within the framework of Bose gases.

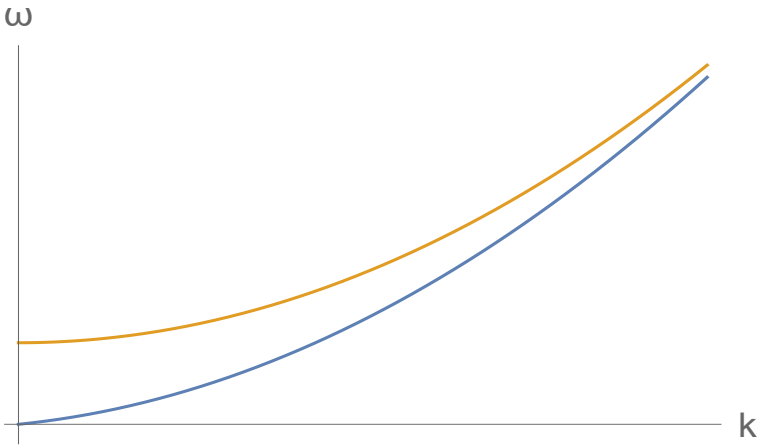

Figure 3.1: The dispersion relation of the Bose gas 3.24 for a one-dimensional system. The orange curve corresponds to the $k \to \infty$ limit of the Bogoliubov dispersion, which appears to be gapped, $n_0 V_{\mathbf{k}} + \frac{\mathbf{k}^2}{2m}$. The threshold between the two limits in Equation 3.24 is determined by the inverse healing length.

Consequently, starting from the Gross-Pitaevskii Equation, 3.4, one can perform the substitution to the density and phase representation, $\Phi = \sqrt{n}e^{i\theta}$, and obtain the equations

$$\partial_t n + \boldsymbol{\nabla} \cdot (n\mathbf{V}) = 0 \tag{3.25}$$

$$\partial_t \theta = -\mu = -\frac{1}{2m}(\boldsymbol{\nabla}\theta)^2 - ng - V_{ext} - V_q, \tag{3.26}$$

where $V_q = -\frac{1}{2m}\frac{\nabla^2\sqrt{n}}{\sqrt{n}}$ is the quantum pressure term, representing the 'stiffness' of the macroscopic wavefunction, and $\mathbf{V} = \frac{\boldsymbol{\nabla}\theta}{m}$ is the irrotational velocity of the condensate[4].

The density and phase representation in the Bogoliubov approximation

$$\hat{\Phi} = \sqrt{n_0 + \hat{n}_1}e^{i(\theta_0 + \hat{\theta}_1)} \tag{3.27}$$

is substituted into Equation 3.4. Then, the following equations can be similarly obtained

$$\partial_t \hat{\theta}_1 = -\mathbf{V} \cdot \boldsymbol{\nabla}\hat{\theta}_1 - \frac{mc^2}{n_0}\hat{n}_1 + \frac{mc^2}{4n_0}\xi^2 \boldsymbol{\nabla} \cdot \left(n_0 \boldsymbol{\nabla}\frac{\hat{n}_1}{n_0}\right) \tag{3.28}$$

$$\partial_t \hat{n}_1 = -\boldsymbol{\nabla} \cdot \left(\hat{n}_1 \mathbf{V} + \frac{n_0}{m}\boldsymbol{\nabla}\hat{\theta}_1\right), \tag{3.29}$$

where the definitions of the healing length, $\xi = \frac{1}{mc}$, and of the local speed of sound have been used[5]. The healing length gives us an approximate length where the condensate is 'healed'. It denotes the threshold where the dispersion relation is linear and behaves like

[4]Unless explicitly mentioned, $\hbar = 1$ will be used in the rest of this chapter.

[5]The healing length ξ should not be confused with the Rindler coordinate ξ used in last chapter. From now on, the symbol ξ will only indicate the healing length.

sound waves (excitations) and where it is quadratic [34]. If the hydrodynamic approximation is satisfied and the last term in Equation 3.29 can be neglected, Equations 3.28 and 3.29 decouple, giving the form for the density

$$\hat{n}_1 = -\frac{n_0}{mc^2}\left(\mathbf{V}\cdot\boldsymbol{\nabla}\hat{\theta}_1 + \partial_t\hat{\theta}_1\right) \Rightarrow \tag{3.30}$$

$$-\left(\partial_t + \boldsymbol{\nabla}\cdot\mathbf{V}\right)\frac{n_0}{mc^2}\left(\partial_t + \mathbf{V}\cdot\boldsymbol{\nabla}\right)\hat{\theta}_1 + \boldsymbol{\nabla}\cdot\left(\frac{n_0}{m}\boldsymbol{\nabla}\hat{\theta}_1\right) = 0, \tag{3.31}$$

which can be reformulated in a matrix form as

$$\partial_\mu\left(f^{\mu\nu}\partial_\nu\hat{\theta}_1\right) = 0, \tag{3.32}$$

with

$$f^{00} = -\frac{n_0}{c^2} \quad f^{0i} = f^{i0} = -\frac{n_0}{c^2}V^i \quad f^{ij} = \frac{n_0}{c^2}\left(c^2\delta^{ij} - V^iV^j\right), \tag{3.33}$$

in terms of the condensate density n and the local velocity V.

After defining Equation 3.32, it is straightforward to define the curved-space scalar d'Alembertian operator in any Lorentzian manifold as

$$\Box = \frac{1}{\sqrt{-g}}\partial_\mu\left(\sqrt{-g}g^{\mu\nu}\partial_\nu\right), \tag{3.34}$$

with $g_{\mu\nu}$ denoting the metric and $g^{\mu\nu}$ denoting its inverse. Then, Equation 3.32 can be rewritten as

$$\Box\hat{\theta}_1 = 0, \tag{3.35}$$

as long as $\sqrt{-g}g^{\mu\nu}$ is identified with the metric $f^{\mu\nu}$,

$$\sqrt{-g}g^{\mu\nu} = f^{\mu\nu}, \tag{3.36}$$

which leads to the effective metric for the BEC case

$$g_{\mu\nu} = \frac{n_0}{mc}\begin{pmatrix} -\left(c^2 - V^2\right) & -V^i \\ -V^j & \delta^{ij} \end{pmatrix}. \tag{3.37}$$

To this end, the Klein-Gordon equation for a massless scalar field propagating in a fictitious spacetime described by the metric $g_{\mu\nu}$ can be mapped onto the equation of motion for the phase fluctuations in a BEC under the hydrodynamic approximation. This is the fundamental result of the gravitational analogy between standard gravitational physics in a Lorentzian manifold and BECs under the hydrodynamic approximation. Otherwise, one can say that the hydrodynamic approximation restricts the dispersion relation only up to those values that the healing length allows. This means that only the linear part of the Bogoliubov spectrum, the sound waves, is dealt with.

Nevertheless, at this point many aspects need to be clarified or further explained. First of all, the general coordinate-transformation-invariance of Equation 3.35 is artificial, as

the real spacetime in which the BEC lives has nothing to do with the Lorentzian spacetime of a relativistic particle. The BEC theory is not invariant under general relativistic coordinate transformations. It is a Newtonian theory with an absolute time, the one of the laboratory frame.

Another special feature of this system, revealed through the metric equation, Equation 3.37, is realized when the flow goes from the normal subsonic case, $|\mathbf{V}| < c$ to supersonic, $|\mathbf{V}| > c$, through any process that can change the velocity of the fluid or the speed of sound. Between the two regions, the subsonic and the supersonic, an analogy with the gravitational system of the spherically symmetric black hole in Gullstrand-Painlevé coordinates can be made. When the velocity of the fluid is greater than the speed of sound, meaning that it enters the supersonic region, sound waves cannot propagate back to the subsonic region and are trapped inside the supersonic one. This is the analogy between the gravitational black hole and an analogue black hole in BECs. This *analogue* or *sonic* black hole possesses an analogue *horizon* where $|\mathbf{V}| = c$.

As a result, it can be seen that in the hydrodynamic approximation, results from the previous chapter, concerning the analysis of the massless scalar field, can be retrieved. But now the analogy is apparent. As a result, one can proceed as in the previous chapter, by obtaining the mode decomposition, finding the 'in' and 'out' vacuum states and showing their unequivalence under the non-trivial mixing of annihilation and creation operators by the Bogoliubov transformation. Finally, one can also obtain the spectrum of thermal radiation, the analogue of Hawking radiation, where the temperature of this blackbody radiation will again be given with respect to the surface gravity, κ, of the *sonic* horizon at the horizon surface:

$$\kappa = \frac{1}{2c}\frac{\mathrm{d}\left(c^2 - \mathbf{V}^2\right)}{\mathrm{d}n}\bigg|_{hor}. \tag{3.38}$$

All this procedure seems quite reasonable, even in the framework of BECs, but it is not quite exact. The hydrodynamic approximation being adopted in this section restricts the validity of the final result. Thus, the BEC framework needs to be re-evaluated in order to obtain an analogue Hawking effect without neglecting the large wavelength part of the spectrum through the hydrodynamic approximation.

3.3 An analogue Black Hole from BECs

In this section, the simplest model which can encode the gravitational analogy in a BEC system will be discussed. Furthermore, one-dimensional condensates with a steplike background profile for the speed of sound will be dealt with, meaning that the configuration in hand consists of two semi-infinite stationary and homogeneous condensates, as in Figure 2.1 for the analogue black hole or Figure 2.2 for the analogue white hole, where the two regions are connected by a steplike discontinuity.

Now, to further analyse the assumptions of the model, one can consider the Gross-Pitaevskii Equation 3.4, and deduce that the background quantities should satisfy

$$V^l_{ext} + n_0 g^l = V^r_{ext} + n_0 g^r, \tag{3.39}$$

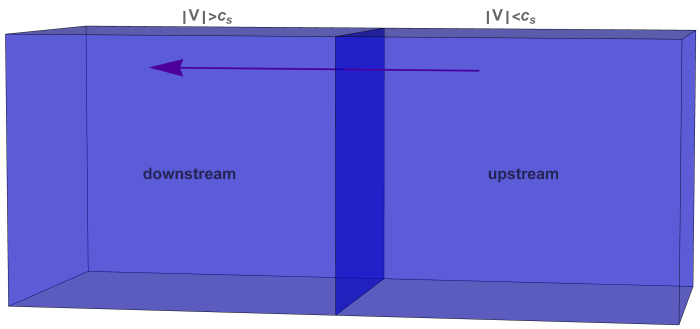

Figure 3.2: An illustration of an analogue black hole where the upstream region is subsonic and the downstream supersonic.

where it is assumed that the external potential and the coupling constant g take the same values across the whole semi-infinite space of its sector. This condition reflects the equality of local chemical potentials across the configuration. Furthermore, it is assumed that the discontinuity point is located at $x = 0$, thus the l-and r- indices reflect each side of the discontinuity (left and right, respectively). From Equation 3.39, the speed of sound across the horizon can be inferred,

$$c^{r/l} = \sqrt{\frac{n_0 g^{r/l}}{m}}. \tag{3.40}$$

Because of the chemical potential conservation relation 3.39, it can be deduced that the Gross-Pitaevskii Equation 3.4 has plane wave solutions of the form

$$\Phi_0 = \sqrt{n_0} e^{-i(\omega_0 t - k_0 x)} \tag{3.41}$$

in both semi-infinite domains. Then $V = \frac{k_0}{m}$ and $\omega_0 = k_0^2/2m + n_0 g$.

Let us now look at the Bogoliubov spectrum of our problem. As a result, the solution for the operator form of the Gross-Pitaevskii Equation 3.4 needs to be decomposed into a mean-field part and a part for the quantum fluctuations, which reduces to

$$\hat{\phi}(t, x) = \sum_j \left(\hat{\alpha}_j \phi_j + \hat{\alpha}_j^\dagger \varphi_j^* \right), \tag{3.42}$$

in the most general case, where the field responsible for quantum fluctuations around the mean-field solution, Φ_0, has been renamed as $\hat{\phi}$.

Operators $\hat{\alpha}_j$ and $\hat{\alpha}_j^\dagger$ represent bosonic creation and annihilation operators satisfying

$$\left[\hat{\alpha}_j, \hat{\alpha}_j^\dagger \right] = \delta_{ij}. \tag{3.43}$$

Introducing the decomposition of the total field

$$\hat{\Phi}(x, t) = \Phi_0(x, t) \left(1 + \hat{\phi}(x, t) \right) e^{-i\mu t}, \tag{3.44}$$

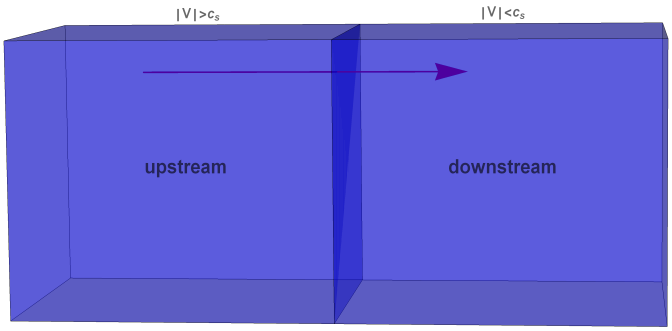

Figure 3.3: An illustration of an analogue white hole where the downstream region is subsonic and the upstream supersonic.

a set of coupled equations for the quantum field or, differently, the Bogoliubov-de Gennes equations,

$$i\frac{\mathrm{d}\hat{\phi}}{\mathrm{d}t} = -\left(\frac{\partial_x^2}{2m} + \frac{1}{m}\frac{\partial_x\Phi_0}{\Phi_0}\partial_x\right)\hat{\phi} + n_0 g(\hat{\phi} + \hat{\phi}^\dagger) \tag{3.45}$$

$$-i\frac{\mathrm{d}\hat{\phi}^\dagger}{\mathrm{d}t} = -\left(\frac{\partial_x^2}{2m} + \frac{1}{m}\frac{\partial_x\Phi_0}{\Phi_0}\partial_x\right)\hat{\phi}^\dagger + n_0 g(\hat{\phi}^\dagger + \hat{\phi}) \tag{3.46}$$

with $n_0 = |\Phi_0|^2$ can be obtained. By substitution of Equation 3.42, Relations 3.45 and 3.46 become

$$\left(\; i(\partial_t + V\partial_x) + \frac{\xi c}{2}\partial_x^2 - \frac{c}{\xi}\right)\phi_j = \frac{c}{\xi}\varphi_j \tag{3.47}$$

$$\left(-i(\partial_t + V\partial_x) + \frac{\xi c}{2}\partial_x^2 - \frac{c}{\xi}\right)\varphi_j = \frac{c}{\xi}\phi_j. \tag{3.48}$$

Due to the specific decomposition of the field, commutators of the following form

$$\left[\hat{\phi}(x,t), \hat{\phi}^\dagger(x',t)\right] = \frac{1}{n_0}\delta(x - x') \tag{3.49}$$

need to be imposed for the quantum fluctuating fields. Equation 3.49 gives for the mode normalization (or scalar product)

$$\int \mathrm{d}x \left(\phi_j \phi_{j'}^* - \varphi_j^* \varphi_{j'}\right) = \pm\frac{\delta_{jj'}}{n_0}. \tag{3.50}$$

Due to the chemical potential conservation equation, Equation 3.39, imposed at the start of this section, plane wave solutions for the Bogoliubov-de Gennes equations across the whole infinite space can be taken into account. As a result, the fields ϕ and φ can assume plane wave solutions of the form

$$\phi_\omega = D(\omega)e^{-i(\omega t - k(\omega)x)} \tag{3.51}$$

$$\varphi_\omega = E(\omega)e^{-i(\omega t - k(\omega)x)}. \tag{3.52}$$

After substituting in Equation 3.47, one obtains

$$\left((\omega - Vk) - \frac{\xi c k^2}{2} - \frac{c}{\xi} \right) D(\omega) = \frac{c}{\xi} E(\omega) \tag{3.53}$$

$$\left(-(\omega - Vk) - \frac{\xi c k^2}{2} - \frac{c}{\xi} \right) E(\omega) = \frac{c}{\xi} D(\omega). \tag{3.54}$$

This system, in order to have nontrivial solutions, needs to satisfy the relation

$$(\omega - Vk)^2 = c^2 \left(k^2 + \frac{\xi^2 k^4}{4} \right), \tag{3.55}$$

with the following dispersion relation

$$\omega = Vk \pm c \sqrt{k^2 + \frac{\xi^2 k^4}{4}}. \tag{3.56}$$

Following the notation given in the previous chapter, the frequency of the comoving frame is further introduced:

$$\Omega_{\pm} = \omega - V_o k = \pm c \sqrt{k^2 + \frac{\xi^2 k^4}{4}}. \tag{3.57}$$

Verifying the behaviour of this profile in the $k \to 0$ and $k \to \infty$ limits, one obtains

$$\omega = \begin{cases} (V \pm c)\, k, & \text{if } k \to 0 \\ \frac{c\xi k^2}{2}, & \text{if } k \to \infty. \end{cases} \tag{3.58}$$

Figures 3.4 and 3.5 represent the dispersion relation for an analogue black and white hole, respectively. Figures 3.6 and 3.8 indicate the different branches of the dispersion profile for an analogue black hole and 3.7 and 3.9 for an analogue white hole for the subsonic and the supersonic regimes, respectively. The dotted parts of the dispersion curves represent negative-norm modes.

The square root in Equation 3.57 consists of two terms. In the absence of the k^4 term, the standard hydrodynamic dispersionless profile is retrieved. This term, which is proportional to the healing length, introduces the dispersive effects in the model. This same term, however, introduces another useful terminology. When it renders the group velocity, V_{gr}, smaller that the speed of sound in the $k \to \infty$ limit, $|V_{gr}| < c$, then we speak of a *subluminal* dispersion relation while, as in our case, the dispersive effects tend to increase the group velocity with increasing wavevector. This case is called *superluminal*. The real dispersion relation for BECs is always superluminal ($|V_{gr}| > c$ for $k \to \infty$).

Such a nonlinear dispersion relation limits the amount of blueshift occurring at the horizon. The existence of infinite-frequency modes is not any more a problem. However, this model needs still to predict the Hawking effect, something that will now be shown in the simplest of settings. Moreover, it can also be shown that thermal radiation emitted at late times from an analogue black hole is still predicted with the high-frequency details of the dispersion relation remain irrelevant to this procedure.

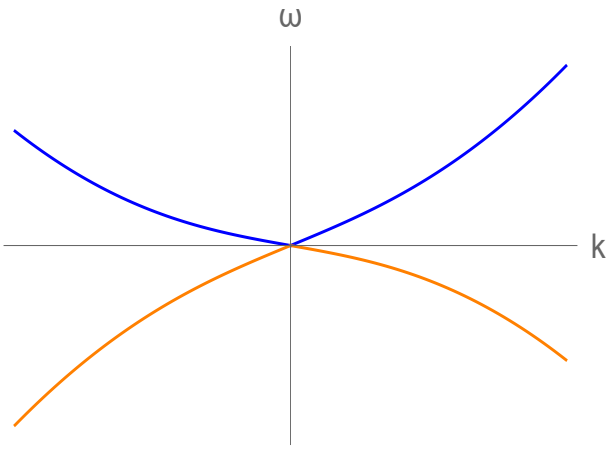

Figure 3.4: The dispersion relation for the subsonic regime of an analogue black hole.

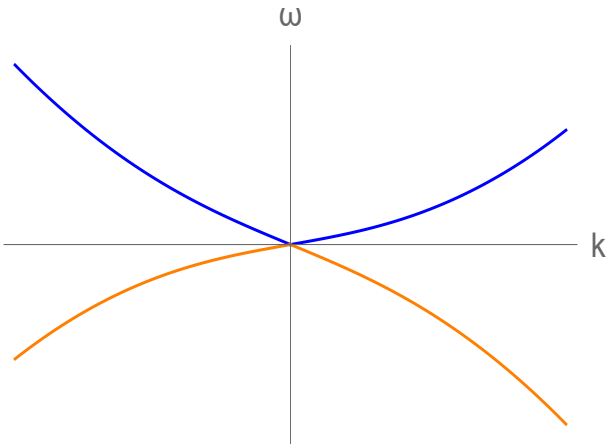

Figure 3.5: The dispersion relation for the subsonic regime of an analogue white hole.

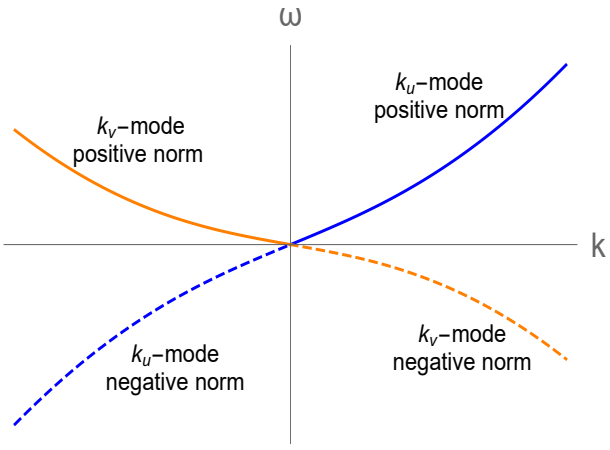

Figure 3.6: The four branches of the dispersion profile for an analogue black hole for background flows $V < 0$ with $|V| < c$.

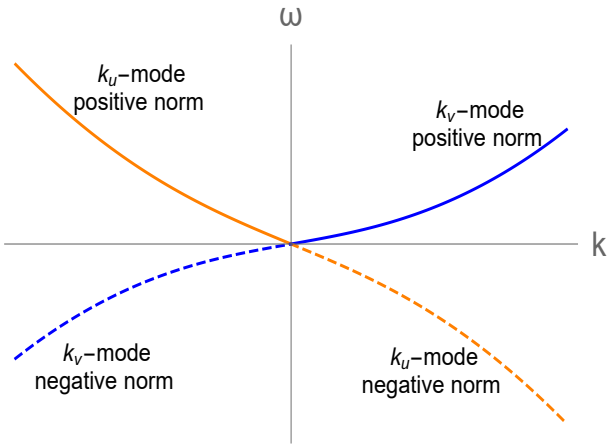

Figure 3.7: The four branches of the dispersion profile for an analogue white hole for background flows $V > 0$ with $|V| < c$. The branches of the analogue white hole follow from the analogue black hole's ones by $V \to -V$ and $k \to -k$.

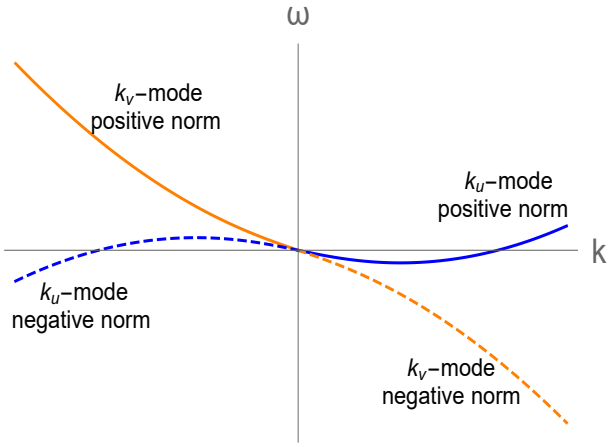

Figure 3.8: The four branches of the dispersion profile for an analogue black hole for background flows $V < 0$ with $|V| > c$.

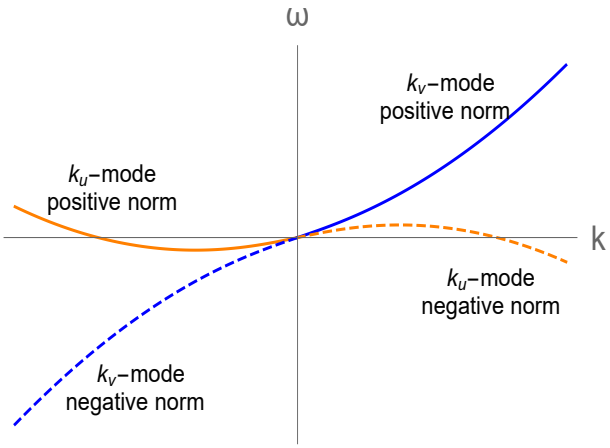

Figure 3.9: The four branches of the dispersion profile for an analogue white hole for background flows $V > 0$ with $|V| > c$.

In the hydrodynamic regime, meaning when $k \to 0$, a linear dispersion profile is obtained, which verifies the initial analogy made with the massless scalar field in Chapter 2. These modes correspond to sound waves in the BEC terminology. For $k \to \infty$, one obtains a quadratic profile in Equation 3.58, when considering the Bogoliubov dispersion relation for BECs (interacting bosonic particles).

Let us return now to find the eigenfunctions of our simple system. The normalization condition when considering the previous advancements can be rephrased as

$$|D(\omega)|^2 - |E(\omega)|^2 = \pm \frac{1}{2\pi n_0} \left| \frac{\mathrm{d}k}{\mathrm{d}\omega} \right|. \tag{3.59}$$

Then, from Equation 3.53, one attains

$$\left.\begin{aligned} \left(\omega - Vk - \tfrac{\xi c k^2}{2}\right) D(\omega) &= \tfrac{c}{\xi} \left(D(\omega) + E(\omega)\right) \\ -\left(\omega - Vk + \tfrac{\xi c k^2}{2}\right) E(\omega) &= \tfrac{c}{\xi} \left(D(\omega) + E(\omega)\right) \end{aligned}\right\} \Rightarrow \tag{3.60}$$

$$\begin{aligned} &\Rightarrow \left(\omega - Vk - \frac{\xi c k^2}{2}\right) D(\omega) = -\left(\omega - Vk + \frac{\xi c k^2}{2}\right) E(\omega) \Rightarrow \\ &\Rightarrow |D(\omega)|^2 - |E(\omega)|^2 = |D(\omega)|^2 \left(1 - \left(\frac{\omega - Vk - \frac{\xi c k^2}{2}}{\omega - Vk + \frac{\xi c k^2}{2}}\right)^2\right) \\ &= |D(\omega)|^2 \frac{2\xi c k^2 (\omega - Vk)}{\left(\omega - Vk + \frac{\xi c k^2}{2}\right)^2} = \pm \frac{1}{2\pi n_0} \left| \frac{\mathrm{d}k}{\mathrm{d}\omega} \right|, \end{aligned} \tag{3.61}$$

which reduces to

$$D(\omega) = \frac{\omega - Vk + \frac{c\xi k^2}{2}}{\sqrt{4\pi n_0 c\xi k^2 \left|(\omega - Vk)\left(\frac{\mathrm{d}k}{\mathrm{d}\omega}\right)^{-1}\right|}} \tag{3.62}$$

$$E(\omega) = -\frac{\omega - Vk - \frac{c\xi k^2}{2}}{\sqrt{4\pi n_0 c\xi k^2 \left|(\omega - Vk)\left(\frac{\mathrm{d}k}{\mathrm{d}\omega}\right)^{-1}\right|}}. \tag{3.63}$$

The mode-description of the system follows. From Equation 3.59, it is obvious that the sign of the normalization defines positive or negative-norm modes respectively, as positive or negative-norm modes correspond to those branches of the dispersion relation with positive or negative comoving frequency, as in the massless scalar field case (see Chapter 2). Any positive-norm branch with frequency ω and wavevector k has its parter negative-norm mode with frequency $-\omega$ and wavevector $-k$. The existing duality between these set of modes can be used to transform the normalization condition in ω-space:

$$\int_0^\infty \mathrm{d}\omega \left(\phi_\omega \phi^*_{\omega'} - \varphi^*_\omega \varphi_{\omega'}\right) = \pm \frac{\delta_{\omega\omega'}}{n_0}. \tag{3.64}$$

Let us take advantage of this simplification and work only on the $\omega > 0$ region of infinite space, as the same arguments will hold for negative-frequencies as well. In this specific case, it is assumed that the background velocity, V, is everywhere constant and the sound speed is step-discontinuous, $c = \Theta(x)c^r + \Theta(-x)c^l$, with $\Theta(x)$ the Heaviside step function. As discussed in the previous section, the k-representation can be used. As a result, by solving the dispersion relation, Equation 3.56, with respect to k, one can find the 4 k-roots. Then, the quantum fluctuating field can be written as a sum over these plane wave solutions

$$\phi_\omega(x,t) = e^{-i\omega t} \sum_{i=1}^{4} A_i^{(\omega)} D_i(\omega) e^{ik_i(\omega)x} \tag{3.65}$$

$$\varphi_\omega(x,t) = e^{-i\omega t} \sum_{i=1}^{4} A_i^{(\omega)} E_i(\omega) e^{ik_i(\omega)x}, \tag{3.66}$$

where $A_i^{(\omega)}$ are the amplitudes of the modes and $D(\omega)$ and $E(\omega)$ their normalizations, obtained in Equations 3.62 and 3.63.

The next step consists in finding the amplitudes of the modes, but, for this, the explicit form of the 4 $k_i(\omega)$ solutions is needed. An approximate analytical treatment for many of the following calculations will be used (see Figures 3.10 and 3.12 for the visualization of the k-solutions for the subsonic and supersonic regions of the analogue black hole configuration)[6].

[6]The system could equally well be described only by a numerical treatment, without any analytical approximation, but we believe that the elegance and meaning of the resulting equations is in this way better exposed and conceptually understood

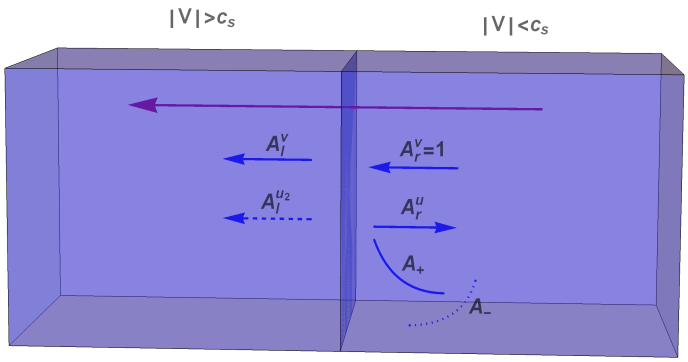

Figure 3.10: The BEC flow for an analogue black hole with the modes in each sector depicted, by assuming an ingoing v-mode in the upstream region.

The mode decomposition in the analogue black hole setting is illustrated in Figure 3.10 and further explained below. Then, the modes are decomposed in the in-going basis for the analogue black hole configuration, as in Figure 3.14[7]. The velocity of the background flow is assumed to be constant everywhere, as depicted in Figure 3.10 and the speed of sound varies from c^r to c^l, by going from the subsonic to the supersonic regime. The coupling constant also varies, $g^{r/l}$, as well as the healing length, $\xi^{r/l}$. The supersonic region is located downstream, the horizon is located at $x = 0$ and the subsonic region is located upstream.

In the subsonic region, as also shown in Figure 3.11, for any constant frequency ω_0, two real solutions for the dispersion curves exist, which belong to the positive-norm branch for $\omega_0 > 0$ and to the negative-norm branch for $\omega_0 < 0$. The k_u mode has positive group velocity, $V_{gr} > 0$, and propagates *against* the fluid, while the k_v mode propagates *with* the fluid flow and thus has negative group velocity, $V_{gr} < 0$. The u/v labels are used in the same way as in Chapter 2. These two modes constitute the hydrodynamic modes.

An approximate form for the k-solutions of these modes for $\omega \to 0$ (or, equally, find a series expansion with respect to the dimensionless variable $z = \frac{\xi\omega}{c}$) will now be found. The dispersion relation equation, Equation 3.56, or equally Equation 3.55, can be written

[7]The field could be equally well expanded in the outgoing basis. Then, results would follow in a similar way for the two approaches, without however the later being identical, due to the horizon occurrence (for more details, see Chapter 2). More details concerning the discontinuous subsonic flow can be found in [56–58]. In this case, where no horizon has formed, the ingoing- and the outgoing-basis treatments are identical.

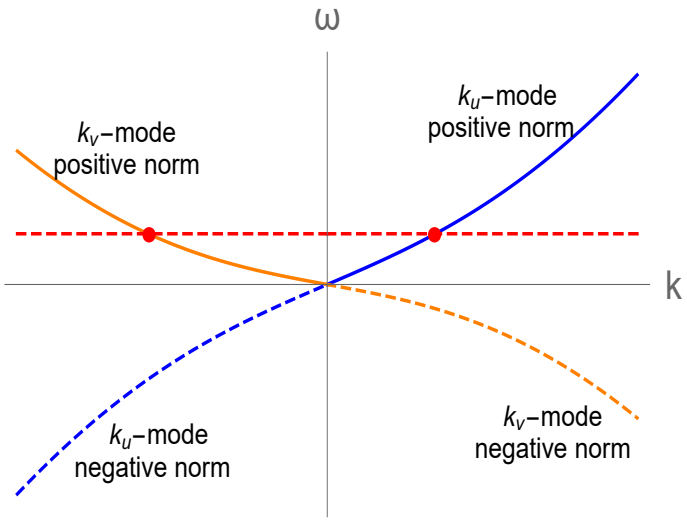

Figure 3.11: The two real k-solutions found for a given frequency are found by the 2 crossings of a specific energy scale, say ω_0, with the dispersion profile. At the same time, the other 2 solutions are complex.

as

$$(\omega - Vk)^2 = c^2\left(k^2 + \frac{\xi^2 k^4}{4}\right) \Rightarrow \frac{c^2\xi^2 k^4}{4} + (c^2 - V^2)k^2 + 2V\omega k - \omega^2 = 0 \Rightarrow$$
$$z^2c^4k^4 + 4\omega^2(c^2 - V^2)k^2 + 8V\omega^3 k - 4\omega^4 = 0 \tag{3.67}$$

For z: small

$$(c^2 - V^2)k_0^2 + 2V\omega k_0 - \omega^2 = 0 \Rightarrow k_0 = \frac{\omega}{V \pm c}, \tag{3.68}$$

Then Equation 3.56 becomes

$$\omega - Vk = \pm ck\sqrt{1 + \frac{z^2c^2k^2}{4\omega^2}} \simeq \pm ck\left(1 + \frac{z^2c^2k^2}{8\omega^2}\right) \Rightarrow$$
$$k_1 = \frac{\omega}{V \pm c\left(1 + \frac{z^2c^2k^2}{8\omega^2}\right)} = \frac{\omega}{V \pm c}\frac{1}{1 \pm \frac{1}{8}\frac{z^2c^3}{(V\pm c)^3}} \tag{3.69}$$

and one obtains

$$k_v = \frac{\omega}{V - c_r}\left(1 + \frac{c_r^3 z^2}{8(V - c_r)^3} + O(z^4)\right) \tag{3.70}$$

$$k_u = \frac{\omega}{V + c_r}\left(1 - \frac{c_r^3 z^2}{8(V + c_r)^3} + O(z^4)\right). \tag{3.71}$$

In the first approximation, the hydrodynamic approximation for the k_v and k_u modes can be verified, based on results from Chapter 2. By including terms of higher order, corrections to the hydrodynamic results are obtained.

By this simple iterative method only the first two real solutions of the fourth order algebraic equation can be found. It is assumed that z is small and, obviously, relation 3.67 leads to the neglect of the fourth order terms. Somehow these terms need to be included as well. This is done by considering singular perturbation theory techniques [59, 60]. These two terms are found as follows. When the fourth order terms are neglected, the previous two equations follow with their solutions found in Equations 3.70-3.71 . As a result, these neglected terms are now indispensable to find the other two solutions as well. By assuming that the fourth order term is big enough and cannot be neglected, the k value needs to be big enough. If the k value is big enough then, the term $2V\omega k$ needs to be much bigger than the constant-in-k term, $4\omega^4$. Thus, this term can be neglected and one can obtain

$$\frac{z^2c^4k^4}{4\omega^2} + (c^2 - V^2)k^2 + 2V\omega k = 0 \Rightarrow k \neq 0 \Rightarrow \tag{3.72}$$

$$\Rightarrow \quad \frac{z^2c^4k^3}{4\omega^2} + (c^2 - V^2)k + 2V\omega = 0 \Rightarrow z^2c^4k^2 + 4\omega^2(c^2 - V^2) = 0. \tag{3.73}$$

For the subsonic case,

$$k_0 = \pm\frac{2i\omega}{zc^2}\sqrt{V^2 - c^2} \tag{3.74}$$

and Equation 3.67 can be written in a form convenient for this purpose:

$$k = \frac{4\omega^4}{z^2c^4k^3} - \frac{8V\omega^3}{z^2c^4k^2} - \frac{4\omega^2(c^2 - V^2)}{z^2c^4k}. \tag{3.75}$$

By using this last equation iteratively and the value of Equation 3.74 obtained earlier, one finds that

$$k_1 = \frac{\omega V}{c^2 - V^2} \pm \frac{2i\sqrt{c^2 - V^2}}{c\xi}\left(1 + \frac{z^2c^4}{4(V^2 - c^2)^4}\right). \tag{3.76}$$

Going to second order in 3.55, the final form of the expansions is found to be

$$k_\pm = \frac{\omega V}{c_r^2 - V^2}\left(1 - \frac{(c_r^2 + V^2)c_r^4z^2}{4(c_r^2 - V^2)^3} + O\left(z^4\right)\right) \pm \frac{2i\sqrt{c_r^2 - V^2}}{c_r\xi}\left(1 + \frac{(c_r^2 + 2V^2)c_r^4z^2}{8(c_r^2 - V^2)^3} + O\left(z^4\right)\right). \tag{3.77}$$

Of course, the fact that only two real solutions could be found indicates that the other two should be a complex conjugate pair, due to the real character of Equation 3.67. These solutions correspond to a positive-imaginary-part solution, representing a decaying mode as $k \to \infty$, k_+, and a negative-imaginary-part mode which represents a growing as $k \to \infty$ mode, k_-. This last mode will be excluded from the procedure of finding the amplitude coefficients of the quantum fields in both the subsonic and the supersonic regime, as it is not square-integrable.

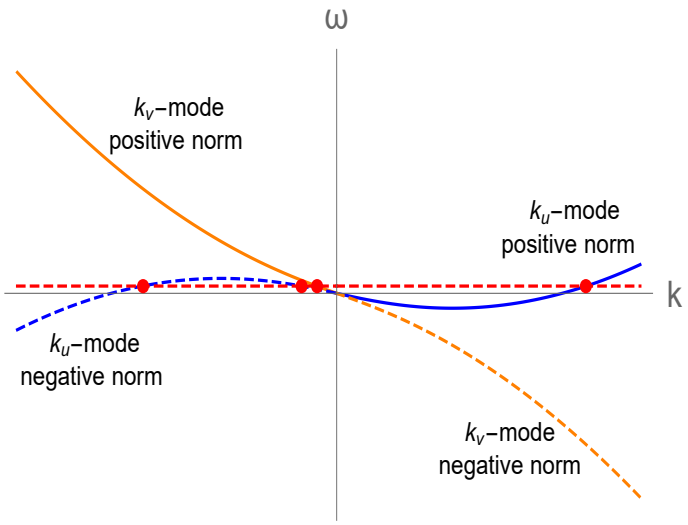

Figure 3.12: The four solutions for a given frequency $\omega_0 < \omega_{max}$ are shown together with the dispersion profile of the supersonic regime. At the same time, above this threshold, the situation resembles the subsonic case where two real modes can be found and other two become complex conjugates.

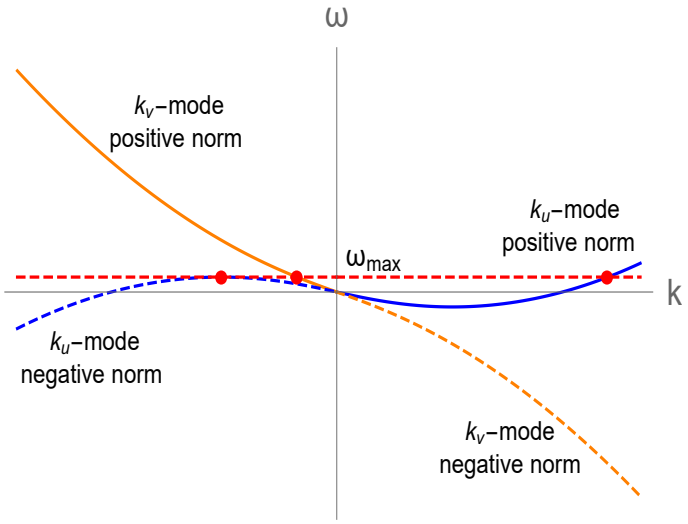

Figure 3.13: The three solutions for a given energy at the threshold frequency, $\omega_0 = \omega_{max}$. The most negative solution is of multiplicity two. As the energy of the system increases for ω_0, the two most negative solutions of the u-branch merge into one at the threshold. For $\omega_0 > \omega_{max}$, the situation resembles the subsonic regime.

In the supersonic region, there are four real solutions for each ω_0 solution up to a maximum frequency ω_{max}, as seen from Figure 3.12. When $\omega_0 > \omega_{max}$, the situation resembles the subsonic case, as there are again two real and two complex solutions. The complex solutions are the ones represented in Equation 3.77. The two real ones consist of one mode propagating with the fluid flow, the v-mode, and one counterpropagating to the fluid flow, the u-mode. It is of interest to note that the mode propagating against the fluid is non-hydrodynamic and is not affected by the nature of the sonic horizon. The threshold frequency ω_{max} is given by the maximum frequency of the negative-norm Bogoliubov mode,

$$\omega_{max} = 2\sqrt{2}\sqrt{|V| + \sqrt{V^2 + 8c_l^2}}\left(\frac{V^2 - c_l^2}{3|V| + \sqrt{V^2 + 8c_l^2}}\right)^{3/2}, \tag{3.78}$$

with c_l the speed of sound in the downstream supersonic region. This phenomenon is shown in Figure 3.12. The two hydrodynamic modes are

$$k_v = \frac{\omega}{V - c_l}\left(1 + \frac{c_l^3 z^2}{8(V - c_l)^3} + O(z^4)\right) \tag{3.79}$$

$$k_{u_2} = \frac{\omega}{V + c_l}\left(1 - \frac{c_l^3 z^2}{8(V + c_l)^3} + O(z^4)\right). \tag{3.80}$$

The crucial difference in this case lies in the nature of the velocity profile and the speed of sound; in the supersonic region, $|V| > c_l$, and thus both modes of the negative-norm u-branch (the u_1- and u_2-modes) have a negative group velocity $V_{gr} < 0$ together with the positive-norm v-mode. These three modes propagate with the background fluid flow, despite the general *counterflow*-character of the u_2-mode. The v-mode, as before, propagates *with* the fluid flow, but the nature of the u-branch-modes has changed. The hydrodynamic u_2-mode now belongs to the *negative* norm branch of the dispersion profile and it is dragged by the flow. The energy carried by that modes is positive despite belonging to the negative-norm sector. The wavevector of the two u- and u_1-modes is nonperturbative in z and found to be

$$k_{u,u_1} = \frac{\omega V}{c_l^2 - V^2}\left(1 - \frac{(c_l^2 + V^2)c_l^4 z^2}{4(c_l^2 - V^2)^3} + O(z^4)\right) \pm \frac{2\sqrt{V^2 - c_l^2}}{c_r \xi}\left(1 + \frac{(c_l^2 + 2V^2)c_l^4 z^4}{8(c_l^2 - V^2)^3} + O(z^4)\right). \tag{3.81}$$

These solutions are analytic continuation of the solutions in Equation 3.77.The k_u mode belongs to the positive-norm sector and has a positive group velocity. The k_{u_1} root has positive group velocity as well, but it belongs to the negative-norm sector.

After this detailed analysis on the decomposition of the modes for the subsonic and the

supersonic flow, the quantum field in each region can finally be written as

$$\phi^l_\omega = e^{-i\omega t}\left(A^l_v D^l_v e^{ik^l_v x} + A^l_u D^l_u e^{ik^l_u x} + A^l_{u_1} D^l_{u_1} e^{ik^l_{u_1} x} + A^l_{u_2} D^l_{u_2} e^{ik^l_{u_2} x}\right) \tag{3.82}$$

$$\varphi^l_\omega = e^{-i\omega t}\left(A^l_v E^l_v e^{ik^l_v x} + A^l_u E^l_u e^{ik^l_u x} + A^l_{u_1} E^l_{u_1} e^{ik^l_{u_1} x} + A^l_{u_2} E^l_{u_2} e^{ik^l_{u_2} x}\right) \tag{3.83}$$

$$\phi^r_\omega = e^{-i\omega t}\left(A^r_v D^r_v e^{ik^r_v x} + A^r_u D^r_u e^{ik^r_u x} + A^r_+ D^r_+ e^{ik^r_+ x} + A^r_- D^r_- e^{ik^r_- x}\right) \tag{3.84}$$

$$\varphi^r_\omega = e^{-i\omega t}\left(A^r_v E^r_v e^{ik^r_v x} + A^r_u E^r_u e^{ik^r_u x} + A^r_+ E^r_+ e^{ik^r_+ x} + A^r_- E^r_- e^{ik^r_- x}\right) \tag{3.85}$$

in each region respectively.

Now, the amplitudes in the last four equations can be found. In the configuration in hand, there is a steplike discontinuity at the horizon. At that point, continuity of the field and its first derivative must be imposed. As a result, one needs to impose the conditions

$$\lim_{\epsilon\to 0}\left(\phi(x+\epsilon) - \phi(x-\epsilon)\right) = 0 \tag{3.86}$$

$$\lim_{\epsilon\to 0}\left(\varphi(x+\epsilon) - \varphi(x-\epsilon)\right) = 0 \tag{3.87}$$

$$\lim_{\epsilon\to 0}\left(\left.\frac{\mathrm{d}\phi}{\mathrm{d}x}\right|_{x+\epsilon} - \left.\frac{\mathrm{d}\phi}{\mathrm{d}x}\right|_{x-\epsilon}\right) = 0 \tag{3.88}$$

$$\lim_{\epsilon\to 0}\left(\left.\frac{\mathrm{d}\varphi}{\mathrm{d}x}\right|_{x+\epsilon} - \left.\frac{\mathrm{d}\varphi}{\mathrm{d}x}\right|_{x-\epsilon}\right) = 0. \tag{3.89}$$

These four conditions lead to a system of four equations with the respect to the four unknown amplitudes in each one of them. This system can be rewritten in a matrix form

$$A^l_i = M_{ij} A^r_j, \tag{3.90}$$

where M is the *matching* matrix. Its explicit form comes from the matching across the horizon relations,

$$W_l \begin{pmatrix} A^l_v \\ A^l_{u_2} \\ A^l_u \\ A^l_{u_1} \end{pmatrix} = W_r \begin{pmatrix} A^r_v \\ A^r_u \\ A^r_+ \\ A^r_- \end{pmatrix}, \tag{3.91}$$

with

$$W_{l/r} = \begin{pmatrix} D^{l/r}_v & D^{l/r}_{u_2/u} & D^{l/r}_{u/+} & D^{l/r}_{u_1/-} \\ ik^{l/r}_v D^{l/r}_v & ik^{l/r}_{u_2/u} D^{l/r}_{u_2/u} & ik^{l/r}_{u/+} D^{l/r}_{u/+} & ik^{l/r}_{u_1/-} D^{l/r}_{u_1/-} \\ E^{l/r}_v & E^{l/r}_{u_2/u} & E^{l/r}_{u/+} & E^{l/r}_{u_1/-} \\ ik^{l/r}_v E^{l/r}_v & ik^{l/r}_{u_2/u} E^{l/r}_{u_2/u} & ik^{l/r}_{u/+} E^{l/r}_{u/+} & ik^{l/r}_{u_1/-} E^{l/r}_{u_1/-} \end{pmatrix} \tag{3.92}$$

and its final form is given by

$$M = W_l^{-1} W_r. \tag{3.93}$$

3.3.1 Scattering decomposition

In order to find the scattering coefficients of the steplike configuration in hand, the modes need to be decomposed into a basis that will be complete and orthonormal. As previously, either the 'in'- or the 'out'-basis can be chosen. In the subsonic case, the u- and v-modes and the decaying mode are taken into account, while for the supersonic region all modes need to be taken into account. The modes in the 'in'-basis need to be expressed in terms of the modes in the 'out'-basis[8]. After the amplitude coefficients for the field are expanded in a specific basis, the explicit form of the quantized field can be constructed and the elements of the scattering matrix be found. Energies with $\omega < \omega_{max}$ for the supersonic region will only be taken into account[9].

The quantum fluctuating field can be decomposed in the 'in'-basis as

$$\phi = \int_0^{\omega_{max}} \mathrm{d}\omega \Big(\hat{\alpha}_\omega^{v,in} \phi_{v,r}^{in} + \hat{\alpha}_\omega^{u,in} \phi_{u,l}^{in} + \hat{\alpha}_\omega^{u_1,in\dagger} \phi_{u_1,l}^{in} + \hat{\alpha}_\omega^{v,in\dagger} \phi_{v,r}^{in,*} + \hat{\alpha}_\omega^{u,in\dagger} \phi_{u,l}^{in*} + \hat{\alpha}_\omega^{u_1,in} \phi_{u_1,l}^{in*} \Big). \tag{3.94}$$

It is important to note that the u_1-mode belongs to the negative-norm branch and thus needs to be complex conjugated with respect to the other modes. This is exactly the feature that is behind the Hawking radiation; the mixing of positive and negative-norm modes in the description of the field for the quantum fluctuations.

The corresponding amplitudes will now be found. By decomposing the modes with respect to the 'in'-basis, the exact form of the modes $\phi_{v,r}^{in}$, $\phi_{u,l}^{in}$ and $\phi_{u_1,l}^{in}$ is found. First, the mode $\phi_{v,r}^{in}$ is considered. It can be defined as of unit initial amplitude. It is flowing in the subsonic region with the fluid towards the horizon, coming from infinity. As this mode impinges on the horizon, a reflected $\phi_{u,r}^{out}$ mode will occur in the subsonic region, as well as a $\phi_{v,l}^{out}$ and a $\phi_{u_2,l}^{out,*}$ mode in the supersonic region. The $\phi_{u_2,l}^{out,*}$ mode is complex conjugated as was also done for the negative-norm mode in the quantization procedure of Chapter 2. Finally, the decaying mode, $\phi_{+,r}^{out}$, in the subsonic region is considered[10]. The matching conditions 3.86-3.89 for the specific mode will then give (see Figure 3.14 for the following analysis)

$$\begin{pmatrix} A_v^l \\ A_{u_2}^l \\ 0 \\ 0 \end{pmatrix} = M \begin{pmatrix} 1 \\ A_u^r \\ A_+^r \\ 0 \end{pmatrix}. \tag{3.95}$$

[8] we could also perform the same calculation but expressing the outgoing modes in the 'in'-basis. Both ways of dealing with the scattering coefficients will give the same taste of the problem, despite defining different vacuum states [57]. More details can also be found in Chapter 2

[9] For $\omega > \omega_{max}$, the nature of the scattering matrix will be completely different. Furthermore, the Hawking signal will be lost, indicating that the Hawking effect is influenced only by the low-frequency dispersion.

[10] This decaying mode will not be included in the scattering matrix decomposition (as it is not a propagating mode in the strict sense) of the field and the necessity of including it will only be revealed by the following matching matrix analysis

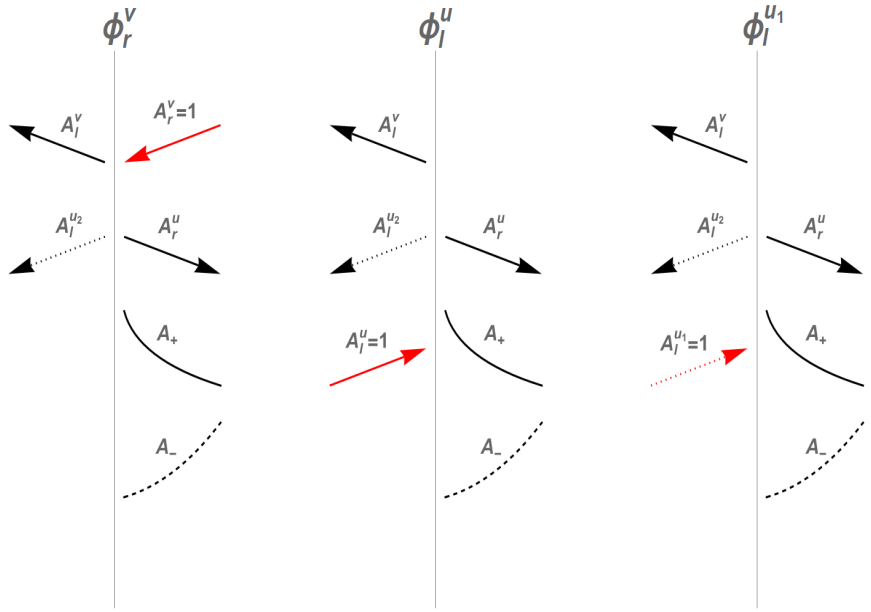

Figure 3.14: The modes of the analogue black hole in the ingoing basis. The mode depicted in red always corresponds to the unit amplitude ingoing mode and the A_- mode is dashed as it is always present, but not taken into account for the matching matrix analysis due to not being square-integrable. The dotted mode $A^l_{u_2}$ corresponds to the negative-norm mode.

Equally for the other two 'in'-modes, as shown in Figure 3.10, it is found that

$$\begin{pmatrix} A^l_v \\ A^l_{u_2} \\ 1 \\ 0 \end{pmatrix} = M \begin{pmatrix} 0 \\ A^r_u \\ A^r_+ \\ 0 \end{pmatrix} \tag{3.96}$$

and

$$\begin{pmatrix} A^l_v \\ A^l_{u_2} \\ 0 \\ 1 \end{pmatrix} = M \begin{pmatrix} 0 \\ A^r_v \\ A^r_+ \\ 0 \end{pmatrix}, \tag{3.97}$$

respectively[11].

These matrix equations can be solved numerically, but a 'glimpse' of the information included in them can also be extracted by using the previous approximation in the expansion of the k-roots. This time, only the leading order terms in z will be considered for

[11] Note the significance of the correct ordering of modes in each regime, $\left(A^l_v,\ A^l_{u_2},\ A^l_u,\ A^l_{u_1}\right)^\intercal$ for the supersonic regime and $(A^r_v,\ A^r_u,\ A^r_+,\ A^r_-)^\intercal$ for the subsonic one. The first two modes for both vectors correspond to the hydrodynamic modes, while the last two in the subsonic regime correspond to the complex conjugate pair. Its analytic continuation to the supersonic regime gives rise to the last two elements as well

simplicity. Then, the amplitudes are found to be

$$A_v^l = \sqrt{\frac{c_r}{c_l}}\frac{V-c_l}{V-c_r} = S_{vl,vr} \tag{3.98}$$

$$A_u^r = \frac{V+c^r}{V-c_r} = S_{ur,vr} \tag{3.99}$$

$$A_{u_2}^l = \sqrt{\frac{c_r}{c_l}}\frac{V+c_l}{c_r-V} = S_{u_2l,vr} \tag{3.100}$$

and

$$A_v^l = \frac{(V^2-c_l^2)^{3/4}(V+c^r)}{c_l^{3/2}\sqrt{2z_l}(c_l+c_r)\sqrt{c_r^2-V^2}}\left(\sqrt{c_r^2-V^2}+i\sqrt{V^2-c_l^2}\right) = S_{vl,ul} \tag{3.101}$$

$$A_u^r = \frac{\sqrt{2c_r}(V^2-c_l^2)^{3/4}(V+c^r)}{c_l\sqrt{z_l}(c_l+c_r)(c_r-c_l)\sqrt{c_r^2-V^2}}\left(\sqrt{c_r^2-V^2}+i\sqrt{V^2-c_l^2}\right) = S_{ur,ul} \tag{3.102}$$

$$A_{u_2}^l = \frac{(V^2-c_l^2)^{3/4}(V+c^r)}{c_l^{3/2}\sqrt{2z_l}(c_l-c_r)\sqrt{c_r^2-V^2}}\left(\sqrt{c_r^2-V^2}+i\sqrt{V^2-c_l^2}\right) = S_{u_2l,ul} \tag{3.103}$$

and

$$A_v^l = \frac{(V^2-c_l^2)^{3/4}(V+c^r)}{c_l^{3/2}\sqrt{2z_l}(c_l+c_r)\sqrt{c_r^2-V^2}}\left(\sqrt{c_r^2-V^2}-i\sqrt{V^2-c_l^2}\right) = S_{vl,u_1l} \tag{3.104}$$

$$A_u^r = \frac{\sqrt{2c_r}(V^2-c_l^2)^{3/4}(V+c^r)}{c_l\sqrt{z_l}(c_l+c_r)(c_r-c_l)\sqrt{c_r^2-V^2}}\left(\sqrt{c_r^2-V^2}-i\sqrt{V^2-c_l^2}\right) = S_{ur,u_1l} \tag{3.105}$$

$$A_{u_2}^l = \frac{(V^2-c_l^2)^{3/4}(V+c^r)}{c_l^{3/2}\sqrt{2z_l}(c_l-c_r)\sqrt{c_r^2-V^2}}\left(\sqrt{c_r^2-V^2}-i\sqrt{V^2-c_l^2}\right) = S_{ul,u_1l}, \tag{3.106}$$

respectively.

It is crucial to note that unitarity imposes the satisfaction of the identity

$$|A_v^l|^2 + |A_u^r|^2 - |A_{u_2}^l|^2 = 1 \tag{3.107}$$

by the first two relations 3.95 and 3.96. The negative sign in front of the $A_{u_2}^l$-mode is due to its negative norm. Respectively, the relation 3.97 satisfies the relation

$$|A_v^l|^2 + |A_u^r|^2 - |A_{u_2}^l|^2 = -1 \tag{3.108}$$

with the negative sign in the right part indicating the negative norm of the initial ingoing mode.

Now that the amplitudes of the modes have been found, the explicit form of the field decomposition 3.94 can be established. The Bogoliubov transformation of the field in the 'in'-basis in terms of the 'out'-basis can then be found to be

$$\begin{pmatrix}\phi_{v,r}^{in}\\ \phi_{u,l}^{in}\\ \phi_{u_1,l}^{in}\end{pmatrix} = \begin{pmatrix}S_{vl,vr} & S_{ur,vr} & S_{u_2l,vr}\\ S_{vl,ul} & S_{ur,ul} & S_{u_2l,ul}\\ S_{vl,u_1l} & S_{ur,u_1l} & S_{u_2l,u_1l}\end{pmatrix}\begin{pmatrix}\phi_{v,l}^{out}\\ \phi_{u,r}^{out}\\ \phi_{u_2,l}^{out}\end{pmatrix}. \tag{3.109}$$

The S-matrix of the transformation obeys the condition

$$S^{\dagger}\eta S = S\eta S^{\dagger}, \tag{3.110}$$

where $\eta = diag(1, 1, -1)$ [20, 58].

The above transformation 3.109 can also be expressed for the creation and annihilation operators, as done in Chapter 2, Equation 2.76,

$$\begin{pmatrix} \hat{\alpha}_{\omega}^{vl,out} \\ \hat{\alpha}_{\omega}^{ur,out} \\ \hat{\alpha}_{\omega}^{u_2l,out\dagger} \end{pmatrix} = \begin{pmatrix} S_{vl,vr} & S_{vl,u_1l} & S_{vl,ul} \\ S_{ur,vr} & S_{ur,u_1l} & S_{ur,ul} \\ S_{u_2l,vr} & S_{u_2l,u_1l} & S_{u_2l,ul} \end{pmatrix} \begin{pmatrix} \hat{\alpha}_{\omega}^{vr,in} \\ \hat{\alpha}_{\omega}^{u_1l,in} \\ \hat{\alpha}_{\omega}^{ul,in\dagger} \end{pmatrix}. \tag{3.111}$$

This mixing of positive and negative-norm modes is behind the form of the η-matrix[12]. Due to this nontriviality of the scattering matrix, the vacuum states of the 'in'- and 'out'-vacuum, $|0, in\rangle$ and $|0, out\rangle$, are not equal[13],

$$|0, in\rangle \neq |0, out\rangle\,. \tag{3.113}$$

The number densities of phonons in each mode are

$$n_{\omega}^{u,r} = \langle 0, in|\hat{\alpha}_{\omega}^{ur,out\dagger}\hat{\alpha}_{\omega}^{ur,out}|0, in\rangle = \left|S_{ur,u_1l}\right|^2 \tag{3.114}$$

$$n_{\omega}^{u_2,l} = \langle 0, in|\hat{\alpha}_{\omega}^{u_2l,out\dagger}\hat{\alpha}_{\omega}^{u_2l,out}|0, in\rangle = \left|S_{u_2l,vr}\right|^2 + \left|S_{u_2l,ul}\right|^2 \tag{3.115}$$

$$n_{\omega}^{v,l} = \langle 0, in|\hat{\alpha}_{\omega}^{vl,out\dagger}\hat{\alpha}_{\omega}^{vl,out}|0, in\rangle = \left|S_{vl,u_1l}\right|^2. \tag{3.116}$$

These equations satisfy the number conservation relation

$$n_{\omega}^{u_2,l} = n_{\omega}^{u,r} + n_{\omega}^{v,l}. \tag{3.117}$$

As of the above equations, it can be seen that the vacuum state $|0, in\rangle$ spontaneously creates particles on both sides of the horizon. But how is the energy-conservation relation preserved? This is due to the negative-frequency modes of the u_2^l-branch. Assuming that particles start at $t = -\infty$, where there are no incoming phonons, Equation 3.117 indicates the creation of equal numbers of positive and negative-norm outgoing modes in the subsonic and supersonic regions, respectively. Spontaneous emission of phonons from the vacuum has occurred. As it can be seen, the total energy produced by the horizon is zero, but there exist emitted particles on both sides.

A hypothetical observer located at $+\infty$ will observe emitted flux [53]

$$\frac{\mathrm{d}N_{\omega}}{\mathrm{d}t\,\mathrm{d}\omega} = \frac{\left|S_{ur,u_1l}\right|^2}{2\pi} \sim \frac{1}{\omega}, \tag{3.118}$$

[12] In a simple setting where both regions across a discontinuity are subsonic, but with different background sound speeds, say $c^{l/r}$, the η-matrix would be replaced by the identity matrix $\mathbb{1}_{2\times 2}$

[13] In the respective case where the flow is discontinuous, but everywhere subsonic, then the two vacuum states satisfy

$$|0, in\rangle = |0, out\rangle\,. \tag{3.112}$$

where the $1/\omega$ dependence comes only from the approximate scheme previously used by taking the first-order terms in the expansion with respect to z. It is clear that this inverse-frequency power is the reminiscent of the blackbody radiation,

$$n_{th} = \frac{1}{e^{\frac{k_B T}{\omega}} - 1} \overset{\omega \to 0}{\simeq} \frac{k_B T}{\omega}. \tag{3.119}$$

From Equations 3.118 and 3.119, the low-frequency effective temperature can be extracted [58]

$$T_{eff} = \frac{1}{k_B} \frac{c_r + V}{c_r - V} \frac{(V^2 - c_l^2)^{3/2}}{c_r^2 - c_l^2} \frac{2c_r}{c_l \xi_l}. \tag{3.120}$$

This temperature is indeed finite. Nevertheless the surface gravity for a steplike profile is infinite, something that causes problems in the interpretation of this effective temperature as the Hawking temperature. The solution to this problem is found by going to smoother profiles, where the quantities across the horizon do not change abruptly. In that case, the temperature found is consistent with Hawking's result as found in [20, 31–33, 61, 62]. Smooth velocity profile across the horizon can also be used [20, 31, 63].

4 An analysis based on Quantum Field Theory

The analysis of the black-hole laser configuration, discussed in next chapters, will mainly focus on the unstable character of the modes characterizing the system. A black-hole laser consists of a two-horizon configuration, when compared to the one-horizon black hole or white hole cases. The description of the black-hole laser will mainly focus on the revelation of its instability to linear perturbations. As a result, in this chapter, the theory of instabilities for BECs will be presented, without making any more contact to the explicit Analogue Gravity framework that will be introduced in next chapter. For this reason, contact with the Klein-Gordon equation will be made, where the formalism of this chapter will be analysed. Then, the description of the instabilities of Bose gases will naturally follow.

To begin with, in order to describe the unstable character of the Klein-Gordon equation or of Bose gases, all the different modes that can occur to this system will be first described. In previous chapters, we have dealt with the standard continuous spectrum which emerges from the real frequency modes. Even if not explicitly said, these modes are asymptotically bound because of their modulus being bounded. They are linear superposition of plane waves with real wavevectors at spatial infinity.

A variety of new types of modes will be now stated, which will be useful for the subsequent analysis. These are the quasi-normal modes, the dynamical instability modes and the bound-state modes. Quasi-normal modes are complex frequency modes that are decaying exponentially in time and are unbounded at spatial infinity. They obey outgoing boundary conditions, meaning that their group velocity points towards infinity ($+\infty$ or $-\infty$), depending on the location of the modes with respect to the potential in question (or the supersonic cavity of the black-hole laser at hand). Dynamical instability modes grow in time and are spatially bounded. A dynamical instability mode is associated with a pair-mode with complex conjugate frequency. This is a consequence of the Hamiltonian (symplectic) symmetry of the problem. These modes are decaying in time. Finally, bound-state modes are stable with real frequencies. Dynamical instability modes and bound-state modes are square-integrable and belong to the discrete sector of the spectrum. Quasi-normal modes are not spatially bound and are thus not square-integrable [64, 65].

The instability character of the Klein-Gordon equation will be discussed with respect to its frequency eigenmodes. The crucial difference between a system with only a continuous real spectrum and one that can, in principle, sustain unstable modes stems from its scalar product, as defined in Equation 2.27.It can be concluded that a system with a positive definite scalar product necessarily possesses a continuous spectrum of real-frequency modes, but no discrete and unstable part. However, when the scalar product of the system

is not positive-definite, instabilities are not formally excluded. There is then no general spectral theorem that guaranties the real character of the modes and its stability. The theory of indefinite metric spaces describes these systems [66–69]. Some basic formalities on indefinite inner product spaces are also given in Appendix C.

Despite the lack of general solutions, in terms of spectral theory, in indefinite inner product spaces, in the case of 1 + 1 dimensional space there is indeed an explicit construction [70]. In the case considered, we will work with an infinite space, which is a necessary condition for obtaining quasi-normal modes and for further studying the Klein-Gordon equation in the presence of an electrostatic potential. The use of the electrostatic potential will be due to historic reasons [45], but also due to its simplicity and analogy with the final goal, the description of instabilities for the black-hole laser case.

After briefly introducing all the different modes that can be encountered when discussing instabilities in the context of the Klein-Gordon equation, the analysis based on the Klein-Gordon equation will be made. In next section, after having established the basics of the theory, the discussion of instabilities will be shifted to the case of BECs.

4.1 Quantum Field Theoretical Treatment of the unstable behaviour of the massless scalar field

To begin with, the Klein-Gordon equation in the presence of an electrostatic field, A_0,

$$(\partial_t + ieA_0(t,x))^2 \phi - \partial_x^2\phi + m^2\phi = 0, \tag{4.1}$$

is considered, where e the charge and m the mass of the system. The scalar product is defined as

$$(\phi_1, \phi_2) = i \int \mathrm{d}x \, (\phi_1^* \pi_2 - \pi_1^* \phi_2) \tag{4.2}$$

with the conjugate momentum of the field ϕ_j, being $\pi_j \equiv (\partial_t + ieA_0)\,\phi_j$ with $j \in \{1, 2\}$.Then, the Laplace transform of Klein-Gordon Equation 4.1,

$$\tilde{\phi}(x;\lambda) \equiv \int_0^\infty \mathrm{d}t \, \phi(x,t) e^{i\lambda t}, \tag{4.3}$$

is defined. For $\lambda \in \mathbb{C}$ and $\mathrm{Im}(\lambda) > 0$, the above integral converges. Then the Laplace transform 4.3 obeys the relation

$$\Big((\lambda - eA_0(x))^2 + \partial_x^2 - m^2 \Big) \tilde{\phi}(x;\lambda) = J^0_\lambda(x) \tag{4.4}$$

with $J^0_\lambda(x) \equiv -\pi(x,0) + i\,(\lambda - eA_0(x))\,\phi(x,0) \equiv J^0_\lambda(x)$ the source term, defined by the initial conditions. Then, the solution of Equation 4.1 is given by

$$\Theta(t)\phi(x,t) = -\frac{1}{2\pi} \int_{D_{ret}} \mathrm{d}\lambda \, \tilde{\phi}(x;\lambda) e^{-i\lambda t}, \tag{4.5}$$

where D_{ret} is a contour in the complex λ-plane above all singularities of $\tilde{\phi}(x;\lambda)$.

The field is obtained for all times, if the field, $\tilde{\phi}(x;\lambda)$, is defined for sufficiently negative $\mathrm{Im}(\lambda)$, so as the corresponding inverse lies below all the singularities of D_{adv}. The final integral is symmetric between the lower- and upper-half complex λ-plane,

$$\phi(x,t) = -\frac{1}{2\pi}\int_{D_{ret}\cup D_{adv}} \mathrm{d}\lambda\, \tilde{\phi}(x;\lambda)e^{-i\lambda t}. \tag{4.6}$$

For the solution of Equation 4.4, its Green's function satisfies

$$\tilde{\phi}(x;\lambda) = \int \mathrm{d}x'\, G_\lambda(x,x')J^0_\lambda(x') \tag{4.7}$$

with

$$\Big((\lambda - eA_0(x))^2 + \partial_x^2 - m^2\Big)G_\lambda(x,x') = \delta(x-x'). \tag{4.8}$$

This equation has a solution constructed with respect to two linearly independent solutions $\phi^{(1)}_\lambda(x)$ and $\phi^{(2)}_\lambda(x)$ of the stationary mode equation

$$\Big((\lambda - eA_0(x))^2 + \partial_x^2 - m^2\Big)\phi_\lambda = 0, \tag{4.9}$$

as their space-ordered product,

$$G_\lambda(x,x') = \frac{1}{W(\lambda)}\begin{cases}\phi^{(1)}_\lambda(x)\phi^{(2)}_\lambda(x'), & \text{if } x < x'\\ \phi^{(1)}_\lambda(x')\phi^{(2)}_\lambda(x), & \text{if } x' > x\end{cases}, \tag{4.10}$$

with

$$W(\lambda) = \phi^{(1)}_\lambda(x)\partial_x\phi^{(2)}_\lambda(x) - \phi^{(2)}_\lambda(x)\partial_x\phi^{(1)}_\lambda(x). \tag{4.11}$$

The Green's function is then uniquely determined by a choice of boundary conditions which select the Jost functions $\phi^{(1)}_\lambda(x)$ and $\phi^{(2)}_\lambda(x)$ [71]. Then, the convergence of Green's-function integral 4.7 is made explicit by assuming that it decays sufficiently fast for $x \to \pm\infty$, a condition that is necessary for solutions of the time-dependent equation, Equation 4.1, with

$$\int \mathrm{d}x\left(|\phi|^2 + |\pi|^2\right) < \infty. \tag{4.12}$$

Thus, the following boundary conditions are imposed:

$$\begin{cases}\phi^{(1)}_\lambda & \text{is } L^2 \text{ for } x \to -\infty\\ \phi^{(2)}_\lambda & \text{is } L^2 \text{ for } x \to +\infty\end{cases} \tag{4.13}$$

for the square-integrable mode-functions.

By using Equations 4.3 and 4.7 in Equation 4.6, the time-dependent solution of the Klein-Gordon equation can be established[1],

$$\phi(x,t) = -\frac{i}{2\pi}\int_{\mathbb{R}}\left(\int_{D_{ret}\cup D_{adv}} e^{-i\lambda t}\left(\lambda - eA_0(x')\right)G_\lambda(x,x')\,\mathrm{d}\lambda\right)\phi_0(x)\,\mathrm{d}x' + i\int_{\mathbb{R}}\left(\int_{D_{ret}\cup D_{adv}} e^{-i\lambda t}G_\lambda(x,x')\,\mathrm{d}\lambda\right)\pi_0(x)\,\mathrm{d}x'\,. \tag{4.14}$$

The contour $D_{ret} \cup D_{adv}$, where the Green's function is calculated, can be deformed to enclose the spectrum.

Let us now try to apply this formulation in the description of a simple problem, the square potential,

$$A_0(x) = \begin{cases} 0, & \text{if } |x| > L \\ A, & \text{if } |x| < L \end{cases}. \tag{4.15}$$

Any solution is of this potential problem is a superposition of two plane waves

$$\phi_\lambda(x) = \alpha_\pm e^{ik_\lambda x} + b_\pm e^{-ik_\lambda x} \tag{4.16}$$

and the momenta in its region satisfy

$$k_\lambda = \begin{cases} \sqrt{\lambda^2 - m^2} & \text{if } |x| > L \\ \sqrt{(\lambda - eA)^2 - m^2} & \text{if } |x| < L \end{cases}. \tag{4.17}$$

In order to obtain globally defined solutions, the same process as in Subsection 3.3.1 is followed; continuity of the field and its first derivative, $\partial_x\phi$, across the point of discontinuity, $x = \pm L$ are then imposed.

When $\lambda \in [-m, m]$, then, $k_\lambda \in \mathbb{C}$. If $\lambda^2 > m^2$, then asymptotically bound modes exist as scattering states (see section 3.3.1). For $\lambda^2 < m^2$, the continuous part of the spectrum does not exist. When $k_\lambda \in \mathbb{C}$, then the field equation, Equation 4.16, needs some vanishing of the coefficients $(\alpha_\pm, b_\pm)$, in order to satisfy the square-integrability condition, Equation 4.13. For this specific choice of coefficients, the Green's function can be constructed. This is not possible unless the Wronskian vanishes. In this case, the Green's function has a pole[2]. For $W(\lambda) = 0$, the fields ϕ_1 and ϕ_2 are dependent on each other and proportional, allowing for the existence of a decaying mode on both sides of the potential step [65].

Bu assuming that there exist complex modes in the spectrum which are, thus, square-integrable, these modes are necessarily pairs of dynamical instability modes. They are pairs because of the Hermiticity of the respective model (See Appendix C), which provokes the Green's function symmetry

$$G^*_\lambda(x,x') = G_{\lambda^*}(x,x'). \tag{4.18}$$

[1] for this reason, we use the Green's function relation in the Laplace transformed version of the Klein-Gordon equation

[2] Note that the Wronskian is composed of continuous functions. As a result, it can only vanish for a discrete set of values. These are the poles of the Green's function.

By analysing the poles of the Green's function, Equation 4.10, the discrete part of the spectrum can be accessed, i.e. the complex frequency modes that describe the dynamical instability [45, 65].

Dynamical instability modes can be regarded as a superposition of equal amount of positive and negative-norm modes of the same frequency. This statement leads to many interesting aspects on their quantization, something that will be analysed in Section 4.2.

In the case $A_0 \to 0$ for $x \to \pm\infty$, the most general form of relation 4.14 can be expressed as[3]

$$\phi(x,t) = \int_{D_{can}} \mathrm{d}\omega \left(\alpha^u_\omega e^{i\omega t}\phi^u_\omega(x) + \alpha^v_\omega e^{-i\omega t}\phi^v_\omega(x)\right) + \sum_{\alpha\in D_{dis}\cap\mathbb{R}} d_\alpha e^{-i\omega_\alpha t}\chi_\alpha(x) + \sum_{\alpha\in D_{dis}\setminus\mathbb{R}} \left(b_\alpha e^{-i\lambda_\alpha t}\phi_\alpha(x) + c_\alpha e^{-i\lambda^*_\alpha t}\psi_\alpha(x)\right), \quad (4.19)$$

where D_{dis} is the discrete spectrum of the system, emerging from the poles of the Green's function. The discrete spectrum has been divided into those modes with vanishing norm, the dynamical instability modes, and those with nonvanishing norm, the bound-state modes. The continuous part of the spectrum is composed of the normal modes, defined and analysed thoroughly in the previous chapter. They arise from the discontinuities across the branch-cut of Green's function. The discrete part of the spectrum has orthogonality relations

$$(\chi_\alpha, \chi_b) = \pm\delta_{\alpha b} \quad (4.20)$$

$$(\phi_\alpha, \phi_b) = (\psi_\alpha, \psi_b) = 0 \quad (4.21)$$

$$(\phi_\alpha, \psi_b) = \delta_{\alpha b}. \quad (4.22)$$

and the energy of the Klein-Gordon equation, Equation 4.1, is

$$E[\phi] = \int \mathrm{d}x \left(|\partial_t\phi|^2 + |\partial_x\phi|^2 + \left(m^2 - e^2A_0^2(x)\right)|\phi|^2\right). \quad (4.23)$$

By substituting Equation 4.19 and using the commutation relations for dynamical instability modes, bound-state modes and normal modes, the energy functional can be reformulated as

$$E = \int_m^\infty \mathrm{d}\omega\,\omega \left(|\alpha^u_\omega|^2 + |\alpha^v_\omega|^2 + |\alpha^u_{-\omega}|^2 + |\alpha^v_{-\omega}|^2\right) + \sum_\alpha^{BSM} \omega_\alpha |d_\alpha|^2 + \sum_\alpha^{DIM} \left(-i\lambda_\alpha b_\alpha c^*_\alpha + i c_\alpha b^*_\alpha\right), \quad (4.24)$$

where the lower integration limit for the part containing contributions from the normal modes reflects their range of validity and DIM indicates the dynamical instability modes

[3] The respective form of Equation 4.19 for the Bogoliubov-de Gennes equations in the BEC framework is given in theorem 7, where bound-state modes are omitted.

and BSM the bound-state modes. The first term inside the integral reflects the continuous character of normal modes, while the discrete bound-state and dynamical instability modes are summed over the discrete spectrum.

To conclude this analysis, quasi-normal modes need to be further studied. As they are not L^2 or asymptotically bound, they are not included in the spectrum. They emerge as poles of the retarded Green's function [65].

There are two types of poles for the retarded Green's function; the ones in the upper complex plane, which are poles of the Green's function, G_λ, as well and those which are located in the lower half plane across the branch cut. The first type of poles are included in the spectrum, as they are poles of G_λ, too. However, poles in the lower complex plane are not included in the spectrum.

By assuming solutions of 4.17 with $\mathrm{Im}\{\lambda\} > 0$, $\mathrm{Im}\{k_\lambda\} > 0$, modes that are square-integrable should asymptotically satisfy the condition

$$\phi_\lambda^{(1)} \sim e^{-ik_\lambda x} \text{ is } L^2 \text{ for } x \to -\infty \tag{4.25}$$

$$\phi_\lambda^{(2)} \sim e^{ik_\lambda x} \text{ is } L^2 \text{ for } x \to +\infty. \tag{4.26}$$

These modes are outgoing[4].

On one hand, when the imaginary part of the frequency is $\mathrm{Im}\{\lambda\} > 0$, the corresponding mode-function decays on both sides of the potential and is thus square-integrable. Retarded Green's function shares these poles with G_λ. On the other hand, when $\mathrm{Im}\{\lambda\} < 0$, the corresponding mode-functions are exponentially increasing on both sides of the potential. These modes do not belong to the spectrum [65].

4.2 Quantum-field theoretic treatment of unstable behaviour of the Bogoliubov-de Gennes equations

Regarding astrophysics, it has been known in a classical basis that a star with ergoregion but no event horizon is unstable to the emission of scalar, electromagnetic or gravitational waves [72]. This classical ergoregion instability is characterized by complex frequency modes. However, it cannot be directly connected with black hole radiation. It resembles more to a laser amplification [73]. The subsequent analysis will mainly focus on general results emerging from the unstable behaviour of BECs.

The linear stability or instability of BECs is usually analysed through the Bogoliubov-de Gennes equations, which follow from linearising the time-dependent Gross-Pitaevskii equation in the quantum fluctuations. Like in the case analysed before, all modes with real eigenvalues can be mapped to the quasiparticle picture and be proven to follow bosonic commutation relations. However, Bogoliubov-de Gennes equations can

[4]This can be seen in the following approximation. Assume that λ is small and then k_λ,

$$k_{\lambda=\omega+i\epsilon} = k_\omega + i\epsilon\frac{\partial k_\omega}{\partial_\omega} + O\left(\epsilon^2\right),$$

possesses an imaginary part which shares the same sign as the group velocity.

sustain complex eigenfrequency modes as well for some specific models, one of these being the multi-component Bose gases [74–77]. Other models where complex eigenfrequencies are important include gap solitons or highly quantized vortices [78, 79].

Condensates can generally have instabilities of two kinds; Landau-type and dynamical instabilities [77, 80, 81]. Instabilities of the Landau type indicate modes with negative energy. For example, in the simplest one horizon model in a BEC which was studied in Chapter 3, there indeed existed modes with negative energies (and positive norm), when dealing with the supersonic region of the configuration. In the subsonic case, all modes with positive energies had positive norms and no Landau instability could be identified. Landau instabilities are responsible for the absence of thermodynamic equilibrium [82]. Dynamical instabilities deal with the decay of the initial condensate's configuration. They are caused by eigenfunctions of Bogoliubov-de Gennes equations with complex eigenvalues. In the case of a highly quantized vortex, complex eigenfrequencies sign the dynamical instability due to the external perturbations [75, 82].

When the field is decomposed with respect to its modes in the framework of black-hole lasers with complex modes present, the exact quantum field theoretic description of these modes will be important. As a result, this analysis will be based not only on the time-dependent Gross-Pitaevskii equation, but also on the underlying Quantum Field Theory. After this formulation will become apparent, time-dependent perturbations or, for example, a linear-response theory treatment of the system will be feasible. As already seen for the case of the Klein-Gordon field in the presence of an electric field, complex eigenvalues give rise to different commutation relations compared to the ones for normal modes. Bogoliubov-de Gennes equations characterize an indefinite metric space, as in the Klein-Gordon case. The complete set of the modes will be needed in order to fully characterize the system. Condensates trapped in a potential will give relevant results to the black-hole laser case, where the supersonic cavity of the black-hole laser takes the place of the potential. For all this subsequent analysis of finding the complete set and the proper mode decomposition, an explicit redefinition of the problem will be made.

Thus, the interacting Bose gas action can be expressed as

$$S = \int \mathrm{d}^4x \left(\hat{\Phi}^\dagger(x) \left(T - T_k - V(\mathbf{x}) + \mu \right) \hat{\Phi}(x) - \frac{1}{2} g \hat{\Phi}^\dagger(x) \hat{\Phi}^\dagger(x) \hat{\Phi}(x) \hat{\Phi}(x) \right) \tag{4.27}$$

with $x = (\mathbf{x}, t)$, $T = i\partial_t$ and $T_k = -\frac{1}{2m}\nabla^2$. The potential term is left arbitrary for this analysis.

Then the substitution

$$\hat{\Phi}(x) = \Phi_0(\mathbf{x}) + \hat{\phi}(x) \tag{4.28}$$

is performed with respect to the classical and quantum fields, respectively, which results

it the equations

$$S_0 = \int \mathrm{d}^4x \left(\Phi_0^*(\mathbf{x}) \left(-T_k - V(\mathbf{x}) + \mu\right) \Phi_0(\mathbf{x}) - \frac{1}{2} g \left|\Phi_0(\mathbf{x})\right|^4 \right) \tag{4.29}$$

$$\begin{aligned} S_1 = \int \mathrm{d}^4x \Big(& \Phi_0^*(\mathbf{x}) \left(-T_k - V(\mathbf{x}) + \mu - g \left|\Phi_0(\mathbf{x})\right|^2\right) \hat{\phi}(x) \\ & + \hat{\phi}^\dagger(x) \left(-T_k - V(\mathbf{x}) + \mu - g \left|\Phi_0(\mathbf{x})\right|^2\right) \Phi_0(\mathbf{x}) \Big) \end{aligned} \tag{4.30}$$

$$\begin{aligned} S_2 = \int \mathrm{d}^4x \Big(& \hat{\phi}^\dagger(x) \left(T - T_k - V(\mathbf{x}) + \mu\right) \hat{\phi}(x) \\ & - \frac{1}{2} g \left(4 \left|\Phi_0(\mathbf{x})\right|^2 \hat{\phi}^\dagger(x)\hat{\phi}(x) + \Phi_0^{*2}(\mathbf{x})\hat{\phi}^{\dagger 2}(x) + \Phi_0^2(\mathbf{x})\hat{\phi}^{\dagger 2}(x)\right) \Big) \end{aligned} \tag{4.31}$$

$$\begin{aligned} S_{3-4} = \int \mathrm{d}^4x \Big(& - g \left(\Phi_0(\mathbf{x})\hat{\phi}^{\dagger 2}(x)\hat{\phi}(x) + \Phi_0^*(\mathbf{x})\hat{\phi}^\dagger(x)\hat{\phi}^2(x)\right) \\ & - \frac{1}{2} g \hat{\phi}^{\dagger 2}(x)\hat{\phi}^2(x) \Big). \end{aligned} \tag{4.32}$$

The quantum field must satisfy the commutation relations

$$\left[\hat{\phi}(\mathbf{x}, t), \hat{\phi}^\dagger(\mathbf{x}', t)\right] = \delta^3(\mathbf{x} - \mathbf{x}') \tag{4.33}$$

$$\left[\hat{\phi}(\mathbf{x}, t), \hat{\phi}(\mathbf{x}', t)\right] = 0 \tag{4.34}$$

$$\left[\hat{\phi}^\dagger(\mathbf{x}, t), \hat{\phi}^\dagger(\mathbf{x}', t)\right] = 0 \tag{4.35}$$

in the canonical formalism in the interaction picture with

$$\begin{aligned} \hat{H}_0 = \int \mathrm{d}^3x \Big(& \hat{\phi}^\dagger(x) \left(T_k + V(\mathbf{x}) - \mu\right) \hat{\phi}(x) \\ & + \frac{1}{2} g \left(4 \left|\Phi_0(\mathbf{x})\right|^2 \hat{\phi}^\dagger(x)\hat{\phi}(x) + \Phi_0^{*2}(\mathbf{x})\hat{\phi}^{\dagger 2}(x) + \Phi_0^2(\mathbf{x})\hat{\phi}^{\dagger 2}(x)\right) \Big) \end{aligned} \tag{4.36}$$

$$\hat{H}_{int} = \int \mathrm{d}^3x \left(g \left(\Phi_0(\mathbf{x})\hat{\phi}^{\dagger 2}(x)\hat{\phi}(x) + \Phi_0^*(\mathbf{x})\hat{\phi}^\dagger(x)\hat{\phi}^2(x)\right) + \frac{1}{2} g \hat{\phi}^{\dagger 2}(x)\hat{\phi}^2(x) \right). \tag{4.37}$$

The classical field is normalized to

$$\int \mathrm{d}^3\mathbf{x} \left|\Phi_0(\mathbf{x})\right|^2 = n_0 \tag{4.38}$$

with the condensate number, n_0. Alternatively, a new field can be defined in the form

$$f(\mathbf{x}) = \frac{1}{\sqrt{n_0}} \Phi_0(\mathbf{x}), \tag{4.39}$$

which is normalized to unity,

$$\int \mathrm{d}^3x \left|f(\mathbf{x})\right|^2 = 1. \tag{4.40}$$

The Gross-Pitaevskii equation can then be brought into the form of Equation 3.20, with $\mathcal{P}$ and $\mathcal{M}$ as defined in Equations 3.12 and 3.13.

For the case of real eigenvalues, the quantum field can be expressed in the quasiparticle basis by diagonalizing the Hamiltonian, Equation 4.37,

$$\hat{\phi}(x) = \sum_{n=1}^{\infty} \left(u_n(\mathbf{x})\hat{\alpha}_n(t) - v_n^*(\mathbf{x})\hat{\alpha}_n^\dagger(t)\right), \tag{4.41}$$

where the operators $\hat{\alpha}$ and $\hat{\alpha}^\dagger$ satisfy bosonic commutations relations. The unperturbed Hamiltonian can then be expressed as

$$\hat{H}_0 = \sum_{n=1}^{\infty} \omega_n \hat{\alpha}_n^\dagger \hat{\alpha}_n, \tag{4.42}$$

up to an irrelevant constant.

Embarking into the description of complex frequency modes[5], the following shorthand notation will be used in order to express more compactly the final results

$$r(\mathbf{x}) = \begin{pmatrix} r_1(\mathbf{x}) \\ r_2(\mathbf{x}) \end{pmatrix} \tag{4.43}$$

$$\begin{aligned}(r, s) &\equiv \int \mathrm{d}^3x\, r^\dagger(\mathbf{x})\sigma_3 s(\mathbf{x}) \\ &= \int \mathrm{d}^3x \begin{pmatrix} r_1^*(\mathbf{x}) & r_2^*(\mathbf{x}) \end{pmatrix} \begin{pmatrix} 1 & 0 \\ 0 & -1 \end{pmatrix} \begin{pmatrix} s_1(\mathbf{x}) \\ s_2(\mathbf{x}) \end{pmatrix} \\ &= \int \mathrm{d}^3x \left(r_1^*(\mathbf{x})s_1(\mathbf{x}) - r_2^*(\mathbf{x})s_2(\mathbf{x})\right)\end{aligned} \tag{4.44}$$

$$\|r\|^2 = \int \mathrm{d}^3x \left(|r_1(\mathbf{x})|^2 - |r_2(\mathbf{x})|^2\right) \tag{4.45}$$

$$x_n(\mathbf{x}) \equiv \begin{pmatrix} u_n(\mathbf{x}) \\ v_n(\mathbf{x}) \end{pmatrix} \tag{4.46}$$

$$y_n(\mathbf{x}) \equiv \sigma_1 x_n^*(\mathbf{x}) = \begin{pmatrix} v_n^*(\mathbf{x}) \\ u_n^*(\mathbf{x}) \end{pmatrix} \quad \forall n \in \mathbb{N} - \{0\} \tag{4.47}$$

$$\sigma_1 = \begin{pmatrix} 0 & 1 \\ 1 & 0 \end{pmatrix} \tag{4.48}$$

$$\sigma_3 = \begin{pmatrix} 1 & 0 \\ 0 & -1 \end{pmatrix}. \tag{4.49}$$

The Bogoliubov-de Gennes equations, Equations 3.20, can then be expressed as

$$K(\mathbf{x})x_n(\mathbf{x}) = \lambda_n x_n(\mathbf{x}) \tag{4.50}$$

with

$$K(\mathbf{x}) = \begin{pmatrix} \mathcal{P}(\mathbf{x}) & \mathcal{M}(\mathbf{x}) \\ -\mathcal{M}^*(\mathbf{x}) & -\mathcal{P}^*(\mathbf{x}) \end{pmatrix} = \sigma_3 \begin{pmatrix} \mathcal{P}(\mathbf{x}) & \mathcal{M}(\mathbf{x}) \\ \mathcal{M}^*(\mathbf{x}) & \mathcal{P}^*(\mathbf{x}) \end{pmatrix}, \tag{4.51}$$

[5]Note that complex frequencies will be denoted with the Greek letter λ and real ones with ω.

where

$$\mathcal{L} = \begin{pmatrix} \mathcal{P}(\mathbf{x}) & \mathcal{M}(\mathbf{x}) \\ \mathcal{M}^*(\mathbf{x}) & \mathcal{P}^*(\mathbf{x}) \end{pmatrix}. \tag{4.52}$$

With the above notation and by ignoring any contributions from the zero-mode state [83–85], $x_0(\mathbf{x})$, the following conditions can be inferred

$$\|x_0(\mathbf{x})\|^2 = 0 \tag{4.53}$$

$$\Big(x_n(\mathbf{x}), x_{n'}(\mathbf{x})\Big) = \delta_{nn'} \tag{4.54}$$

$$\Big(y_n(\mathbf{x}), y_{n'}(\mathbf{x})\Big) = 0 \tag{4.55}$$

$$\Big(y_n(\mathbf{x}), x_{n'}(\mathbf{x})\Big) = 0 \tag{4.56}$$

$$\sum_{n=1}^{\infty} \Big(x_n(\mathbf{x}) x_n^\dagger(\mathbf{x}') - y_n(\mathbf{x}) y_n^\dagger(\mathbf{x}')\Big) = \sigma_3 \delta^{(3)}(\mathbf{x} - \mathbf{x}') \tag{4.57}$$

with the commutation relation

$$\Big[\hat{\phi}(\mathbf{x}, t), \hat{\phi}^\dagger(\mathbf{x}', t)\Big] = \delta^{(3)}(\mathbf{x} - \mathbf{x}'). \tag{4.58}$$

Properties of complex modes in the context of BECs are then discussed based on [74, 79, 82, 86–88].

Theorem 1. *If* $Im(\lambda_n) \neq 0$*, then* $\|x_n\|^2 = 0$.

Proof. Due to the conjugate symmetry of the inner product,

$$(s, t) = (t, s)^*, \tag{4.59}$$

it can be deduced that

$$\begin{aligned} \lambda_n^*(x_n(\mathbf{x}), x_n(\mathbf{x})) &= (Kx_n(\mathbf{x}), x_n(\mathbf{x})) = (x_n(\mathbf{x}), Kx_n(\mathbf{x})) \\ &= \lambda_n(x_n(\mathbf{x}), x_n(\mathbf{x})) \xRightarrow{Im(\lambda_n)\neq 0} \|x_n\|^2 = 0. \end{aligned} \tag{4.60}$$

□

Theorem 2. *If* $(x_n(\boldsymbol{x}), x_m(\boldsymbol{x})) \neq 0$*, then* $\lambda_n^* = \lambda_m$.

Proof.

$$\begin{aligned} \lambda_n^*(x_n(\mathbf{x}), x_m(\mathbf{x})) &\overset{(4.62)}{=} (Kx_n(\mathbf{x}), x_m(\mathbf{x})) = (x_n(\mathbf{x}), Kx_m(\mathbf{x})) \\ &\overset{(4.50)}{=} \lambda_m(x_n(\mathbf{x}), x_m(\mathbf{x})), \end{aligned} \tag{4.61}$$

while using in the first equation the property

$$(Kx_n)^* = \lambda_n^* x_n^*. \tag{4.62}$$

□

Corollary 2.1. *When theorem 2 is applied to Equation 3.20, the complex eigenvalues arise in pairs of complex conjugates, due to the symplectic structure of the Bogoliubov-de Gennes equations. When complex modes arise, the condensate will have a dynamically unstable ground state [89].*

Theorem 3. *If $\lambda_n^* \neq \lambda_m$, then $(x_n(\boldsymbol{x}), x_m(\boldsymbol{x})) = 0$.*

Corollary 3.1. *Two modes satisfying Theorem 3 are orthogonal to each other.*

Corollary 3.2. *Complex modes are orthogonal to real ones.*

Theorem 4. *If x_n is an eigenvector belonging to the complex sector with*

$$K(\boldsymbol{x})x_n(\boldsymbol{x}) = \lambda_n x_n(\boldsymbol{x}), \tag{4.63}$$

then it satisfies the equation

$$K(\boldsymbol{x})y_n(\boldsymbol{x}) = -\lambda_n^* y_n(\lambda) \tag{4.64}$$

as well.

This means that when x_n is an eigenvector, then y_n is also an eigenvector with eigenvalue $-\lambda_n^*$.

Theorem 5. *When all eigenvalues of the matrix $\mathcal{L}$ in Equation 4.52 are positive, then the eigenvalues λ_n must be real, $\lambda_n = \omega_n$.*

Discussion. *The matrix $\mathcal{L}$ is hermitian and as a result will be equipped with a set of real eigenvalues. Then, Equation 4.63, after being multiplied by σ_3 and $x_n^\dagger(\boldsymbol{x})$ will be reduced to*

$$x_n^\dagger(\boldsymbol{x})\mathcal{L}x_n(\boldsymbol{x}) = \lambda_n x_n^\dagger(\boldsymbol{x})\sigma_3 x_n(\boldsymbol{x}). \tag{4.65}$$

Since the matrix $\mathcal{L}$ is always real, the left hand side of 4.65 is always real and λ_n can be complex only if $x_n^\dagger(\boldsymbol{x})\mathcal{L}x_n(\boldsymbol{x}) = x_n^\dagger(\boldsymbol{x})\sigma_3 x_n(\boldsymbol{x}) = 0$. When all eigenvalues of $\mathcal{L}$ are positive, $x_n^\dagger(\boldsymbol{x})\mathcal{L}x_n(\boldsymbol{x})$ must be positive and then $\lambda_n \in \mathbb{R}$. They also carry the same sign as $x_n^\dagger(\boldsymbol{x})\sigma_3 x_n(\boldsymbol{x})$.

As a result, it has been proven that an energetic instability is a prerequisite for the occurrence of dynamical instabilities. A system energetically unstable is not necessarily dynamically unstable. A system dynamically unstable is necessarily energetically unstable.

Theorem 6 (Complete set)**.** *Let us define a pair of complex modes with no degeneracy between them, satisfying the commutation relations*

$$(x_\mu, x_{*\nu}) = \delta_{\mu\nu} \tag{4.66}$$

and

$$(y_\mu, y_{*\nu}) = -\delta_{\mu\nu} \tag{4.67}$$

with

$$Kx_\mu = \lambda_\mu x_\mu \tag{4.68}$$
$$Kx_{*\mu} = \lambda_{*\mu} x_{*\mu} = \lambda_\mu^* x_{*\mu}, \tag{4.69}$$

where further $y_\mu \equiv \sigma_1 x_\mu^*$, $y_{*\mu} \equiv \sigma_1 x_{*\mu}^*$, $x_\mu = \begin{pmatrix} u_\mu(\boldsymbol{x}) \\ v_\mu(\boldsymbol{x}) \end{pmatrix}$ *and* $x_{*\mu} = \begin{pmatrix} u_{*\mu}(\boldsymbol{x}) \\ v_{*\mu}(\boldsymbol{x}) \end{pmatrix}$.

Then, a complete set can be formed, that will satisfy the above theorems

$$\sum_n \left(x_n(\boldsymbol{x}) x_n^\dagger(\boldsymbol{x}') - y_n(\boldsymbol{x}) y_n^\dagger(\boldsymbol{x}') \right) + \sum_\mu \left(x_\mu(\boldsymbol{x}) x_{*\mu}^\dagger(\boldsymbol{x}') + x_{*\mu}(\boldsymbol{x}) x_\mu^\dagger(\boldsymbol{x}') \right.$$
$$\left. - y_\mu(\boldsymbol{x}) y_{*\mu}^\dagger(\boldsymbol{x}') - y_{*\mu}(\boldsymbol{x}) y_\mu^\dagger(\boldsymbol{x}') \right) = \sigma_3 \delta^{(3)}(\boldsymbol{x} - \boldsymbol{x}'). \tag{4.70}$$

Theorem 7 (Free-Hamiltonian representation)**.** *From the complete set defined above, the equation of the field in the Schrödinger picture can be deduced*

$$\hat{\phi}(\boldsymbol{x}) = \sum_n \left(\hat{\alpha}_n u_n(\boldsymbol{x}) - \hat{\alpha}_n^\dagger v_n^*(\boldsymbol{x}) \right) + \sum_\mu \left(\hat{A}_\mu u_\mu(\boldsymbol{x}) + \hat{B}_\mu u_{*\mu}(\boldsymbol{x}) - \hat{A}_\mu^\dagger v_\mu^*(\boldsymbol{x}) - \hat{B}_\mu^\dagger v_{*\mu}^*(\boldsymbol{x}) \right) \tag{4.71}$$

$$\hat{\phi}^\dagger(\boldsymbol{x}) = \sum_n \left(\hat{\alpha}_n^\dagger u_n^*(\boldsymbol{x}) - \hat{\alpha}_n v_n(\boldsymbol{x}) \right) + \sum_\mu \left(\hat{A}_\mu^\dagger u_\mu^*(\boldsymbol{x}) + \hat{B}_\mu^\dagger u_{*\mu}^*(\boldsymbol{x}) - \hat{A}_\mu v_\mu(\boldsymbol{x}) - \hat{B}_\mu v_{*\mu}(\boldsymbol{x}) \right), \tag{4.72}$$

where the index n refers to the real modes and the index μ to the complex ones. The operators $\hat{A}_\mu$, $\hat{A}_\mu^\dagger$, $\hat{B}_\mu$ *and* $\hat{B}_\mu^\dagger$ *are introduced to describe the complex modes which characterize the dynamical instability modes. The operators used in 4.71 and 4.72 satisfy*

$$\left[\hat{\alpha}_m, \hat{\alpha}_n^\dagger \right] = \delta_{mn} \tag{4.73}$$
$$\left[\hat{A}_\mu, \hat{B}_\nu^\dagger \right] = \delta_{\mu\nu} \tag{4.74}$$
$$\left[\hat{A}_\mu, \hat{A}_\nu^\dagger \right] = 0 \tag{4.75}$$
$$\left[\hat{B}_\mu, \hat{B}_\nu^\dagger \right] = 0 \tag{4.76}$$
$$\left[\hat{A}_\mu, \hat{B}_\nu \right] = 0. \tag{4.77}$$

The free Hamiltonian is then defined as

$$\hat{H}_0 = \sum_n \omega_n \hat{\alpha}_n^\dagger \hat{\alpha}_n + \sum_\mu \left(\lambda_\mu^* \hat{A}_\mu^\dagger \hat{B}_\mu + \lambda_\mu \hat{B}_\mu^\dagger \hat{A}_\mu \right). \tag{4.78}$$

The time evolution of the complex-sector operators is

$$\hat{A}_\mu(t) = e^{-i\lambda_\mu t} \hat{A}_\mu$$
$$\hat{B}_\mu(t) = e^{-i\lambda_\mu * t} \hat{B}_\mu$$
$$\hat{A}_\mu^\dagger(t) = e^{i\lambda_\mu^* t} \hat{A}_\mu^\dagger$$
$$\hat{B}_\mu^\dagger(t) = e^{i\lambda_\mu t} \hat{B}_\mu^\dagger \tag{4.79}$$

and the field can be finally expressed in terms of the contributions from normal mode and from dynamical instability modes in the form

$$\begin{aligned}\hat{\phi}(\boldsymbol{x},t) = &\sum_n \left(\hat{\alpha}_n e^{-i\omega_n t} u_n(\boldsymbol{x}) - \hat{\alpha}_n^\dagger e^{i\omega_n t} v_n^*(\boldsymbol{x})\right) \\ &+ \sum_\mu \left(\hat{A}_\mu e^{-i\lambda_\mu t} u_\mu(\boldsymbol{x}) + \hat{B}_\mu e^{-i\lambda_\mu^* t} u_{*\mu}(\boldsymbol{x})\right. \\ &\left. - \hat{A}_\mu^\dagger e^{i\lambda_\mu^* t} v_\mu^*(\boldsymbol{x}) - \hat{B}_\mu^\dagger e^{i\lambda_\mu t} v_{*\mu}^*(\boldsymbol{x})\right) \end{aligned} \tag{4.80}$$

and

$$\begin{aligned}\hat{\phi}^\dagger(\boldsymbol{x},t) = &\sum_n \left(\hat{\alpha}_n^\dagger e^{i\omega_n t} u_n^*(\boldsymbol{x}) - \hat{\alpha}_n e^{-i\omega_n t} v_n(\boldsymbol{x})\right) \\ &+ \sum_\mu \left(\hat{A}_\mu^\dagger e^{i\lambda_\mu^* t} u_\mu^*(\boldsymbol{x}) + \hat{B}_\mu^\dagger e^{i\lambda_* t} u_{*\mu}^*(\boldsymbol{x})\right. \\ &\left. - \hat{A}_\mu e^{-i\lambda_\mu t} v_\mu(\boldsymbol{x}) - \hat{B}_\mu e^{-i\lambda_\mu^* t} v_{*\mu}(\boldsymbol{x})\right). \end{aligned} \tag{4.81}$$

It can be checked that Equations 4.80 and 4.81 satisfy the bosonic commutation relations, Equations 4.33-4.35.

The nature of the complex-sector operators can be easier understood if they are expressed in terms of some new operators that will satisfy bosonic commutation relations [74, 79, 87]. In this representation, the following operators can be deduced

$$\begin{pmatrix}\hat{A}_\mu \\ \hat{B}_\mu\end{pmatrix} = \frac{1}{\sqrt{2}}\hat{b}_\mu \begin{pmatrix}1\\1\end{pmatrix} + i\tilde{b}_\mu^\dagger \begin{pmatrix}1\\-1\end{pmatrix} \Rightarrow \begin{pmatrix}\hat{b}_\mu \\ \tilde{b}_\mu\end{pmatrix} = \frac{1}{\sqrt{2}}\begin{pmatrix}\hat{A}_\mu + \hat{B}_\mu \\ i\left(\hat{A}_\mu^\dagger - \hat{B}_\mu^\dagger\right)\end{pmatrix}, \tag{4.82}$$

satisfying

$$\left[\hat{b}_\mu, \hat{b}_\nu^\dagger\right] = \delta_{\mu\nu} \tag{4.83}$$

$$\left[\tilde{b}_\mu, \tilde{b}_\nu^\dagger\right] = \delta_{\mu\nu}. \tag{4.84}$$

The free Hamiltonian 4.78 is then transformed into the form

$$\hat{H}_0 = \sum_n \omega_n \hat{\alpha}_n^\dagger \hat{\alpha}_n + \sum_\mu \left(\mathrm{Re}\{\lambda_\mu\}\left(\hat{b}_\mu^\dagger \hat{b}_\mu - \tilde{b}_\mu^\dagger \tilde{b}_\mu\right) + \mathrm{Im}\{\lambda_\mu\}\left(\hat{b}_\mu^\dagger \tilde{b}\mu^\dagger + \tilde{b}_\mu \hat{b}_\mu\right)\right). \tag{4.85}$$

Theorem 8. *The modes of the complex sector of Hamiltonian of 4.85 cannot be diagonalized by a Bogoliubov transformation [74].*

All this analysis has enlightened the properties of indefinite metric spaces (or Krein spaces as seen in Appendix C) describing the emergence of complex modes in the description of unstable BECs. The existence of two inner product spaces, the positive semi-definite one (the bosonic annihilation and creation operators for the normal modes) and the indefinite one, corresponding to the complex modes (describing dynamical instability modes), has further been elucidated.

Another important aspect that needs clarification is that the emergence of complex modes does not instantly imply the occurrence of dynamical instabilities. As in experiments, the quantity under consideration (for example the initial distribution of the density) remains static until some external perturbation perturbs the system under consideration. Then, the exponential decay/increase emerges.

The existence of complex modes is encased in the occurrence of an energy degeneracy between a positive and a negative-norm mode. Differently said, dynamical instabilities are the result of the resonant coupling between a phonon mode and an anti-phonon mode (between a positive and a negative-norm mode for a given frequency, in the black-hole laser case.). The fact that complex eigenvalues emerge as pairs in the Bogoliubov-de Gennes equations is due to the matrix, K, in 3.20 being real (See Appendix C). The total energy is conserved and, thus, dynamical instability modes have zero norm. The energy spectrum of Equation 4.52 can, in principle, contain some negative-frequency modes. As a result, if all eigenvalues of Equation 4.52 were positive, there would be no complex modes (and no possibility for a dynamical instability) in the Bogoliubov-de Gennes spectrum, Equation 4.50. The possibility of emergence of dynamical instability modes is enabled by the existence of energetic instabilities. Moreover, the system cannot be energetically stable when it is dynamically unstable, but it can be dynamically stable when energetically unstable.

When some of the eigenvalues of the matrix T in Equation 3.11 are negative, then an energetic or Landau-type instability occurs to the system. Elementary excitations are favored and the superfluid character of the condensate is lost, as the Landau criterion,

$$V < V_{cr} = \frac{\epsilon_0(\mathbf{q})}{|\mathbf{q}|}, \tag{4.86}$$

is not satisfied. In this equation, $\epsilon_0(\mathbf{q})$ is the energy of some excitations in the background of the moving fluid.

5 Black-Hole Lasers

5.1 A Classical Treatment

In this chapter, a configuration often termed *black-hole laser*, due to its resemblance with the laser effect and the subsequent growth of modes happening there will be discussed in depth. Analogue gravity models possessing one horizon consist of a really restricted set of different configurations, the analogue black hole, the simplified version of which has already been discussed, and the analogue white hole, the time-symmetric of the analogue black hole. By introducing a second horizon in an analogue configuration, many novel effects appear (see Figures 5.1 and 5.2). Inhomogeneous profiles with one horizon, in the BEC context, can be dynamically stable, but are necessarily energetically unstable, due to the emergence of negative-frequency modes; thus the appearance of superradiance effects, meaning the spontaneous production of correlated phonon pairs, one at each side of the horizon, with opposite energies. Now, by the introduction of a second horizon, flows with a finite supersonic Region in between of two infinite and asymptotically homogeneous subsonic ones are unstable because of a mechanism that leads to the amplification of the superradiant effects at each horizon. The black-hole laser consists of an analogue black hole and an analogue white hole.

The dynamical instability of the black-hole laser can be characterized by a complex spectrum in the Bogoliubov-de Gennes level in the BEC framework (and also in the linear regime for other configurations as well) with the unstable resonant cavity of the supersonic region triggering the introduction of more complex frequency modes by the increase of its width [90].

Before embarking on a fully BEC-based analysis of the effect, a more classical description will be given, based on a simple massless scalar field, as done in Chapter 2. This will bring back to attention the analogy between gravitational modes and the mean-field analysis with regard to Bose gases. The process of explaining the black-hole laser in this section will be based on Figure 5.1.

An incident wavepacket in the right subsonic region will be assumed, being in the mode ϕ_v^r and propagating with negative group velocity (see Figure 5.3). At the horizon, a mode-conversion process will occur. A reflected wavepacket will then be scattered in Region III in the ϕ_u^r mode, while the decaying mode ϕ_+^r also needs to be included in the description for a complete scattering description, as done in Section 3.3.1. In Region II, there will be two outgoing modes. Firstly, the ϕ_v^c mode belonging to the v-branch has positive frequency and negative group velocity and, then, the $\phi_{u_2}^c$ mode (which is a mode of counterpropagating-to-the-fluid nature) has negative-norm and negative group velocity and is being dragged by the flow, as the speed of sound, c, is smaller that the fluid velocity in this region. This mode-scattering analysis is redone by reaching the other

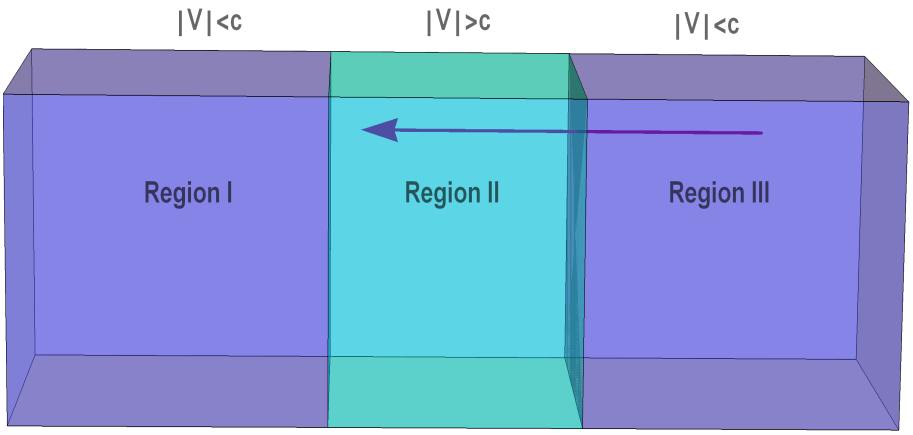

Figure 5.1: The black-hole laser consists of two subsonic regions, Region I and III, which extend towards infinity. The intermediate finite supersonic Region II acts as a resonant cavity giving rise to an exponential increase of negative norm modes.

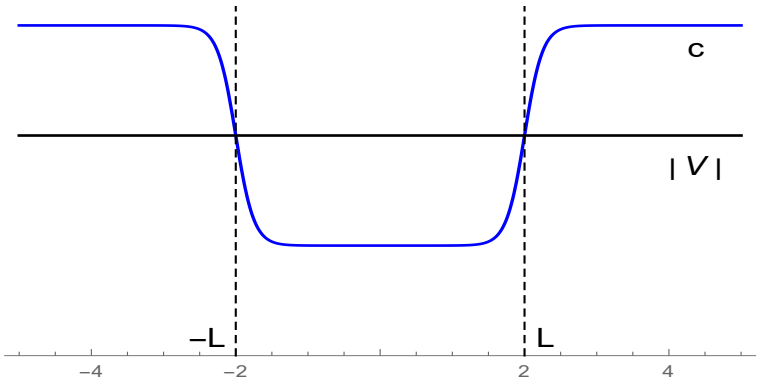

Figure 5.2: A constant velocity and a smooth speed of sound profile for the black-hole laser. The dashed lines indicate the horizons (scale is arbitrary).

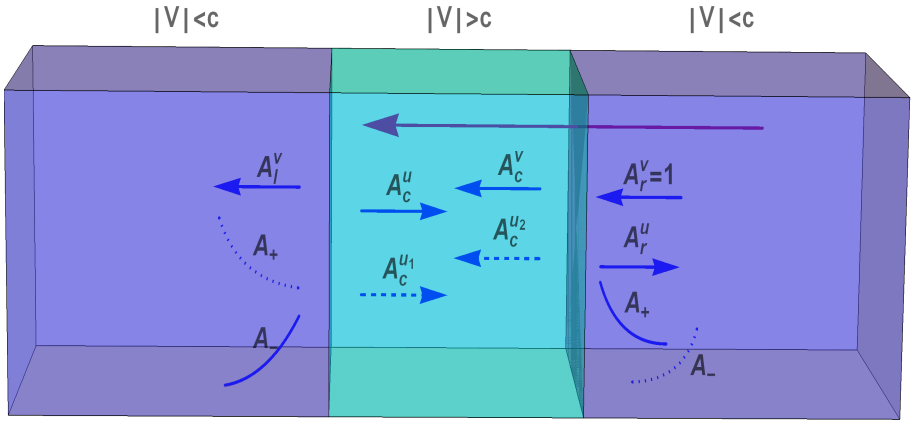

Figure 5.3: The mode decomposition for the black-hole laser. The modes are decomposed based on the same decomposition done for the analogue black hole case in Chapter 3. Negative-norm modes are indicated as dashed. The exponentially increasing or decreasing away from the horizon modes are represented with dotted and solid lines, respectively.

horizon as well, but with the difference that now the subsonic flow is downstream and the supersonic one upstream, on contrast to the analogue black hole's horizon decomposition. The second horizon resembles an analogue white hole. Across the analogue white hole's horizon, a second conversion process occurs. The ingoing modes lead to the existence, in Region I, of a travelling with positive norm and negative group velocity mode belonging to the ϕ_v^l sector and the decaying mode ϕ_-^l. In the supersonic regime, the positive-norm mode with positive group velocity ϕ_u^c and the negative-norm mode with positive group velocity $\phi_{u_1}^c$ exist. After the scattering across the analogue white hole's horizon, the two right-going modes in Region II propagate towards the analogue black hole horizon, where a new conversion process will occur. The two modes in the supersonic sector will give rise to a new ϕ_v^r and ϕ_+^r set of modes. In the supersonic region a new set of $\phi_{u_2}^c$ and ϕ_v^c modes will appear and the process will continue (see Figure 5.4) until the analogue black or white hole evaporates or until some nonlinear effects prevail.

Importantly, the norm of this evolving solution is conserved. This means that in each conversion process, equal amounts of negative and positive frequency occur, preserving energy in each process. With each bounce at a horizon, it can be seen that the negative-frequency mode in the supersonic region gets more 'populated'. After some conversions, an exponential increase will be manifest. As before, the size of the negative-frequency mode will define the particle production, as in the gravitational picture; but the number of particles in this mode is exponentially increased. This is the manifestation of the black-hole laser effect [37–40].

This process, analytically explained in the previous paragraphs, can be described by a four-level process, as can be readily seen from Figures 5.1-5.4. The process followed below is heavily influenced by the seminal works of [37, 38].

The Bogoliubov transformation that underlies linear particle creation can be visualised

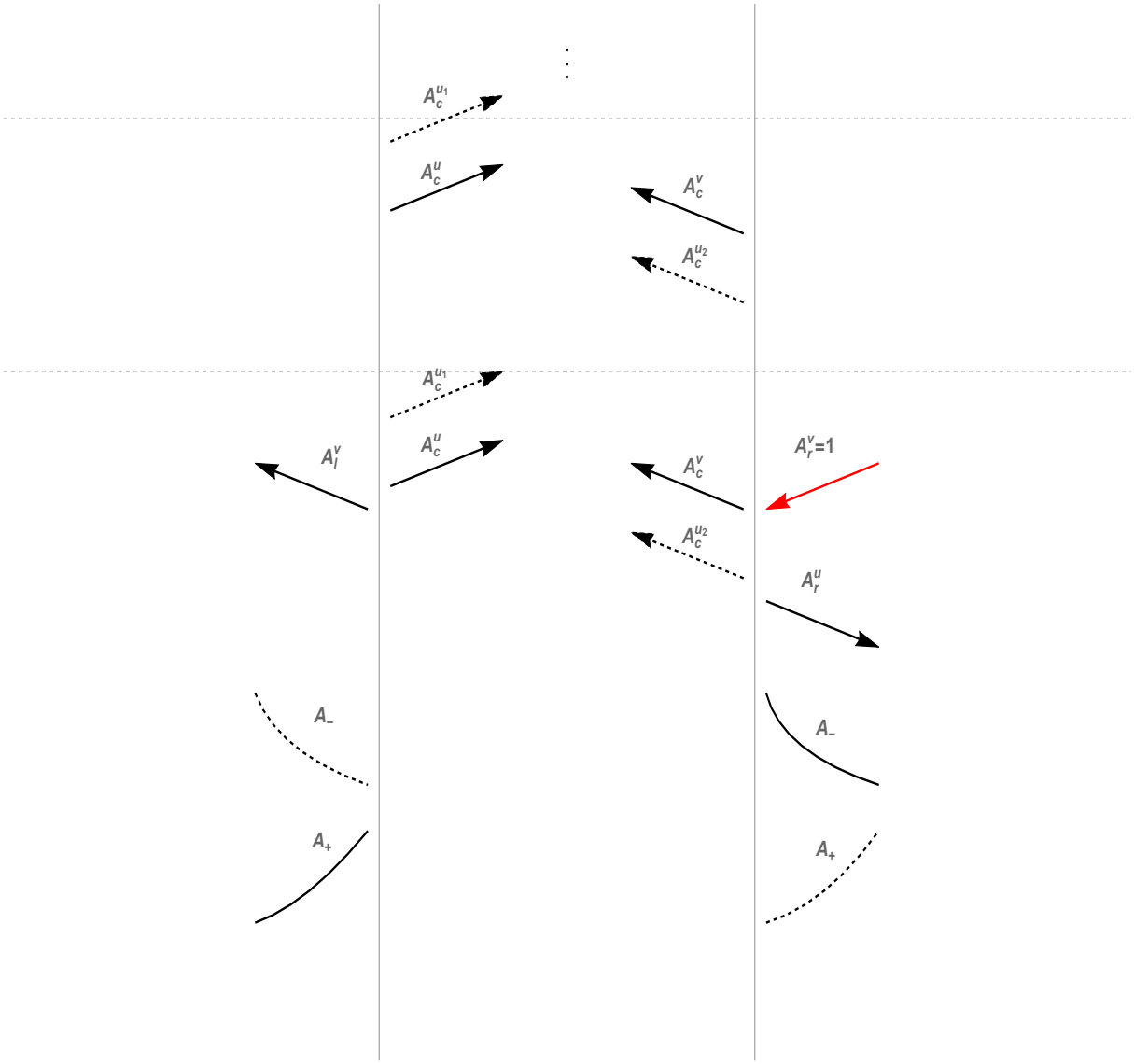

Figure 5.4: The black hole lasing effect described in cycles indicated by the horizontal dotted lines. Each cycle contributes to the exponential increase of the negative-frequency mode in the supersonic region, Region II.

as a general transformation of ingoing annihilation and creation operators, transformed in the outgoing basis as

$$\begin{pmatrix} \hat{\alpha}'_1 \\ \hat{\alpha}'_2 \\ \vdots \\ \hat{\alpha}'_{n-1} \\ \hat{\alpha}'_n \\ \hat{\alpha}'^{\dagger}_1 \\ \hat{\alpha}'^{\dagger}_2 \\ \vdots \\ \hat{\alpha}'^{\dagger}_{n-1} \\ \hat{\alpha}'^{\dagger}_n \end{pmatrix} = S \begin{pmatrix} \hat{\alpha}_1 \\ \hat{\alpha}_2 \\ \vdots \\ \hat{\alpha}_{n-1} \\ \hat{\alpha}_n \\ \hat{\alpha}^{\dagger}_1 \\ \hat{\alpha}^{\dagger}_2 \\ \vdots \\ \hat{\alpha}^{\dagger}_{n-1} \\ \hat{\alpha}^{\dagger}_n \end{pmatrix}, \tag{5.1}$$

where the scattering matrix is constrained by equation

$$S \eta S^{\dagger} = \eta \tag{5.2}$$

with

$$\eta = \begin{pmatrix} I & 0 \\ 0 & -I \end{pmatrix}, \tag{5.3}$$

where the identity matrix I has been introduced. Its dimension can vary, depending on the exact problem at hand. Scattering matrices belong to the $U(n, n)$ group and an example matrix is the

$$S = \begin{pmatrix} \cosh\rho & 0 & 0 & \sinh\rho \\ 0 & \cosh\rho & \sinh\rho & 0 \\ 0 & \sinh\rho & \cosh\rho & 0 \\ \sinh\rho & 0 & 0 & \cosh\rho \end{pmatrix}, \tag{5.4}$$

which is described similarly to the parametric amplifier case in optics [91]. The quantity ρ can be defined with respect to the surface gravity across the horizon and the frequency of the modes considered.

As a result, the Bogoliubov transformations due to the analogue white and black holes can be written as

$$\begin{pmatrix} \hat{\alpha}'_1 \\ \hat{\alpha}'^{\dagger}_2 \end{pmatrix} = \begin{pmatrix} \cosh\zeta & -\sinh\zeta \\ -\sinh\zeta & \cosh\zeta \end{pmatrix} \begin{pmatrix} \hat{\alpha}_1 \\ \hat{\alpha}^{\dagger}_2 \end{pmatrix} \tag{5.5}$$

and

$$\begin{pmatrix} \hat{\alpha}'_1 \\ \hat{\alpha}'^{\dagger}_2 \end{pmatrix} = \begin{pmatrix} \cosh\rho & \sinh\rho \\ \sinh\rho & \cosh\rho \end{pmatrix} \begin{pmatrix} \hat{\alpha}_1 \\ \hat{\alpha}^{\dagger}_2 \end{pmatrix}, \tag{5.6}$$

respectively.

The four-step process described previously can be visualized by the following unitary 'Bogoliubov' matrices

$$U = U_4U_3U_2U_1 = \begin{pmatrix} e^{-i\theta_0} & 0 \\ 0 & 1 \end{pmatrix}\begin{pmatrix} \cosh\zeta & -\sinh\zeta \\ -\sinh\zeta & \cosh\zeta \end{pmatrix}\begin{pmatrix} e^{i\theta_-} & 0 \\ 0 & e^{i\theta_+} \end{pmatrix}\begin{pmatrix} \cosh\rho & \sinh\rho \\ \sinh\rho & \cosh\rho \end{pmatrix} \tag{5.7}$$

and then the scattering matrix will be of the form

$$S = U^n, \tag{5.8}$$

where n denotes the number of amplification steps. Each step includes the action of U_1, U_2, U_3 and U_4. The matrix U_1 describes the mode conversion process across the black hole horizon, U_2 the propagation of modes in Region II, U_3 the conversion process across the analogue white hole's horizon and U_4 the propagation back to the black hole horizon. This four-step process can take place multiple times, until some external constraints are imposed. At each propagation time between the two horizons, the two modes acquire separate phases. One phase is a free parameter and can be set to zero.

When the Bogoliubov matrices U_i satisfy the equation of the scattering matrix equation, Equation 5.2, then the elements of the matrix U should satisfy equations

$$|U_{11}|^2 - |U_{12}|^2 = 1 \tag{5.9}$$

$$|U_{21}|^2 - |U_{22}|^2 = 1 \tag{5.10}$$

$$U_{11}^* U_{21} - U_{12}^* U_{22} = 0 \tag{5.11}$$

due to unitarity and then, as U should be a $U(1,1)$ matrix,

$$U = e^{i\kappa}\begin{pmatrix} \mu & \nu^* \\ \nu & \mu^* \end{pmatrix} \tag{5.12}$$

with $|\mu|^2 - |\nu|^2 = 1$ and

$$\begin{aligned} |\mu|^2 &= \frac{1}{2}\Big(1 + \cosh(2\rho)\cosh(2\zeta) - \cos(\theta_+ + \theta_-)\sinh(2\rho)\sinh(2\zeta)\Big) \Rightarrow \\ |\mu|^2 &= \begin{cases} \frac{1}{2}\Big(1 + \cosh(2\rho)\cosh(2\zeta) - \sinh(2\rho)\sinh(2\zeta)\Big) \\ \frac{1}{2}\Big(1 + \cosh(2\rho)\cosh(2\zeta) + \sinh(2\rho)\sinh(2\zeta)\Big) \end{cases} \end{aligned} \tag{5.13}$$

with the two choices indicating maximal suppression ($\cos(\theta_+ + \theta_-) = 1$) and maximal amplification ($\cos(\theta_+ + \theta_-) = -1$), respectively. The maximal amplification condition translates into

$$\theta_+ + \theta_- = 2\pi\left(m + \frac{1}{2}\right), \tag{5.14}$$

with $m \in \mathbb{Z}$. The phase θ_0 is not included in this relation, as modes from the subsonic regions have no phase sensitivity. Indeed, the phase content that is included is the phase difference between the two modes $\theta_+ + \theta_-$ that propagate across the supersonic regime.

After n-amplification steps, the negative-frequency mode trapped in the supersonic region leads the annihilation operator to obtain a form

$$\hat{\alpha}'_{-n} = e^{in\kappa}\mu^n\hat{\alpha}_{-1} + \nu^* \sum_{l=1}^{n} e^{i(n-l+1)\kappa}\mu^{n-l}\hat{\alpha}^\dagger_{+l} \tag{5.15}$$

and the respective of the positive-frequency mode in the subsonic region to be

$$\hat{\alpha}'^\dagger_{+n} = e^{in\kappa}\nu\mu^{n-1}\hat{\alpha}_{-1} + |\nu|^2 \sum_{l=1}^{n-1} e^{i(n-1)\kappa}\mu^{n-l-1}\hat{\alpha}^\dagger_{+l} + e^{i\kappa}\mu^*\hat{\alpha}^\dagger_{+n} \tag{5.16}$$

with the vacuum conditions

$$\begin{aligned} \hat{\alpha}_{-1}\,|0\rangle &= 0 \\ \hat{\alpha}_{+l}\,|0\rangle &= 0 \end{aligned} \tag{5.17}$$

and $l = 1, \ldots, n$. The particle number content for modes in the supersonic and subsonic regions is respectively found to be

$$\begin{aligned} \left\langle \hat{N}_{-n} \right\rangle &= \left\langle \hat{\alpha}'^\dagger_{-n}\hat{\alpha}'_{-n} \right\rangle \\ &= |\mu|^{2n} - 1 \end{aligned} \tag{5.18}$$

and

$$\left\langle \hat{N}_{+n} \right\rangle = \left\langle \hat{\alpha}'^\dagger_{+n}\hat{\alpha}'_{+n} \right\rangle \tag{5.19}$$

$$= |\mu|^{2n}\left(1 - \frac{1}{|\mu|^2}\right). \tag{5.20}$$

5.2 Mode analysis for the black-hole laser

In configurations where the speed of sound crosses the velocity of the moving fluid once (see Figure 1.1), it has been seen that there exist 2 travelling modes, one exponentially decreasing and another exponentially increasing in the subsonic region and two ingoing and two outgoing modes in the supersonic region. For the black-hole laser, the situation is a bit more intricate, as complex frequency modes 'usually' occur as well (see Chapter 4). Now, the matching conditions at the horizons for the two 'discontinuities' encountered between the three regions of a black-hole laser will be introduced. For the rest of this section, steplike profiles for the speed of sound across the configuration will be used, while the background velocity will be considered constant.

For this reason, the field in each region is expressed as a superposition of the available mode-functions. On the left and on the right side, the field can be decomposed as

$$\phi_\omega = \sum_i \mathcal{L}^i_\omega \phi^{i,l}_\omega \tag{5.21}$$

$$\phi_\omega = \sum_i \mathcal{R}^i_\omega \phi^{i,r}_\omega, \tag{5.22}$$

where l, r denote the left and right to the supersonic cavity regions I and III and $\mathcal{L}^i_\omega$ and $\mathcal{R}$ are the coefficients of this decomposition. The field ϕ is used in the same way as in Equation 3.42[1]. By matching modes $\phi^{i,l/r}_\omega$ across the horizons with the components of the decomposed in Region II field, one obtains

$$\phi^{i,l}_\omega = \sum_j \mathfrak{Q}^{ij}_\omega \phi^{j,c}_\omega \tag{5.23}$$

$$\phi^{i,r}_\omega = \sum_j \mathfrak{R}^{ij}_\omega \phi^{j,c}_\omega \tag{5.24}$$

and the matrix equation

$$\sum_{i=u,v,dec} \left(\mathcal{L}^i_\omega \sum_{j=v,u,u_1,u_2} \mathfrak{Q}^{ij}_\omega - \mathcal{R}^i_\omega \sum_{j=v,u,u_1,u_2} \mathfrak{R}^{ij}_\omega \right) \phi^{j,c}_\omega = 0 \tag{5.25}$$

with *dec* denoting the decaying mode towards infinity in each case. This reduces to the equation

$$\sum_i \mathfrak{R}^{ij}_\omega \mathcal{R}^i_\omega = \sum_i \mathfrak{Q}^{ij}_\omega \mathcal{L}^i_\omega. \tag{5.26}$$

The notation $\phi^{l/c/r}$ is used for the field in each left, central and right region, respectively with

$$\mathcal{L}^u_\omega \mathfrak{Q}^{u\,v}_\omega + \mathcal{L}^v_\omega \mathfrak{Q}^{v\,v}_\omega + \mathcal{L}^{dec}_\omega \mathfrak{Q}^{dec\,v}_\omega = \mathcal{R}^u_\omega \mathfrak{R}^{u\,v}_\omega + \mathcal{R}^v_\omega \mathfrak{R}^{v\,v}_\omega + \mathcal{R}^{dec}_\omega \mathfrak{R}^{dec\,v}_\omega \tag{5.27}$$

$$\mathcal{L}^u_\omega \mathfrak{Q}^{u\,u}_\omega + \mathcal{L}^v_\omega \mathfrak{Q}^{v\,u}_\omega + \mathcal{L}^{dec}_\omega \mathfrak{Q}^{dec\,u}_\omega = \mathcal{R}^u_\omega \mathfrak{R}^{u\,u}_\omega + \mathcal{R}^v_\omega \mathfrak{R}^{v\,u}_\omega + \mathcal{R}^{dec}_\omega \mathfrak{R}^{dec\,u}_\omega \tag{5.28}$$

$$\mathcal{L}^u_\omega \mathfrak{Q}^{u\,u_1}_\omega + \mathcal{L}^v_\omega \mathfrak{Q}^{v\,u_1}_\omega + \mathcal{L}^{dec}_\omega \mathfrak{Q}^{dec\,u_1}_\omega = \mathcal{R}^u_\omega \mathfrak{R}^{u\,u_1}_\omega + \mathcal{R}^v_\omega \mathfrak{R}^{v\,u_1}_\omega + \mathcal{R}^{dec}_\omega \mathfrak{R}^{dec\,u_1}_\omega \tag{5.29}$$

$$\mathcal{L}^u_\omega \mathfrak{Q}^{u\,u_2}_\omega + \mathcal{L}^v_\omega \mathfrak{Q}^{v\,u_2}_\omega + \mathcal{L}^{dec}_\omega \mathfrak{Q}^{dec\,u_2}_\omega = \mathcal{R}^u_\omega \mathfrak{R}^{u\,u_2}_\omega + \mathcal{R}^v_\omega \mathfrak{R}^{v\,u_2}_\omega + \mathcal{R}^{dec}_\omega \mathfrak{R}^{dec\,u_2}_\omega \tag{5.30}$$

for a single mode-function (doubled for both of them).

This is a system of four equations with six unknowns, coefficients $\mathcal{L}$ and $\mathcal{R}$, when considering just one of the mode-functions, as stated above. The real modes of the system will now be dealt with. For both mode-functions of the system, there are eight equations

[1]Note that the total field can be decomposed as

$$\hat{\phi} = \int_0^\infty \mathrm{d}\omega \Big(e^{-i\omega t} \Big(\hat{\alpha}^u_\omega \phi^u_\omega + \hat{\alpha}^v_\omega \phi^v_\omega + \theta(\omega_{max} - \omega) \sum_{i=u_1,u_2} \hat{\alpha}^{(i)\,\dagger}_{-\omega} \varphi^{(i)\,*}_{-\omega} \Big) + e^{i\omega t} \Big(\hat{\alpha}^{u\,\dagger}_\omega \varphi^{u\,*}_\omega + \hat{\alpha}^{v\,\dagger}_\omega \varphi^{v\,*}_\omega + \theta(\omega_{max} - \omega) \sum_{i=u_1,u_2} \hat{\alpha}^{(i)}_{-\omega} \phi^{(i)}_{-\omega} \Big) \Big)$$

in the supersonic and as

$$\hat{\phi} = \int_0^\infty \mathrm{d}\omega \left(e^{-i\omega t} \left(\hat{\alpha}^u_\omega \phi^u_\omega + \hat{\alpha}^v_\omega \phi^v_\omega \right) + e^{i\omega t} \left(\hat{\alpha}^{u\,\dagger}_\omega \varphi^{u\,*}_\omega + \hat{\alpha}^{v\,\dagger}_\omega \varphi^{v\,*}_\omega \right) \right)$$

in the subsonic region, respectively.

in total with twelve unknowns. Each mode-function has a set of two linearly independent solutions. For this reason, any combinations of these modes can be chosen. For example, for one of the mode-functions, one of these combinations could be the modes $\phi_\omega^{u,in}$ and $\phi_\omega^{v,in}$. For this solution, the coefficients are $\mathcal{L}_u = 1, \mathcal{R}_v = 0$ or $\mathcal{L}_u = 0, \mathcal{R}_v = 1$ for the two right-going and left-going modes, respectively. With the help of the Bogoliubov transformation, these modes can be written as

$$\phi_\omega^{u,in} = \mathcal{T}_\omega \phi_\omega^{u,out} + \mathcal{R}_\omega \phi_\omega^{v,out} \tag{5.31}$$

$$\phi_\omega^{v,in} = \tilde{\mathcal{R}}_\omega \phi_\omega^{u,out} + \tilde{\mathcal{T}}_\omega \phi_\omega^{v,out}, \tag{5.32}$$

with unitarity condition

$$|\mathcal{T}_\omega|^2 + |\mathcal{R}_\omega|^2 = \left|\tilde{\mathcal{T}}_\omega\right|^2 + \left|\tilde{\mathcal{R}}_\omega\right|^2 = 1 \tag{5.33}$$

$$\mathcal{R}_\omega \tilde{\mathcal{T}}_\omega^* + \mathcal{T}_\omega \tilde{\mathcal{R}}_\omega^* = 0. \tag{5.34}$$

For the case of complex eigenvalues, $\lambda = \omega + i\Gamma$, the situation is different. We again need to impose that modes are asymptotically bound. After the acquisition of an imaginary part, $\Gamma > 0$, the mode k_λ^u gains a positive imaginary part and thus diverges at $x \to -\infty$, unless $\mathcal{L}^u = 0$. Furthermore, the v-mode will acquire an imaginary part and diverge at $x \to +\infty$, unless $\mathcal{R}^v = 0$. These two conditions mean that the system 5.26 will only have the solution $\mathcal{L}^i = \mathcal{R}^i = 0$, when considering both mode-functions, or that the determinant from the respective equations, Equations 5.27-5.30, will vanish[2]. This is exactly the condition for finding the complex frequency modes in a black-hole laser. This is the matrix condition that will be used in order to find the emergence of instability in the black-hole laser case for a one-component BEC.

5.2.1 Semiclassical analysis for real modes for a black-hole laser from a one-component BEC

Let us now continue the treatment of the previous section, improving the example-based classical description of the black-hole laser in Section 5.1. The same process in constructing the scattering matrix (found in Figure 5.5) will follow, but with the inclusion of an important new constraint. In this case, the most general case for the unitary matrices will be discussed, after gaining the experience needed from the specific example already dealt with.

For the analysis, steplike velocity profiles will be considered. For smooth profiles, a WKB (Wentzel-Kramers-Brillouin) analysis is usually performed for treating the asymptotic regions [48, 92]. In this case, the wavevectors acquire some spatial dependence in first approximation [48, 92].

Numerical results have shown that in a first approximation, one can safely assume no mixing between u- and v-modes [20, 31, 40]. This means that in the scattering analysis,

[2]The analysis follows the same path for both mode-functions. Results found for one of them can be just duplicated in order to get the full picture.

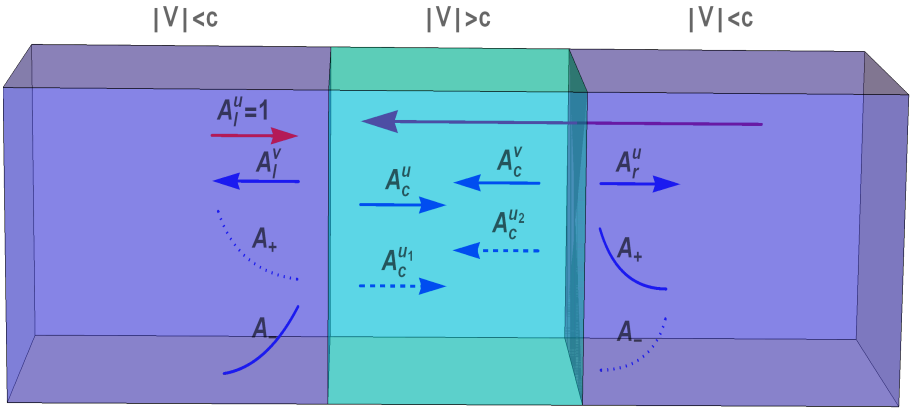

Figure 5.5: A one-component BEC with a background flow forming a black-hole laser. When compared with Figures 5.4 and 5.3, an ingoing u^l mode is now used.

one can ignore the v-modes and discuss only the effects coming from the u-modes. In this approximation, the u-modes completely characterize the black-hole laser effect. The ingoing u-mode in Region I, as in Figure 5.5, can be expressed in terms of the modes in the central supersonic regime

$$\phi_\omega^{u,in} = \mathcal{A}_\omega \phi_\omega^u + \mathcal{B}_\omega^{u_1 *} \phi_{-\omega}^{u_1 *} + \mathcal{B}_\omega^{u_2 *} \phi_{-\omega}^{u_2 *}. \tag{5.35}$$

The modes of negative norm are included as complex conjugated. Then, the scattering of ingoing modes in terms of outgoing ones from one horizon to the other needs to be taken into account. As the v-modes have been omitted in this analysis, the the scattering can be described by a two-component vector[3],

$$\Phi = \begin{pmatrix} \phi_\omega^u \\ \phi_{-\omega}^{tr*} \end{pmatrix}, \tag{5.36}$$

with tr denoting the trapped mode of negative norm (meaning the $\phi_{-\omega}^{u_1}$ or the $\phi_{-\omega}^{u_2}$ modes) and the modes of u-character, meaning the u-modes in the subsonic regions I and III and the supersonic regime (see Figure 5.5). In this treatment, the example-based analysis of Section 5.1 will be abandoned and the most general forms of the same unitary matrices will be used. The first matrix, U_1, will again describe the scattering of the incoming right-going mode ϕ_ω^u and of the incoming left-going negative-norm mode $\phi_\omega^{(2)}$ across the analogue white hole's horizon, the second, U_2, the propagation towards the analogue black hole's horizon in the central supersonic regime, the third matrix, U_3, the scattering across the analogue black hole's horizon and the fourth, U_4, the propagation back towards the analogue white hole's horizon for the trapped mode and through the right subsonic

[3]Note that here the capital letter Φ is used to denote the following vector and is not related with the same symbol as used in Chapter 3

region for the right-going u-mode,

$$U_1 = \begin{pmatrix} \alpha_\omega & \alpha_\omega z_\omega \\ \tilde{\alpha}_\omega z_\omega * & \tilde{\alpha}_\omega \end{pmatrix} \tag{5.37}$$

$$U_2 = \begin{pmatrix} e^{iS^u_\omega} & 0 \\ 0 & e^{-iS^{(1)}_{-\omega}} \end{pmatrix} \tag{5.38}$$

$$U_3 = \begin{pmatrix} \gamma_\omega & \gamma_\omega w_\omega \\ \tilde{\gamma}_\omega w_\omega * & \tilde{\gamma}_\omega \end{pmatrix} \tag{5.39}$$

$$U_4 = \begin{pmatrix} 1 & 0 \\ 0 & e^{-iS^{(2)}_{-\omega}} \end{pmatrix}, \tag{5.40}$$

with[4]

$$|\alpha_\omega|^2 = |\tilde{\alpha}_\omega|^2 \tag{5.41}$$

$$|\gamma_\omega|^2 = |\tilde{\gamma}_\omega|^2 \tag{5.42}$$

$$|\alpha_\omega|^2 \left(1 - |z_\omega|^2\right) = |\gamma_\omega|^2 \left(1 - |w_\omega|^2\right) = 1, \tag{5.43}$$

due to the unitarity of the U_i matrices[5], and

$$S^u_\omega = \int_{-L}^{L} \mathrm{d}x\, k^u_\omega(x) = 2Lk^u_\omega \tag{5.44}$$

$$S^{u_1}_{-\omega} = \int_{L_\omega}^{R_\omega} \mathrm{d}x \left(-k^{u_1}_\omega(x)\right) = -2Lk^{u_1}_\omega \tag{5.45}$$

$$S^{u_2}_{-\omega} = \int_{L_\omega}^{R_\omega} \mathrm{d}x \left(-k^{u_2}_\omega(x)\right) = -2Lk^{u_2}_\omega. \tag{5.46}$$

The last equality for Equations 5.44-5.46 holds for steplike profiles.

The limits of integration denote the length of the supersonic regime, extending from $-L$ to L. The points L_ω and R_ω generally do not correspond to the horizons. They correspond to the turning points [31]. In first approximation, any nontrivial effects can be neglected and the wavevectors are assumed to possesses no spatial dependence, which considerably reduces the integrals involved.

From this scattering process, the elements of the scattering matrix can be found in terms

[4]The unit element in U_4 reflects the freedom of choosing the initial ingoing mode in the left region, being of unit amplitude, see also Sections 5.1 or 3.3.1.

[5]Note that unitarity in 5.31 sums the respective elements of each row, while here it subtracts. This is exactly the influence (and the signature) of the negative-norm mode (see also Section 3.3.1)

of the coefficients of the unitary matrices in 5.37-5.40, as

$$S_{11} = \alpha_\omega \gamma_\omega e^{iS^u_\omega} \left(1 + \frac{\tilde{\alpha}_\omega}{\alpha_\omega} z^*_\omega w_\omega e^{-iu\left(S^u_\omega + S^{u_1}_{-\omega}\right)}\right) \tag{5.47}$$

$$S_{12} = \alpha_\omega \gamma_\omega e^{iS^u_\omega} \left(z_\omega + \frac{\tilde{\alpha}_\omega}{\alpha_\omega} w_\omega e^{-iu\left(S^u_\omega + S^{u_1}_{-\omega}\right)}\right) \tag{5.48}$$

$$S_{21} = \tilde{\alpha}_\omega \tilde{\gamma}_\omega e^{-i\left(S^{u_1}_\omega - S^{u_2}_\omega\right)} \left(z^*_\omega + \frac{\alpha_\omega}{\tilde{\alpha}_\omega} w^*_\omega e^{iu\left(S^u_\omega + S^{u_1}_{-\omega}\right)}\right) \tag{5.49}$$

$$S_{22} = \tilde{\alpha}_\omega \tilde{\gamma}_\omega e^{-i\left(S^{u_1}_\omega - S^{u_2}_\omega\right)} \left(1 + \frac{\alpha_\omega}{\tilde{\alpha}_\omega} z_\omega w^*_\omega e^{iu\left(S^u_\omega + S^{u_1}_{-\omega}\right)}\right). \tag{5.50}$$

Now, the scattering matrix will describe the propagation of the ingoing u-mode from Region I, through Region II, to Region III, but also the bouncing of the negative-norm mode at the horizons. This process will give rise to the lasing effect. After each time, Φ, which represents physical solutions of the scattering, is imposed to be *single-valued*. The value of the negative-norm mode impinging on the analogue white hole's horizon, due to U_4, will have the same amplitude before and after the action of the scattering matrix S on it. The same follows for the other negative mode as well.

Then, the scattering can be characterized by the equation

$$\begin{pmatrix} e^{i\theta_\omega} \\ b_\omega \end{pmatrix} = S \begin{pmatrix} 1 \\ b_\omega \end{pmatrix}, \tag{5.51}$$

where the amplitude $B^{u_2}_\omega$ is assumed to be $B^{u_2}_\omega = b_\omega$ and the phase θ_ω is real from unitarity. This means that

$$b_\omega = \frac{S_{21}}{1 - S_{22}} \tag{5.52}$$

$$e^{i\theta_\omega} = S_{11} + S_{12} b_\omega = -\frac{S_{11}}{S_{22}*} \frac{1 - S^*_{22}}{1 - S_{22}}, \tag{5.53}$$

where the last property is a direct consequence of the unitarity of S. From Equation 5.35, $\mathcal{A}_\omega$ and $\mathcal{B}^{u_1}_\omega$ can now be found from U_1 by setting $\mathcal{B}^{u_2}_\omega = b_\omega$[6],

$$\mathcal{A}_\omega = \alpha_\omega \left(1 + z_\omega b_\omega\right) \tag{5.54}$$

$$\mathcal{B}^{u_1}_\omega = \tilde{\alpha}_\omega \left(z^*_\omega + b_\omega\right) \tag{5.55}$$

$$\mathcal{B}^{u_2}_\omega = b_\omega. \tag{5.56}$$

After having concluded with the analysis for no u-v mixing, these results can also be extended to include u-v mixing. The inclusion of the v-modes in the analysis hardly makes any changes. The ingoing field in the subsonic left region is now

$$\phi^{u,in}_\omega = \mathcal{A}_\omega \phi^u_\omega + \mathcal{A}^v_\omega \phi^v_\omega + \mathcal{B}^{u_1 *}_\omega \phi^{u_1 *}_{-\omega} + \mathcal{B}^{u_2 *}_\omega \phi^{u_2 *}_{-\omega}, \tag{5.57}$$

[6]The outgoing modes from the analogue white hole's horizon are expressed via the unitary matrix U_1 as

$$\begin{pmatrix} \mathcal{A}_\omega \\ \mathcal{B}^{u_1}_\omega \end{pmatrix} = \begin{pmatrix} \alpha_\omega & \alpha_\omega z_\omega \\ \tilde{\alpha}_\omega z^*_\omega & \tilde{\alpha}_\omega \end{pmatrix} \begin{pmatrix} 1 \\ b_\omega \end{pmatrix}$$

for this reason.

but with

$$\phi^{u,in}_{\omega} = \phi^{u}_{\omega} + \mathcal{R}_{\omega}\phi^{v}_{\omega} \tag{5.58}$$

in the left region, while in the right subsonic region it asymptotes to $\mathcal{T}_{\omega}\phi^{u}_{\omega}$. The coefficients of this decomposition are again be found from the matching conditions across the two horizons. Now, at each horizon a triplet of modes (compared to the doublet, for no mixing) exists,

$$\begin{pmatrix} \phi^{u}_{\omega} \\ \phi^{v}_{\omega} \\ \phi^{tr*}_{-\omega} \end{pmatrix}. \tag{5.59}$$

From the scattering at each horizon, the following equations are found

$$\begin{pmatrix} \mathcal{A}_{\omega} \\ \mathcal{R}_{\omega} \\ \mathcal{B}^{u_1}_{\omega} \end{pmatrix} = S_{WH} \begin{pmatrix} 1 \\ \mathcal{B}_{\omega} \\ \mathcal{B}^{u_2}_{\omega} \end{pmatrix} \tag{5.60}$$

and

$$\begin{pmatrix} \mathcal{T}_{\omega} e^{iS^{u}_{\omega}} \\ \mathcal{A}^{v}_{\omega} e^{iS^{v}_{\omega}} \\ \mathcal{B}^{u_2}_{\omega} e^{-iS^{u_2}_{-\omega}} \end{pmatrix} = S_{BH} \begin{pmatrix} \mathcal{A}^{u}_{\omega} e^{iS^{u}_{\omega}} \\ 0 \\ \mathcal{B}^{u_1}_{\omega} e^{-iS^{u_1}_{-\omega}} \end{pmatrix}, \tag{5.61}$$

which fix the coefficients $\mathcal{A}^{i}_{\omega}$ and $\mathcal{B}^{j}_{\omega}$, with $i = \{u, v\}$ and $j = \{u_1, u_2\}$ and the $\mathcal{R}_{\omega}$ and $\mathcal{T}_{\omega}$ functions.

Each of the elements in the matrices S_{WH} and S_{BH} are found through the analysis of the ingoing modes in terms of the outgoing ones (or, equally, by constructing the outgoing modes in terms of the ingoing ones), as done in Chapter 3 based on Figure 3.14. To find the scattering decomposition for the analogue black hole's horizon, the three sets of four coupled equations (in total twelve equations) for the analogue black hole's horizon and the respective three sets for the analogue white hole's horizon need to be solved. In total, there are thirty equations (twelve for the scattering across the analogue white hole's horizon, twelve for the scattering across the analogue black hole's horizon and six from Equations 5.60 and 5.61), which need to be solved numerically (or analytically in some lower order approximation, as done in Chapter 3), in order to fully characterize the real modes across the black-hole laser configuration.

5.2.2 Semiclassical analysis for complex modes for a black-hole laser from a one-component BEC

Let us now deal with the possibility of the emergence of complex-frequency modes. The same scattering decomposition is again followed, but different conditions for the outgoing modes are now imposed.

At first, the complex frequencies $\lambda = \omega + i\Gamma$ are assumed to have $\Gamma > 0$[7]. In Region I, the ingoing u-mode will need to vanish in order to ensure its finiteness for $t \to -\infty$. The trapped mode is again assumed to be single-valued. It can be chosen to have unit amplitude and, then, the relation for the complex-mode scattering gets

$$\begin{pmatrix} \beta \\ 1 \end{pmatrix} = \begin{pmatrix} S_{11} & S_{12} \\ S_{21} & S_{22} \end{pmatrix} \begin{pmatrix} 0 \\ 1 \end{pmatrix} \tag{5.62}$$

with

$$\beta = S_{12} \tag{5.63}$$

$$S_{22} = 1. \tag{5.64}$$

From the two parallel analyses followed for real and complex modes, a relation between them can be identified; when a complex frequency exists for Equation 5.64, it is also a pole for the coefficient $\mathcal{B}_{\omega}^{u_2} = b_{\omega}$ in Equation 5.52. When Γ is small, then $\mathcal{B}_{\omega}^{u_2}$ is dominated by the contribution of the pole[8].

Having concluded the scattering analysis, what follows is the calculation of the dynamical instability modes for the black-hole laser. In later stages of the evolution of the black-hole laser, the real modes will be drown by the exponential amplification caused by the complex modes. As it has become clear until now, there exist two equally valid processes for their acquisition. We have chosen to follow the matching matrix route, through Equation 5.26. The next section will be devoted to this analysis.

5.3 Matching matrix analysis for complex frequencies

Let us consider stationary solutions of the Gross-Pitaevskii equation ($\hbar = m = c = 1$),

$$i\partial_t \psi = -\frac{1}{2}\partial_x^2 \psi + V_j(x)\psi + g_j |\psi|^2 \psi, \tag{5.65}$$

of the form

$$\psi(t, x) = e^{-i\mu t} f(x) e^{i\theta(x)}, \tag{5.66}$$

with μ denotes the chemical potential and $f = n^2$ denotes the amplitude of the wavefunction[9].

Then, by using the definition of the conserved current (with respect to the velocity, $V = \partial_x \theta$),

$$J = V = n\partial_x \theta = f^2 \partial_x \theta, \tag{5.67}$$

[7] This is always the signal of some dynamically instability mode. Modes with $\Gamma < 0$ will denote the complex conjugates of each pair of complex modes, which are decaying in time, as shown in Chapter 4

[8] For further details, see [39, 92].

[9] In this section, the variable f instead of the density, n, will be used which will simplify some of the calculations for the matching matrix.

the ordinary differential equation

$$\partial_x^2 f = 2g_j f^3 - 2\mu_j f + \frac{J^2}{f^3} \tag{5.68}$$

is obtained, where the index j takes values in the set $j = \{\mathrm{I}, \mathrm{II}, \mathrm{III}\}$ of the respective region of the black-hole laser.

Then, a homogeneous solution with $f = f_0$ is also assumed to exist across all regions of the black-hole laser (with subsonic flow in regions I and III and supersonic flow for Region II [93]). Perturbations of the homogeneous solution, with $c_j^2 = g_j f_0^2$, $J = V f_0^2$ are being used for the equilibrium value $f = f_0$ and $\theta_0(x) = \frac{xJ}{f_0^2}$, of the form

$$f(t, x) = f_0 + \delta f(t, x) \tag{5.69}$$

$$\theta(t, x) = \theta_0(x) + \delta\theta(t, x). \tag{5.70}$$

The zeroth-order resulting equation reads

$$\mu_j = \frac{1}{2} f_0 V^2 + g_j f_0^2, \tag{5.71}$$

where it is used that $\mu_j = \mu - V_j(x)$, with $V_j(x)$ the potential in each region (see Equation 5.65).

The first-order equations are found to be

$$(\partial_t + V\partial_x)\,\delta f = -f_0 \partial_x^2 \delta\theta \tag{5.72}$$

$$f_0\,(\partial_t + V\partial_x)\,\delta\theta = \left(\mu_j - 3g_j f_0^2 - \frac{V^2}{2} + \frac{1}{2}\partial_x^2\right)\delta f. \tag{5.73}$$

Then, solutions of Equations 5.72 and 5.73 in the plane wave form are assumed,

$$\delta f = A_f e^{-i(\omega t - kx)} \tag{5.74}$$

$$\delta\theta = A_\theta e^{-i(\omega t - kx)}. \tag{5.75}$$

The resulting linear equations give

$$\frac{A_\theta}{A_f} = \frac{-2i\Omega}{f_0 k^2} \tag{5.76}$$

with

$$\Omega = \omega - kV = \pm\sqrt{c_j^2 k^2 + \frac{1}{4}k^4}. \tag{5.77}$$

Eight matching conditions for the two horizons are being used to construct the matching matrix. Two conditions correspond to each mode, $\delta\theta$ and δn, and two more for the continuity of their derivatives across each horizon (in total eight conditions). For this reason, the complex frequencies that give rise to dynamical instabilities of the black-hole

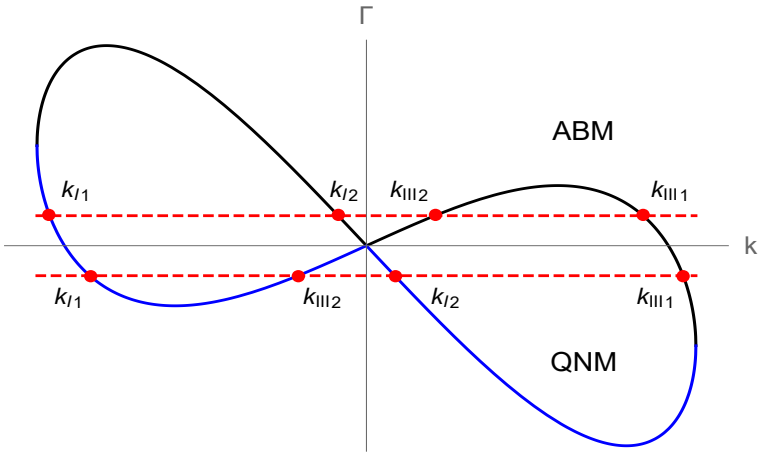

Figure 5.6: Subsonic dispersion relation for $\omega \to i\omega$ and $k \to ik$.

laser need to be considered. The modes of the spectrum responsible for this phenomenon are asymptotically bound at each side of the horizon. Two such modes exist in each subsonic regime, which are named k_{I_1} and k_{I_2} for Region I and k_{III_1} and k_{III_1} for Region III (see Figure 5.6 for their analytic continuations in $\Gamma = \mathrm{Im}\,\omega > 0$). Figure 5.6 is obtained by the transition to the discrete complex part of the spectrum by $\omega \to i\omega$ and $k \to ik$ with the new variables $k \in \mathbb{R}$ and $\omega \in \mathbb{R}$, which leads to a dispersion relation of the form

$$(\omega - Vk)^2 = c_j^2 k^2 - \frac{1}{4}k^4. \tag{5.78}$$

Note that from now on and until the end of this section, the specific character of each mode will no more used. Modes will be just numbered as in Figure 5.6. This reflects their identification as the first, second, etc. mode for each sector, *I*, *II* or *III*. No more information regarding them will be needed for the subsequent analysis.

For real frequencies, these two modes corresponded to the outgoing and the exponential decaying wave in regions I and III. It is evident, from our selection method of Figure 5.6 that asymptotically bound modes need to be square-integrable (for the general analysis, see 4.25). As a result, we retain four modes for the outer subsonic regions I and III. For Region II, all four solutions are retained. By concluding,the eight k-modes for every low-frequency solution in total will be considered, evaluated at the analogue black and white hole's horizons, which are assumed being placed at $x = -L$ and $x = +L$. By varying the position of the analogue black and white hole's horizons, the onset of instability is detected[10].

The instability onset (see Figure 5.8) for the black-hole laser case can be explained through the inclusion of quasi-normal modes in the analysis[11]. Quasi-normal modes are not square-integrable and are not included in the spectrum. From their definition in Chapter 4, quasi-normal modes are found depicted for $\Gamma < 0$, as in Figures 5.6 and 5.7. It is

[10]Take into account that by placing the two horizons symmetrically across the origin, only symmetric variations of the supersonic regime are taken into account.

[11]For a more in-depth analysis, see Chapter 4 and references therein.

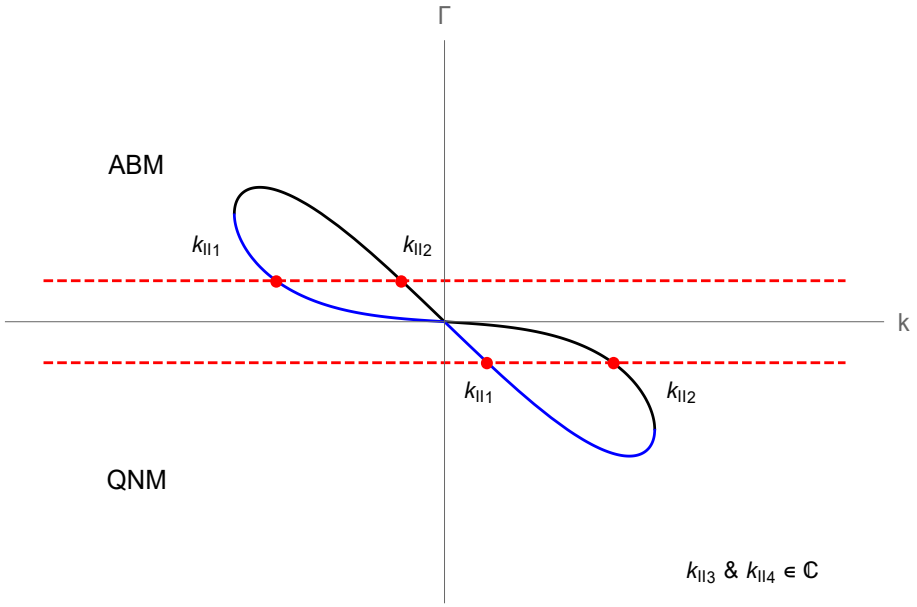

Figure 5.7: Supersonic dispersion relation for $\omega \to i\omega$ and $k \to ik$.

stressed that not all modes with $\Gamma < 0$ are quasi-normal modes; there exist also dynamical instability modes having $\Gamma < 0$. These set of modes, however, will not be included in the following figures. As shown in Chapter 4, quasi-normal modes obey outgoing boundary conditions. Solutions k_{I_2} and k_{III_2} interchange their character in order to satisfy outgoing boundary conditions, as they correspond to poles of the retarded Green's function that are not poles of the G_λ.

The first four columns of the matrix which gives rise to the dynamical instability of the system are presented below:

$$M_{i(1-4)} = \begin{pmatrix} e^{-ik_{I_1}L}k_{I_1}^2 & e^{-ik_{I_2}L}k_{I_2}^2 & e^{-ik_{II_1}L}k_{II_2}^2 & e^{-ik_{II_3}L}k_{II_{2c}}^2 \\ e^{-ik_{I_1}L}k_{I_1}^3 & e^{-ik_{I_2}L}k_{I_2}^3 & e^{-ik_{II_1}L}k_{II_1}^3 & e^{-ik_{II_2}L}k_{II_2}^3 \\ e^{-ik_{I_1}L}\Omega_{I_1} & e^{-ik_{I_2}L}\Omega_{I_2} & e^{-ik_{II_1}L}\Omega_{II_1} & e^{-ik_{II_2}L}\Omega_{II_2} \\ e^{-ik_{I_1}L}k_{I_1}\Omega_{I_1} & e^{-ik_{I_2}L}k_{I_2}\Omega_{I_2} & e^{-ik_{II_1}L}k_{II_1}\Omega_{II_1} & e^{-ik_{II_2}L}k_{II_2}\Omega_{II_2} \\ 0 & 0 & e^{ik_{II_1}L}k_{II_1}^2 & e^{ik_{II_2}L}k_{II_2}^2 \\ 0 & 0 & e^{ik_{II_1}L}k_{II_1}^3 & e^{ik_{II_2}L}k_{II_2}^3 \\ 0 & 0 & e^{ik_{II_1}L}\Omega_{II_1} & e^{ik_{II_2}L}\Omega_{II_2} \\ 0 & 0 & e^{ik_{II_1}L}k_{II_1}\Omega_{II_1} & e^{ik_{II_2}L}k_{II_2}\Omega_{II_2} \end{pmatrix}. \tag{5.79}$$

This matrix condition emerges out of the imposed continuity and differentiability across the horizons. Columns of the matching matrix correspond to the eight k-modes and rows to the eight matching conditions. The first four rows are evaluated across the analogue black hole's horizon, while the last four across the analogue white hole's horizon. The first and third rows consider the modes δn and $\delta\theta$, while the second and fourth rows their derivatives. All matrix elements are multiplied with a factor k^2 in order to avoid numerical errors while searching for the solutions of the determinant problem. Third and fourth rows correspond to $\frac{A_\theta}{A_n}e^{ikz}$ with $f_0 = 1$, by the inclusion of the normalization factors.

The last four columns, not presented here (but exactly symmetric to the presented ones), correspond to the last two modes for the supersonic regime, the modes k_{II_3} and k_{II_4}, and the two modes for the subsonic Region III, k_{III_1} and k_{III_2}. The zeros in the first two columns of the matching matrix are due to the fact that modes in Region I give no contribution to the continuity and differentiability of the modes at the analogue black hole's horizon. The same phenomenon occurs for the first four elements of columns seven and eight, as the modes in Region III give no contribution to the matching conditions at $x = -L$. The frequency Ω_i corresponds to the comoving frequency of the system, which is defined in Equation 5.77 or 3.57. For the calculation of the figures in the rest of this section, $V = 1$, $c_I = c_{III} = 1.5$ and $c_{II} = 0.5$ has been used. With this selection of values, we are able to verify existing results of the bibliography and also extend the theoretical framework of the emergence of dynamical instability modes in the black-hole laser. In the determinant equation of the matrix 5.79,

$$\det(M) = 0, \tag{5.80}$$

the only free parameter is the distance of the two horizons, $2L$. By varying this distance for some specific range of complex frequencies, we can produce the following graphs. Figure 5.8 includes the first two complex frequency modes belonging to the discrete part of the spectrum. Blue and red curves correspond to the real parts of the mode solutions while black and gray to their respective imaginary parts.

By initializing the system with a fluid flow being everywhere subsonic, no emergence of complex frequency modes is initially predicted, something that is verified by the numerical calculations for $L = 0$. The system is then stable. By initializing the supersonic cavity, the first nonzero complex frequency mode appears as a purely imaginary mode with a real degree of freedom. This happens before the 'healing-length' scale is reached (found for $L = 1$). When this mode hits the axis again, a nonzero real part emerges and the mode becomes complex. Before $L = 2.3$, the next nonzero imaginary frequency mode emerges. Its immigration to the complex plane occurs for approximately $L = 3.2$. As L increases, new modes will become nonzero. The imaginary part of the first mode varies with decreasing maximum as $L \to \infty$. At this limit,it is expected that a supersonic flow with range $L \to \infty$ would correspond to a flow that would give no instability (all imaginary parts of the complex modes would tend to zero). This exact behaviour of the decrease of the imaginary part of all complex modes is shown in all the relevant figures.

Figure 5.9 depicts the real parts of the first five modes. It is evident that for increasing L, the real parts tend to saturate to a maximum frequency which has a frequency of $\omega \lesssim 0.3$ and corresponds to the maximum allowed frequency-mode, as seen in Figures 5.6 and 5.7 or as computed in Equation 3.78.

The third dynamical instability mode is depicted in Figure 5.10. The pattern that the first two modes follow is also found for the third mode[12].

By going to $n > 3$, the existence of modes that follow the exact same pattern as the first three branches can be verified. The initial maximum, reached by the imaginary part of the

[12]Note that we speak of the 'third' mode, but we start our enumeration from $n = 0$. This will become apparent when the points where complex modes first appear will be discussed.

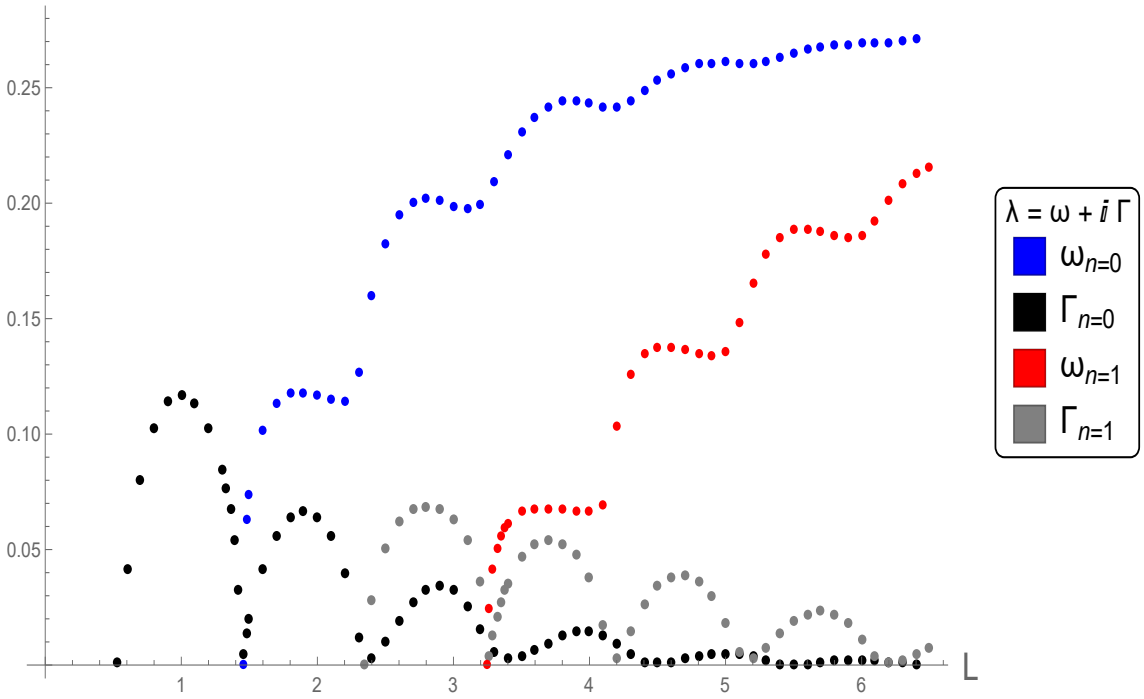

Figure 5.8: The first two dynamical instability modes of the one-component black-hole laser. Blue and red (small dots) curves indicate the respective real parts of the modes and black and gray their imaginary parts.

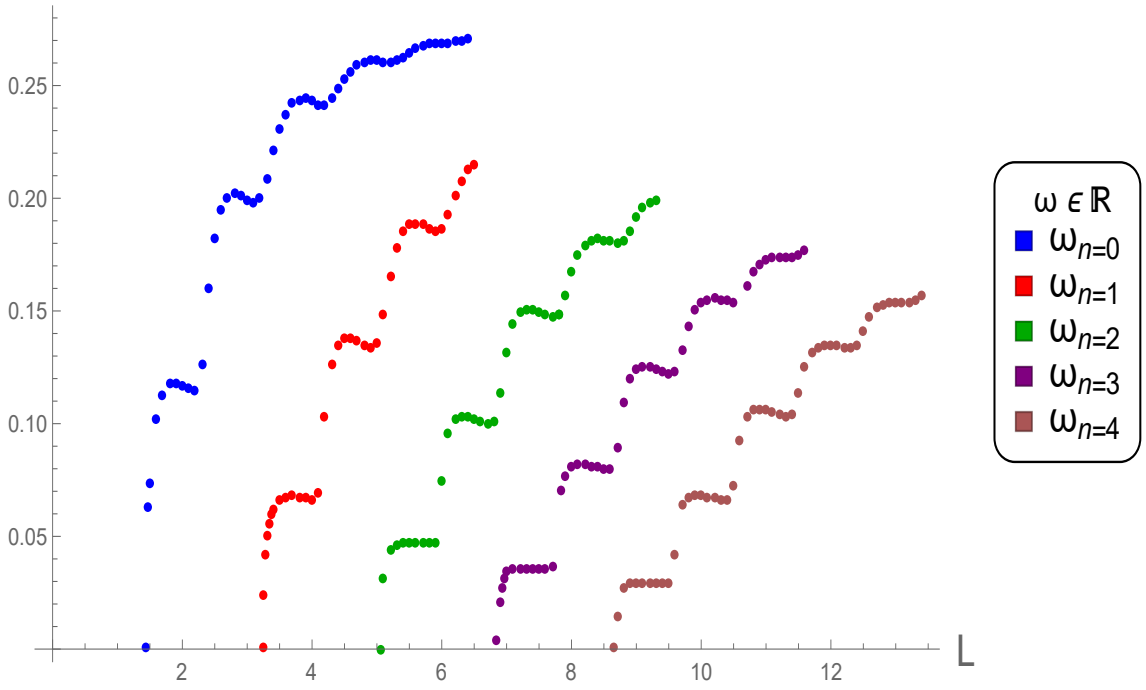

Figure 5.9: The real parts of the first five dynamical instability modes.

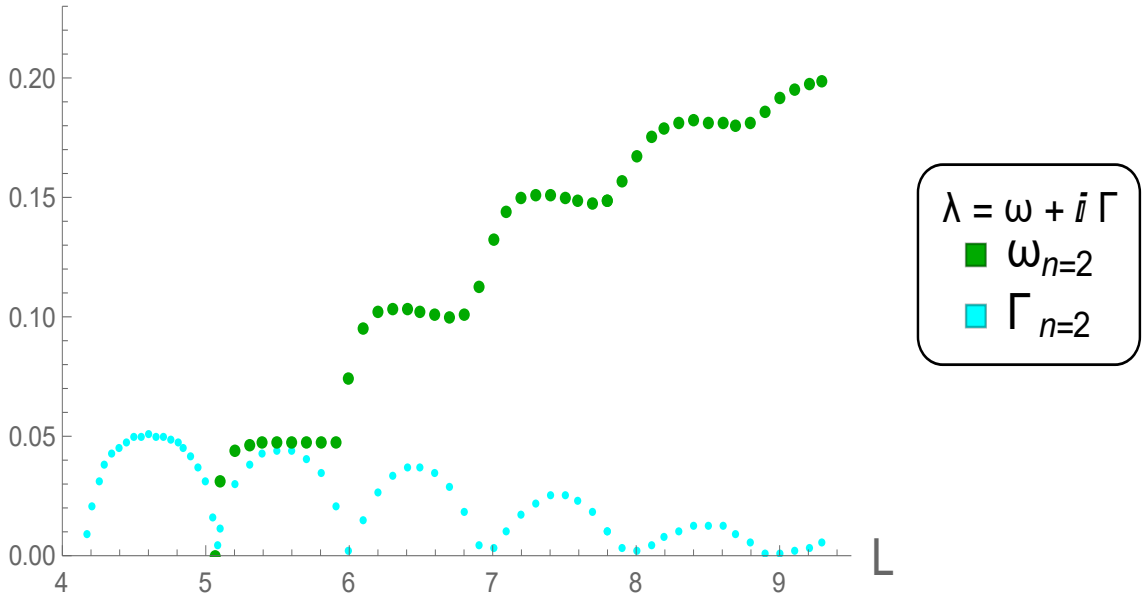

Figure 5.10: Third dynamical instability mode with its real (green) and imaginary (cyan) parts.

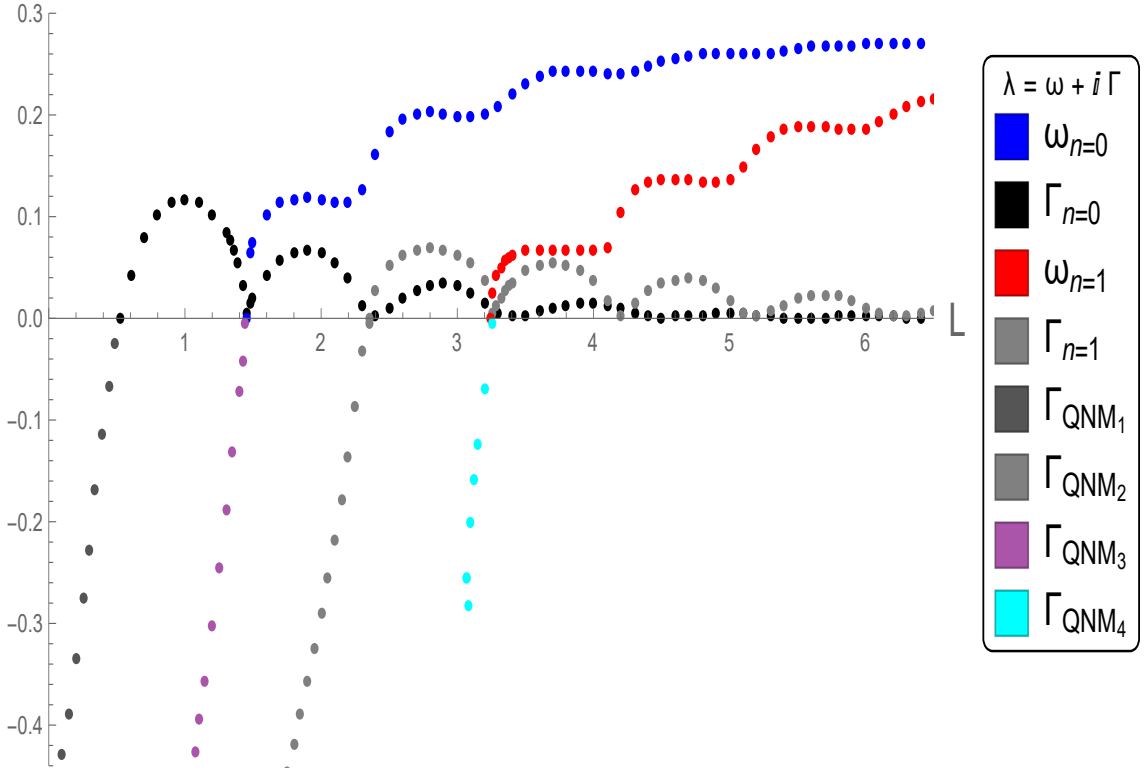

Figure 5.11: The origin of dynamically unstable modes, explicitly shown for the first two dynamical instability modes. For $\Gamma < 0$, the four quasi-normal modes are indicated. When they hit the real axis, they give rise to a degenerate dynamical instability mode. The second (purple) and fourth (cyan) quasi-normal modes give rise to a degenerate dynamical instability mode that instantly leads to the production of a nondegenerate dynamical instability mode with the help of the already existing degenerate dynamical instability ones.

respective mode decreases as the length L is increased. At the same time, more complex modes emerge.

Figure 5.11 includes the first indication of the origin of the instability. By increasing the length L, a quasi-normal mode exists in the system from the point that the supersonic Region II is initialized. As the length of the supersonic cavity is increased, quasi-normal modes move closer to the real axis. When the first quasi-normal mode (the gray in colour, Γ_{QNM_1}) hits the real axis, it gives rise to the imaginary dynamical instability mode for $\Gamma > 0$. After L is increased more, this imaginary dynamical instability mode will hit the real axis at the point where another quasi-normal mode hits it as well. Then, the first complex frequency mode arises. The same process is found for the second dynamical instability mode as well ($n = 1$) and for the quasi-normal mode Γ_{QNM_2}. Note that the first two quasi-normal modes are of imaginary frequency.

The situation for the description of quasi-normal modes differentiates for the third

quasi-normal mode, which is of complex frequency. When the real part of the third quasi-normal mode hits the real axis, a scattering of the imaginary part of the quasi-normal mode occurs. Before $L = 3.1$, the third complex-frequency quasi-normal mode has splitted by a scattering process into two modes of imaginary frequencies. These two modes hit the real axis at some values of L giving rise to dynamical instability modes, as seen in Figure 5.12. In this last figure, all the information of the last figures is gathered together; small dots (blue, red and green) indicate the real part of the complex frequencies for dynamically unstable modes.

The instability onset will now be explained. To begin with, an intriguing aspect of Figures 5.8-5.12 consists of their periodic onset. For this reason, Equation 5.68 is linearised in δf

$$\partial_x^2 f = \left(-2\mu_j f_0 + 2g_j f_0^3 + \frac{J^2}{f_0^3}\right) + \left(-2\mu_j + 6g_j f_0^2 - \frac{3}{J^2}\right)\delta f \overset{2\mu_j = 2c_j^2 + V^2}{=\!=} 4\left(c^2 - V^2\right)\delta f. \tag{5.81}$$

Its solution reads

$$\delta f = \begin{cases} A_I e^{2\sqrt{c_I^2 - V^2}x}, & z < -L \\ A_{II}\cos\left(2\sqrt{V^2 - c_{II}^2}x + \phi\right), & -L < z < L \\ A_{III} e^{-2\sqrt{c_I^2 - V^2}x}, & z > L \end{cases} \tag{5.82}$$

with A_I, A_{II}, A_{III} and ϕ constants.

Then continuity and differentiability of the function δf at the horizons are imposed, leading to the equations

$$A_I e^{2\sqrt{c_I^2 - V^2}(-L)} = A_{II}\cos\left(2\sqrt{V^2 - c_{II}^2}(-L) + \phi\right) \tag{5.83}$$

$$A_{III} e^{-2\sqrt{c_I^2 - V^2}L} = A_{II}\cos\left(2\sqrt{V^2 - c_{II}^2}L + \phi\right) \tag{5.84}$$

$$2\sqrt{c_I^2 - V^2}A_I e^{2\sqrt{c_I^2 - V^2}(-L)} = -2\sqrt{V^2 - c_{II}^2}A_{II}\sin\left(2\sqrt{V^2 - c_{II}^2}(-L) + \phi\right) \tag{5.85}$$

$$-2\sqrt{c_I^2 - V^2}A_{III} e^{-2\sqrt{c_I^2 - V^2}L} = -2\sqrt{V^2 - c_{II}^2}A_{II}\sin\left(2\sqrt{V^2 - c_{II}^2}L + \phi\right), \tag{5.86}$$

which reduce to

$$\sqrt{\frac{c_I^2 - V^2}{V^2 - c_{II}^2}} = -\tan\left(2\sqrt{V^2 - c_{II}^2}(-L) + \phi\right) \tag{5.87}$$

$$\sqrt{\frac{c_I^2 - V^2}{V^2 - c_{II}^2}} = \tan\left(2\sqrt{V^2 - c_{II}^2}L + \phi\right). \tag{5.88}$$

From the properties of the inverse tangent function, the length, L, can be obtained as

$$L_m = \frac{1}{2\sqrt{V^2 - c_{II}^2}}\arctan\left(\sqrt{\frac{c_I^2 - V^2}{V^2 - c_{II}^2}}\right) + \frac{\pi m}{2\sqrt{V^2 - c_{II}^2}}. \tag{5.89}$$

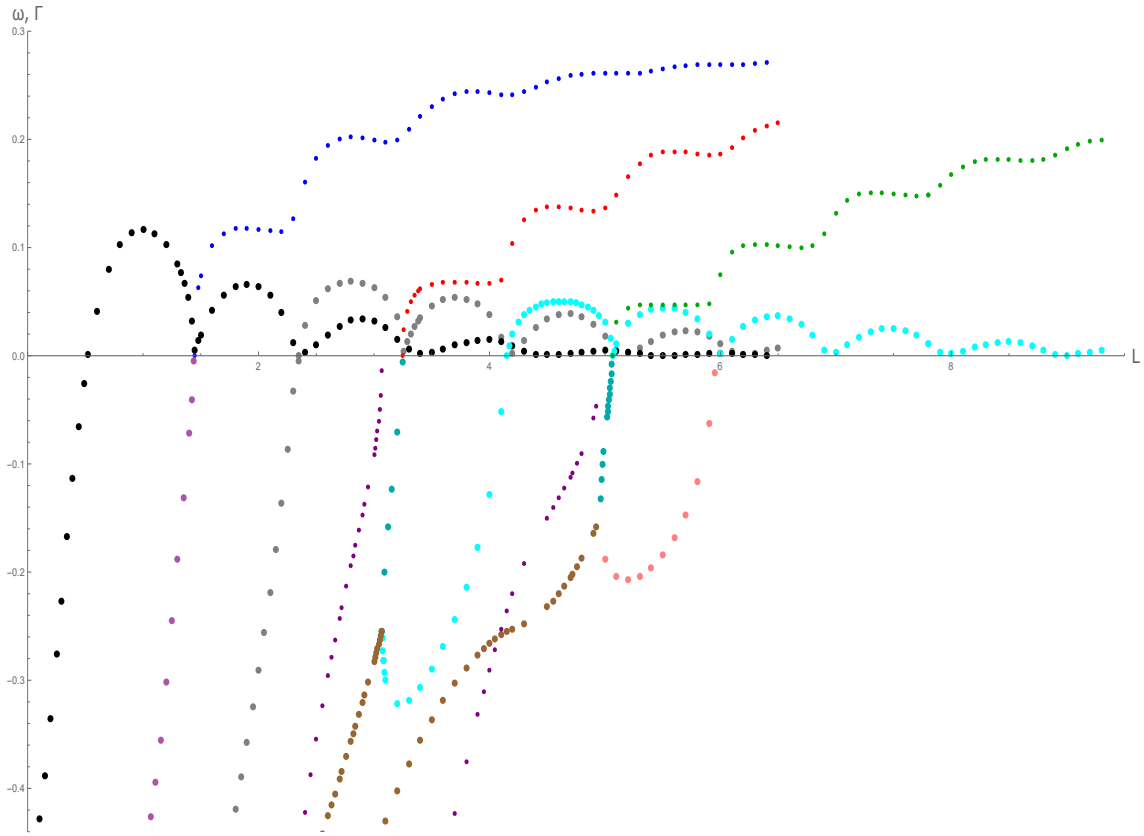

Figure 5.12: All dynamical instability modes for $n \leq 2$ with the relative quasi-normal modes are represented. Note that small dots (blue, red and green for positive frequencies and the dark purple ones for negative frequencies represent the real parts of the respective modes) and the thicker ones the corresponding imaginary parts. The first three quasi-normal modes are imaginary, while the fourth and fifth are complex. They split into two imaginary ones when their real parts hit the imaginary axis and the two newly born imaginary modes for its previously complex quasi-normal mode give rise to two degenerate dynamical instability modes.

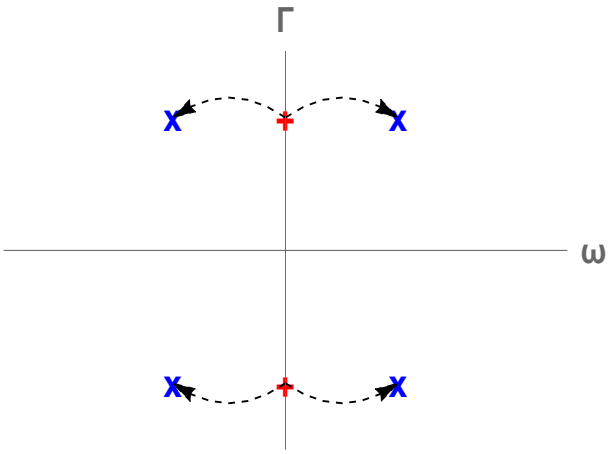

Figure 5.13: The Hamiltonian-Hopf bifurcation. The two imaginary modes (red crosses) will split with the variation of a parameter of the system giving rise to a quartet of complex modes (the four blue crosses). The theory revealing this phenomenon is explained below, in Chapter 4 and in appendix C.

For $m \in \mathbb{N}$, it can be seen that a new dynamical instability mode of imaginary frequency emerges from a quasi-normal mode, while the latter hits the real axis. For $L_{m+1/2}$ that same mode enters the complex plane. For $L = L_0$ the system becomes unstable. This same length corresponds also to the point where a nontrivial nonlinear solution becomes energetically favorable when compared to the homogeneous one [90].

To conclude this section, the instability onset of the one-component black-hole laser configuration in terms of the theory formulated in Chapter 4 will demonstrated and some of the conclusions made there will be readdressed.

Based on considerations in that chapter it can be stated that the occurrence of a dynamical instability mode is interwoven with energetic instabilities, occurring for the same values of the parameters of the system. Due to the Hamiltonian origin of the respective Bogoliubov-de Gennes equations, the symplectic structure of the system explains the emergence of two kinds of dynamical instability modes; pairs of imaginary modes with a real degree of freedom, the *degenerate modes*, and quartets of complex modes, the *nondegenerate modes*. As shown in Figures 5.8-5.12, the process that the system follows in becoming unstable can be summarized as follows; a quasi-normal mode hits the real axis and gives rise to a degenerate dynamical instability mode for some length $L = L_0$. Then another quasi-normal mode hits the real axis and gives rise to a second degenerate dynamical instability mode for $L = L_1 > L_0$. Finally, the two degenerate instability modes merge in order to create a nondegenerate dynamical instability mode for $L = L_2$. In this specific case, $L_1 = L_2$ and the second degenerate instability mode is instantly scattered with the first degenerate dynamical instability mode, giving rise to the complex nongenerate dynamical instability mode. A second nongenerate dynamical instability mode will occur in the system by another similar step for the third and fourth degenerate dynamical instability modes.

Since the Bogoliubov-de Gennes matrix is real, it can sustain only complex frequencies,

which arise in conjugate pairs, and real eigenvalues. If there is a doublet of nonreal eigenvalues, this necessarily corresponds to a pair of degenerate dynamical instability modes and this pair can be described by the imaginary-frequency harmonic oscillator [94]. If four eigenvalues are complex, then they correspond to a quartet of complex nondegenerate dynamical instability modes (λ, $-\lambda^*$, $-\lambda$ and λ^*) and are described by the complex harmonic oscillator theory of Chapter 4. Alternatively, they can correspond to two sets of imaginary modes that have not evolved to create nondegenerate dynamical instability modes. This case is not found in the black-hole laser system, but it is observed in other systems [65]. The energy of the system is conserved in time and this means that dynamical instability modes have necessarily zero energy. The previous existence of energetic instabilities in the system is necessary for the subsequent occurrence of dynamical instability modes (see theorem 5 and the following discussion). This means that for the occurrence of a zero-energy dynamical instability mode, two eigenvalues of opposite signs of the matrix, Equation 4.52, are needed. When all eigenvalues of that matrix have the same sign, there is no way to support the onset of dynamical instability modes and the system is stable. For an eigenvalue of the that matrix changing sign, a degenerate dynamical instability mode is created in (or erased from) the system. When a second eigenvalue of this matrix changes sign, then the previous degenerate dynamical instability mode is erased from the system or a new one emerges (see theorem 1). A further merging of these two degenerate dynamical instability modes gives rise to a quartet of complex nondegenerate dynamical instability modes. This phenomenon is represented in Figure 5.13. The axis are the real and imaginary parts of the respective complex frequency. The two imaginary modes bifurcate and give rise to a quartet of complex modes, after some scattering process that will trigger the imaginary modes to do so. This is called a *Hamiltonian-Hopf* bifurcation, as by varying a parameter of the system (the length L in this case), the splitting of the two imaginary modes into the quartet of four complex modes is witnessed.

All the conclusions made in this chapter regarding the onset of the instability of the black-hole laser configuration can be strictly formulated through the theory of nonhermitian Hamiltonians via the identification of the *Krein signature*[13]. Some introductory concepts and theorems will be given in appendix C.

5.4 Conditions for the emergence of dynamical instability modes for black-hole lasers

In Chapter 4, the possibilities for the emergence of energetic or dynamical instabilities in BECs were discussed. General arguments, when applied to the black-hole laser case, give a set of criteria that, when satisfied, the black-hole laser will possess dynamical instability modes.

Prerequisite for the emergence of dynamical instability modes is the occurrence of energetic instability modes. For energetic instabilities to occur the following conditions need to be satisfied:

[13]For more details see [66, 95–97] or, for coupled nonlinear Schroödinger equations, [98]

- There exists a region of frequency values where the field equations admit both positive and negative-norm (asymptotic) modes.
- These modes (of both positive and negative-norm) are mixed when considering globally exact solutions of the mode equations.

Further conditions apply for the occurrence of dynamical instabilities:

- One of the solutions mentioned above needs to be trapped.
- The depth of the potential (or the length of the supersonic region) needs to be large enough to sustain at least one pair of complex modes.

These conditions need to be satisfied in order for the dynamical instability to appear [39, 65, 90].

6 Rabi-coupled condensates-Countersuperflow

Bose-Einstein condensates (BECs) with one component, as studied in the previous chapters, enable a simplistic analysis for the respective theory. However, due to their spin degrees of freedom, multi-component BECs, open a whole new world of possibilities for exploring spin waves, phase separation, quantum tunnelling, Rabi oscillations, vortices and topological defects and many more [99–104].

In this section, a two-component Bose gas with Rabi coupling will be considered. Furthermore, it will be assumed that the condensates have no background velocities. After having finished this analysis, the differencies, when a nonzero background flow between the two components is included, creating a countersuperflow, will be analysed [105, 106].

Starting with no background flow between the two components, the Lagrangian describing the system can be expressed in the form

$$L = \int \mathrm{d}x\, i\hbar \left(\psi_1^\dagger \frac{\partial \psi_1}{\partial t} + \psi_2^\dagger \frac{\partial \psi_2}{\partial t} \right) - E \tag{6.1}$$

with the energy functional E

$$E = \int \mathrm{d}x \Bigg(\sum_{j=1}^{2} \left(\frac{\hbar^2}{2m} \left| \frac{\partial \psi_j}{\partial x} \right|^2 - \mu_j \left| \psi_j \right|^2 + \sum_{k=1}^{2} \frac{g_{jk}}{2} \left| \psi_j \right|^2 \left| \psi_k \right|^2 \right) - \hbar\Omega \left(\psi_1 \psi_2^\dagger + \psi_2 \psi_1^\dagger \right) \Bigg) \tag{6.2}$$

and m_j the atomic masses of the components and μ_j their respective chemical potentials. The coefficients $g_{jk} = \frac{2\pi\hbar^2 \alpha_{jk}}{m_{jk}}$ of the density-density interaction are represented by the effective masses of the j-th components as $m_{jk}^{-1} = m_j^{-1} + m_k^{-1}$ and the scattering lengths, α_{jk}, satisfy $\alpha_{jk} = \alpha_{kj}$ between the j-th and the k-th components. The last term on the right hand side of Equation 6.2 represents the Rabi coupling, which will later be assumed $\Omega > 0$.

Equations 6.1 and 6.2 represent two BECs in two hyperfine levels (spin states). Theoretical investigations on coupled BECs had initially been triggered based on the Landau-Khalatnikov two-fluid model for one-component BECs and then extended on the stability of ground state, to their properties and to their collective excitations as well. Hartree-Fock theory has also been successfully tested to two-component systems [107–110].

Generally, many properties of two-component BECs (or, in general, binary BECs) emerge out of symmetry arguments. Two-component systems sustain a wealth of symmetry and symmetry breaking patterns. Condensation for binary condensates corresponds to

the spontaneous breaking of two $U(1)$ global symmetries which are related by Nöther's theorem to the conservation of each of the atom numbers of the two species. The coupling of a system of two condensates populating two different spin states is specifically enabled by, for example, an electromagnetic tuning to the transition frequency. In this case, atoms can be converted back and forth between the two spin states and the numbers of atoms of the two species are not conserved separately, as atoms always move between components due to the coupling drive. In this case, only the total number of particles is conserved. As a result, one of the two initial $U(1)$ symmetries remains exact, but the other is broken. The preserved $U(1)$ symmetry originates to the total particle number conservation and is reflected to equal-amount changes on the phases of the two components. No more a change of $\psi_1 \rightarrow e^{i\theta_1}\psi_1$ and $\psi_2 \rightarrow e^{-i\theta_2}\psi_2$ remains a symmetry of the total system 6.1, unless $\theta_1 = \theta_2$. The violated symmetry corresponds to the relative phase between the two components. As a result, the presence of the electromagnetic coupling lifts the degeneracy of the ground state with respect to the relative phase.

We proceed by obtaining the equations of motion, based on Equation 6.1. By taking variations of the action (and restoring the operator-form of the fields),

$$S = \int \mathrm{d}t\, \mathrm{d}x\, L, \tag{6.3}$$

the coupled equations are found to be

$$i\hbar\partial_t\hat{\psi}_1 = -\left(\frac{\hbar^2}{2m}\partial_x^2 + V(x)\right)\hat{\psi}_1 + \left(g_{11}\left|\hat{\psi}_1\right|^2 + g_{12}\left|\hat{\psi}_2\right|^2\right)\hat{\psi}_1 - \hbar\Omega\hat{\psi}_2 \tag{6.4}$$

$$i\hbar\partial_t\hat{\psi}_2 = -\left(\frac{\hbar^2}{2m}\partial_x^2 + V(x)\right)\hat{\psi}_2 + \left(g_{12}\left|\hat{\psi}_2\right|^2 + g_{22}\left|\hat{\psi}_1\right|^2\right)\hat{\psi}_2 - \hbar\Omega\hat{\psi}_1, \tag{6.5}$$

where it is first assumed that $g_{jk} = \gamma g$ and γ is arbitrary but real[1]. Initially, the general analysis will be considered and no constraint to γ will be imposed (when $\gamma = 1$, the Manakov limit is reached, see [111] for the amazing properties of the system under this constraint). It is further assumed that there is no external potential, $V(x) = 0$. The term proportional to Ω gives rise to phase correlations of the two components. For the case of a mixture of two Bose gases it is usually renamed through $\Omega \rightarrow J$ [112]. When Ω is used, one of the next two processes is usually inferred: a two photon Rabi process or a direct Rabi coupling between the two components.

Starting with $\Omega = 0$ and by dealing with the ground state of the two-component gas [113], the wavefunctions ψ_j will have nonzero expectation values. These values can be found by the minimization of the 'potential' energy in Equation 6.1, with respect to ψ_1 and ψ_2. This procedure will involve the densities of the two components $n_j = \left|\psi_j\right|^2$, as

$$g_{11}n_1 + g_{12}n_2 = \mu_1 \tag{6.6}$$

$$g_{21}n_1 + g_{22}n_2 = \mu_2, \tag{6.7}$$

[1]For the mean-field solutions of Equations 6.4-6.5, the substitution $\hat{\psi}_i \rightarrow \psi_i$ is used.

where $g_{12} = g_{21}$. These equations restrict to the extrema of the 'potential' energy of Equation 6.1. For finding the respective minima, the quadratic form

$$g_{11}n_1^2 + 2g_{12}n_1n_2 + g_{22}n_2^2 \tag{6.8}$$

is used, which needs to be positive definite. Furthermore, the following condition needs to be satisfied:

$$g_{11}g_{22} - g_{12}^2 > 0. \tag{6.9}$$

This equation ensures the stability of a mixture of two Bose superfluids and their thermodynamic stability against segregation [80]. When $g_{11} = g_{12} = g_{22}$, the respective Hamiltonian has $SU(2)$ symmetry and some very interesting properties [111].

By returning to the Lagrangian with nonvanishing Rabi coupling, the symmetry

$$\psi_1 \to e^{i\theta_1}\psi_1 \tag{6.10}$$

$$\psi_2 \to e^{i\theta_2}\psi_2 \tag{6.11}$$

for the case $\Omega = 0$ is not conserved. The total particle numbers of each component, $N_1 = \int \mathrm{d}x\, \psi_1^\dagger \psi_1$ and $N_2 = \int \mathrm{d}x\, \psi_2^\dagger \psi_2$ are not conserved. Nevertheless, their sum, $N = N_1 + N_2$, is conserved (no inelastic scattering effects are taken into account). With $\Omega \neq 0$, the Lagrangian is invariant only under a subset of the initial $U(1) \times U(1)$ symmetry. When $\Omega = 0$, from Goldstone theorem, there exist two gapless modes, while initiating a nonzero Rabi coupling leads one of them to acquire a gap. The gapless modes are the phonon excitation (sound waves) also encountered for one-component Bose gases.

By substituting $\psi_i = e^{-i\mu_i t}\Psi_i$, in the equations of motion, Equations 6.4 and 6.5, and following the same process as in Section 3.3, the dispersion profile of the Bogoliubov spectrum can be obtained. This procedure will be further analysed in Section 6.2. Stationary profiles of the Equations 6.4 and 6.5 can be obtained only when $\mu_1 = \mu_2 = \mu$.

Before this analysis, the stability of ground states will be discussed and the mode analysis will only then be performed.

6.1 Stability of ground states

In this section, the ground states of Rabi coupled condensates will be considered. As a result, a two-component system of homogeneous Bose gases which interact via s-wave contact interactions together with a coherent coupling is taken into account. The description of the system is enabled through the coupled GP model 6.4-6.5.

The ground state energy of the system, based on Equation 6.2 is

$$\epsilon = \frac{1}{2}g_{11}n_1^2 + \frac{1}{2}g_{22}n_2^2 + g_{12}n_1n_2 - 2\Omega\sqrt{n_1n_2}\cos(\phi_2 - \phi_1) - \mu(n_1 + n_2), \tag{6.12}$$

where generally the Rabi coupling can be complex, $\Omega = |\Omega|\, e^{i\phi_\Omega}$. The minimum of the energy corresponds to

$$\phi = \phi_2 - \phi_1 + \phi_\Omega = 2\kappa\pi, \quad \forall \kappa \in \mathbb{Z}. \tag{6.13}$$

General extrema of the energy are found only for values of the total phase $\phi = 0$ or $\phi = \pi$. Assuming, as before, without loss of generality, that $\Omega \in \mathbb{R}$ and that $\Omega > 0$, the minimum of the energy of the Rabi-coupled system corresponds to the conditions

$$\begin{aligned} \frac{\partial \epsilon}{\partial \phi} &= 2\Omega \sqrt{n_1 n_2} \sin \phi = 0 \\ \frac{\partial^2 \epsilon}{\partial \phi^2} &= 2\Omega \sqrt{n_1 n_2} \cos \phi > 0, \end{aligned} \tag{6.14}$$

which are satisfied for $\phi_1 = \phi_2,\ \phi_\Omega = 0$. For $\frac{\partial^2 \epsilon}{\partial \phi^2} < 0$, the system will possess other local energy extrema [114–116]

From now on, the assumption that $g_{11} = g_{22} = g$ will be considered. The stability criterion becomes

$$\begin{aligned} \frac{\partial \epsilon}{\partial n_1} = \frac{\partial \epsilon}{\partial n_2} = 0 \Rightarrow \left(g - g_{12} + \frac{\Omega \cos \phi}{\sqrt{n_1 n_2}} \right) (n_1 - n_2) = 0 \Rightarrow \\ \begin{cases} n_1 = n_2 = n_0 = \frac{n}{2}, & \text{symmetric ground state} \\ \sqrt{n_1 n_2} = -\frac{\Omega \cos \phi}{g - g_{12}}, & \text{polarized ground state} \end{cases} \end{aligned} \tag{6.15}$$

with the necessary condition

$$\frac{\Omega \cos \phi}{g - g_{12}} < 0, \quad \forall\, \Omega, g, g_{12}, \phi. \tag{6.16}$$

The relation of the densities of the polarized ground state can then be found to be

$$n_1 - n_2 = \pm n \sqrt{1 - \left(\frac{2\Omega \cos \phi}{(g - g_{12}) n} \right)^2} = \pm n \sqrt{1 - \left(\frac{2\Omega}{n(g - g_{12})} \right)^2}, \tag{6.17}$$

as $\cos \phi = (-1)^\kappa$ for the ground state, with the total density

$$n_1 + n_2 = n. \tag{6.18}$$

Generally, the nature of the extrema can be detected from the behaviour of the Hessian

$$\mathcal{H}\epsilon = \begin{pmatrix} \frac{\partial^2 \epsilon}{\partial \phi^2} & \frac{\partial^2 \epsilon}{\partial \phi \partial n_1} & \frac{\partial^2 \epsilon}{\partial \phi \partial n_2} \\ \frac{\partial^2 \epsilon}{\partial n_1 \partial \phi} & \frac{\partial^2 \epsilon}{\partial n_1^2} & \frac{\partial^2 \epsilon}{\partial n_1 \partial n_2} \\ \frac{\partial^2 \epsilon}{\partial n_2 \partial \phi} & \frac{\partial^2 \epsilon}{\partial n_2 \partial n_1} & \frac{\partial^2 \epsilon}{\partial n_2^2} \end{pmatrix}, \tag{6.19}$$

where $\mathcal{H}$ is regarded as an operator acting on the energy of the system. For a three variable function as in this case, $\epsilon = \epsilon(\phi, n_1, n_2)$, it is found that the following quantities need to

A	B	D	Type
> 0	> 0	> 0	Minimum
< 0	> 0	< 0	Maximum
otherwise			saddle point

Table 6.1: Stability criteria for the Hessian

be taken into account:

$$A = \left| \frac{\partial^2 \epsilon}{\partial \phi^2} \right| \tag{6.20}$$

$$B = \begin{vmatrix} \frac{\partial^2 \epsilon}{\partial \phi^2} & \frac{\partial^2 \epsilon}{\partial n_1 \partial \phi} \\ \frac{\partial^2 \epsilon}{\partial \phi \partial n_1} & \frac{\partial^2 \epsilon}{\partial n_1^2} \end{vmatrix} \tag{6.21}$$

$$D = \begin{vmatrix} \frac{\partial^2 \epsilon}{\partial \phi^2} & \frac{\partial^2 \epsilon}{\partial n_1 \partial \phi} & \frac{\partial^2 \epsilon}{\partial \phi \partial n_2} \\ \frac{\partial^2 \epsilon}{\partial \phi \partial n_1} & \frac{\partial^2 \epsilon}{\partial n_1^2} & \frac{\partial^2 \epsilon}{\partial n_1 \partial n_2} \\ \frac{\partial^2 \epsilon}{\partial \phi \partial n_2} & \frac{\partial^2 \epsilon}{\partial n_1 \partial n_2} & \frac{\partial^2 \epsilon}{\partial n_2^2} \end{vmatrix}. \tag{6.22}$$

Then, the different cases for the extrema of the energy function are summarized in Table 6.1 The analysis of the matrix results in 4 cases:

- an extremum being a saddle point (with $A < 0$, $B < 0$, respectively)
- an extremum being a maximum for $g_{12} < \tilde{g}_{12}$ (defined only for $g_{12} < g$)
- an extremum being a global minimum for $g_{12} < \bar{g}_{12}$ and a saddle for $g_{12} > \bar{g}_{12}$ (the symmetric state)
- an extremum being a saddle for $g_{12} < \bar{g}_{12}$ and a global minimum for $g_{12} > \bar{g}_{12}$ (the polarized state),

where

$$\bar{g}_{12} = g - \frac{2\Omega}{n} \tag{6.23}$$

$$\tilde{g}_{12} = g + \frac{2\Omega}{n}. \tag{6.24}$$

A bifurcation occurs to the ground state (see Figure 6.1) when $g_{12} = \bar{g}$. For $g_{12} < \bar{g}$, the symmetric ground state is the global ground state. For $g_{12} > \bar{g}$, the polarized ground state is the global ground state (see Figure 6.1).

The bifurcation point has been found to correspond to a Schrödinger cat state [114]. The stability case briefly summarized for no Rabi coupling can discern the miscible from a phase separated or immiscible phase. This phase transition is different from the one between a miscible and an immiscible mixture without Rabi coupling [80]. Here, as also

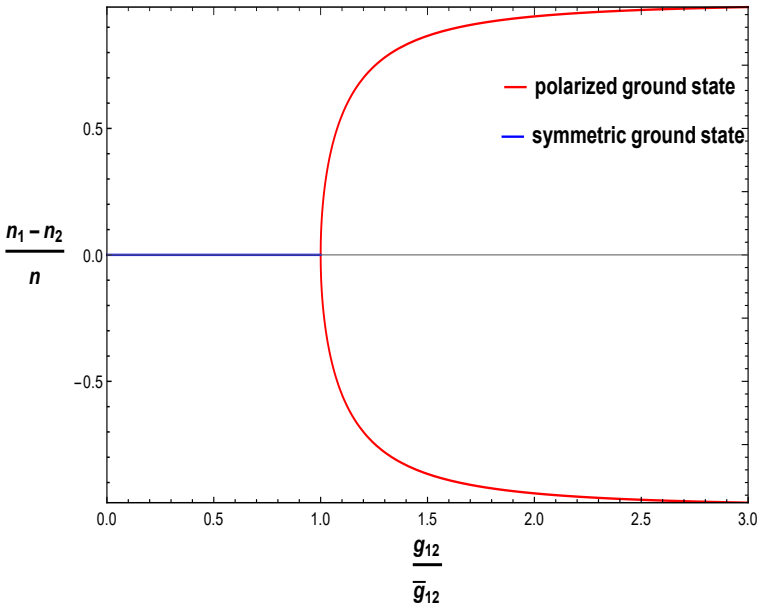

Figure 6.1: The bifurcation of the ground state. The respective regions of validity for the symmetric and the polarized ground states have been indicated ($\Omega = 0.5ng$ has been used).

shown in the stability diagram 6.6, this critical value is shifted to higher interspecies interaction values. Phase separation is prevented by the polarization (or, differently said, by the population imbalance). For the polarized ground state fixed point, self-trapping dynamics would just emerge, while for the symmetric ground state closed orbits are observed [117]. This bifurcation has been first described experimentally in [118].

6.2 Mode analysis

In this section, a Rabi-coupled two-component Bose gas with no background flow ($V = 0$) will be analysed. The background flow will be first introduced in Section 6.3.

The linear spectrum obtained from the Bogoliubov-de Gennes equations emerges from Equations 6.4-6.5. By substituting solutions of the form

$$\hat{\psi}_i(x,t) = \psi_{o_i}(x)\left(1 + \hat{\phi}_i(x,t)\right)e^{-i\mu t} \tag{6.25}$$

with $\psi_{o_i}(x)$ the symmetric ground state with $\psi_{o_1}(x) = \psi_{o_2}(x) = \sqrt{n_0}$, the Bogoliubov-de Gennes equations are

$$i\partial_t\hat{\phi}_1 = -\left(\frac{\partial_x^2}{2m} + \frac{1}{m}\frac{\partial_x\Psi_{o_1}}{\Psi_{o_1}}\partial_x\right)\hat{\phi}_1 + n_o g\left(\hat{\phi}_1 + \hat{\phi}_1^\dagger\right) + \gamma n_o g\left(\hat{\phi}_2 + \hat{\phi}_2^\dagger\right) - \Omega\hat{\phi}_2 \tag{6.26}$$

$$i\partial_t\hat{\phi}_2 = -\left(\frac{\partial_x^2}{2m} + \frac{1}{m}\frac{\partial_x\Psi_{o_2}}{\Psi_{o_2}}\partial_x\right)\hat{\phi}_2 + n_o g\left(\hat{\phi}_2 + \hat{\phi}_2^\dagger\right) + \gamma n_o g\left(\hat{\phi}_1 + \hat{\phi}_1^\dagger\right) - \Omega\hat{\phi}_1. \tag{6.27}$$

The fields ϕ_i are decomposed as

$$\hat{\phi}_1 = \sum_j \left(\hat{\alpha}_j \phi_j(t,x) + \hat{\alpha}_j^\dagger \varphi_j^*(t,x)\right) \tag{6.28}$$

$$\hat{\phi}_2 = \sum_j \left(\hat{\alpha}_j \chi_j(t,x) + \hat{\alpha}_j^\dagger X_j^*(t,x)\right) \tag{6.29}$$

with the boson commutation relation $\left[\hat{\alpha}_,\hat{\alpha}_j^\dagger\right] = \delta_{ij}$ and, then, expanded in plane wave form

$$\phi_\omega = D(\omega)e^{-i\omega t + ik(\omega)x} \tag{6.30}$$

$$\varphi_\omega = E(\omega)e^{-i\omega t + ik(\omega)x} \tag{6.31}$$

$$\chi_\omega = F(\omega)e^{-i\omega t + ik(\omega)x} \tag{6.32}$$

$$X_\omega = G(\omega)e^{-i\omega t + ik(\omega)x}. \tag{6.33}$$

The final form of the eigenvalue problem reads

$$K\begin{pmatrix} D(\omega) \\ E(\omega) \\ F(\omega) \\ G(\omega) \end{pmatrix} = \omega \begin{pmatrix} D(\omega) \\ E(\omega) \\ F(\omega) \\ G(\omega) \end{pmatrix}, \tag{6.34}$$

where the matrix K is defined as

$$K = \begin{pmatrix} -\frac{1}{2}\partial_x^2 + n_0 g - \Omega & n_0 g & n_0 g_{12} + \Omega & n_0 g_{12} \\ n_0 g & -\frac{1}{2}\partial_x^2 + n_0 g - \Omega & n_0 g_{12} & n_0 g_{12} + \Omega \\ n_0 g_{12} + \Omega & n_0 g_{12} & -\frac{1}{2}\partial_x^2 + n_0 g - \Omega & n_0 g \\ n_0 g_{12} & n_0 g_{12} + \Omega & n_0 g & -\frac{1}{2}\partial_x^2 + n_0 g - \Omega \end{pmatrix}, \tag{6.35}$$

with the spatial derivative formally being substituted by $\partial_x^2 \to -k^2$ and $\frac{1}{m}\frac{\partial_x \Psi_{o_i}}{\Psi_{o_i}} = 0$, due to the static background. The dispersion relation obtained from the matrix equation, Equation 6.34, is

$$\omega_{1,2}^2 = \frac{k^2}{2m}\left(\frac{k^2}{2m} + 2n_0 g(1+\gamma)\right) \tag{6.36}$$

$$\omega_{3,4}^2 = \left(\frac{k^2}{2m} + 2\Omega\right)\left(\frac{k^2}{2m} + 2\Omega + 2n_0 g(1-\gamma)\right), \tag{6.37}$$

where $g_{12} = \gamma g$ is used. For the miscible phase, γ satisfies $\gamma < 1$ and for the immiscible $\gamma > 1$. The dispersion relations in dimensionless variables reads[2]

$$\tilde{\omega}_{1,2}^2 = \tilde{k}^2\left(\tilde{k}^2 + 4(1+\gamma)\right) \tag{6.38}$$

$$\tilde{\omega}_{3,4}^2 = \left(\tilde{k}^2 + 2\omega_R\right)\left(\tilde{k}^2 + 2\omega_R + 4(1-\gamma)\right) \tag{6.39}$$

[2]The plots for the dispersion relations include dimensionless variables obtained from Equations 6.36 and 6.37 with the wavefunction, length, time and energy scaling as $\psi = \sqrt{n_0}\psi'$, $\xi = \frac{\hbar}{\sqrt{mgn_0}}$, $\frac{\hbar}{n_0 g}$ and $n_0 g/2$.

with $\omega_R = \frac{2\Omega}{n_0 g}$ (R: Rabi). The notation $\omega_{1,2}$ and $\omega_{3,4}$ is used to further indicate the density and polarization modes, respectively. From now on, the definition of the rescaled dimensionless eigenfrequencies and eigenmomenta with the tilde will be abandoned and denoted simply by ω and k; adimensionalization will be implied.

The eigenvalues of the matrix 6.35 organize themselves in two 'branches' of different nature. One of them has a gap for low momenta, Equation 6.37, while Equation 6.36 is gapless (see Figure 6.2 or 6.3).

For the dispersion relation, Equation 6.36, it can be shown that for low momenta the dispersion profile is linear and, thus, takes the form

$$\omega_{1,2}^2 = 4k^2(1+\gamma) = c_s^2 k^2 \tag{6.40}$$

with

$$c_s = \lim_{k\to 0} \frac{\omega_{1,2}}{k} = 2\sqrt{1+\gamma}. \tag{6.41}$$

The dispersion relation 6.37 possesses a gap, Δ, for low momenta,

$$\Delta^2 = \lim_{k\to 0} \omega_{3,4}^2 = \lim_{k\to 0} \left(4\omega_R\left(\omega_R + 2(1-\gamma)\right)\right) + O\left(k^2\right). \tag{6.42}$$

For the limit to infinity, the eigenfrequencies read

$$\lim_{k\to\infty} \omega_{1,2,3,4} = k^2, \tag{6.43}$$

in dimensionless form[3].

From the polarization dispersion branch, a stability criterion can be inferred by observing that Equation 6.37 vanishes for a momentum scale that satisfies

$$k_*^2 = 4(\gamma - 1) - 2\omega_R. \tag{6.44}$$

It is of importance to verify that for $\omega_R \to 0$, or $\Omega \to 0$, stability is indeed ensured, only when $\gamma < 1$ [119]. For $k \to 0$, the criterion becomes

$$\gamma = 1 + \frac{\omega_R}{2}, \tag{6.45}$$

which can be interpreted as that the Rabi coupling between the two components ensures stability in an extended region of phase space, when compared to the two-component Bose gas with $\Omega = 0$. The two cases are identical only in the limit $k \to 0$. As k increases, the region of stability increases for the Rabi-coupled system as well (see Figure 6.6).

For $k \to 0$ and

$$\gamma > 1 + \frac{\omega_R}{2}, \tag{6.46}$$

[3]Restoring dimensions, $\omega \xrightarrow{k\to\infty} \frac{\hbar^2 k^2}{2m}$.

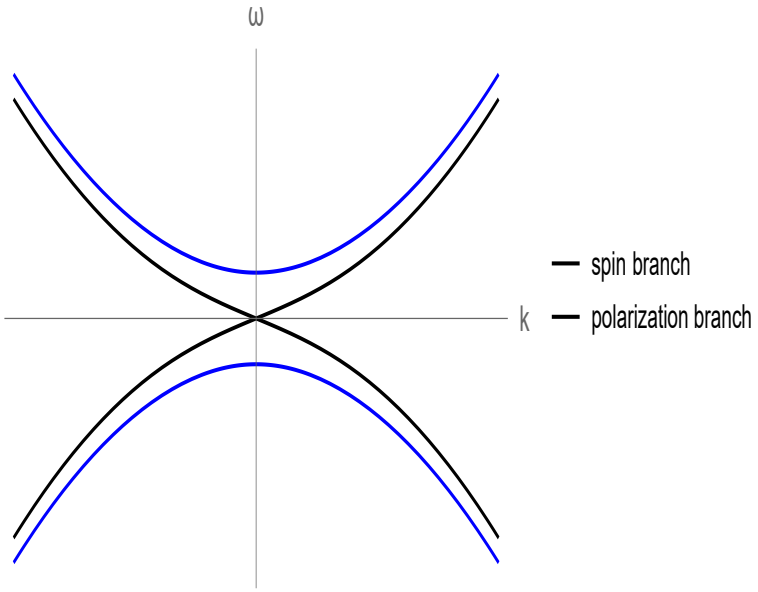

Figure 6.2: Dispersion relation for Rabi-coupled condensates for $\omega_R = 0.6$ and $\gamma = 0.3$. The spin and polarization branches are denoted with black and blue, respectively, with the later being gapped.

the polarization mode becomes unstable. This is a sign of dynamical instability, by using the language of Chapter 4. The appearance of a dynamical instability mode is always traced back to an energetic instability of the corresponding matrix 4.52.

The behaviour of the polarization modes as $k \to 0$ can be summarized as follows:

$$\text{for } \gamma > 1 + \frac{\omega_R}{2},\ \omega_{3,4} \in i\mathbb{R}$$
$$\text{for } \gamma < 1 + \frac{\omega_R}{2},\ \omega_{3,4}\text{: gapped, with } \Delta = \pm\sqrt{4\omega_R\left(\omega_R + 2(1-\gamma)\right)}.$$

When $\Delta > 0$ ($\Delta = 0$) the polarization modes, $\omega_{3,4}$, cross the modes $\omega_{1,2}$ at some value $\bar{k}$ ($\bar{k} = 0$),

$$k^2\left(k^2 + 4(1+\gamma)\right) = k^2\left(k^2 - 4\omega_R + 4(1-\gamma)\right) + 2\omega_R\left(2\omega_R + 4(1-\gamma)\right) \Rightarrow$$
$$\bar{k}^2 = \frac{\omega_R\left(\omega_R + 2(1-\gamma)\right)}{2\gamma - \omega_R}. \tag{6.47}$$

If $2\gamma = \omega_R$ the point of intersection of the two branches moves to infinity. As it can also be inferred from Figure 6.2, there does not always exist a point of intersection.

Let us now assume that in an asymptotic analysis for a configuration with Rabi-coupled condensates in the context of Analogue Gravity, we obtain this model (Equations 6.36 and 6.37). Then, the discussion of the modes of the system in the k-representation in the sense of Chapter 3 follows[4]. Four k-modes for the spin branch and another four for the

[4]This is just an arbitrary assumption and the statement is not justified, but this analysis will be used for accessing the black-hole laser instabilities in Chapter 7. As a result, even if it seems a bit arbitrary now, it will be of fundamental importance for the analysis of Chapter 7.

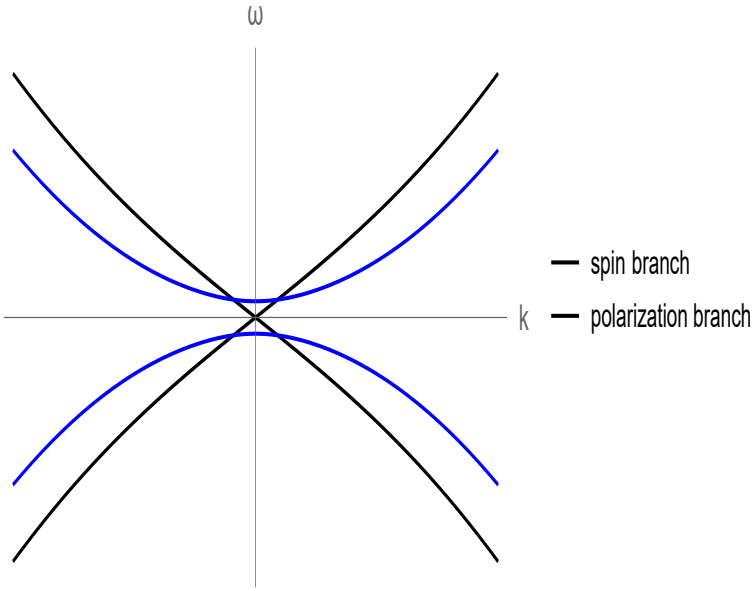

Figure 6.3: Dispersion relation for Rabi-coupled condensates for $\omega_R = 0.1$ and $\gamma = 0.8$. For this specific range of parameters the two branches cross each other. The polarization branch is again gapped.

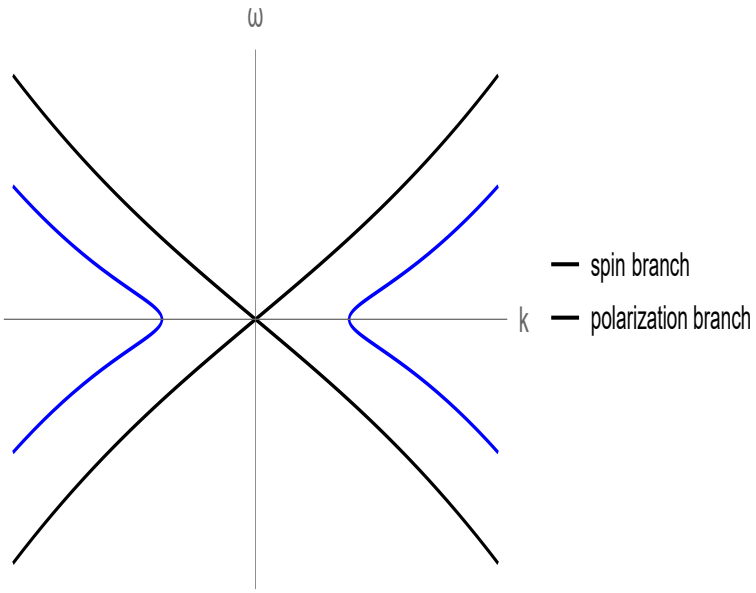

Figure 6.4: Dispersion relation for Rabi-coupled condensates for $\omega_R = 0.3$ and $\gamma = 1.3$ for the immiscible regime of the phase diagram of Rabi-coupled condensates (see Figure 6.6 for the phase diagram of Rabi-coupled condensates).

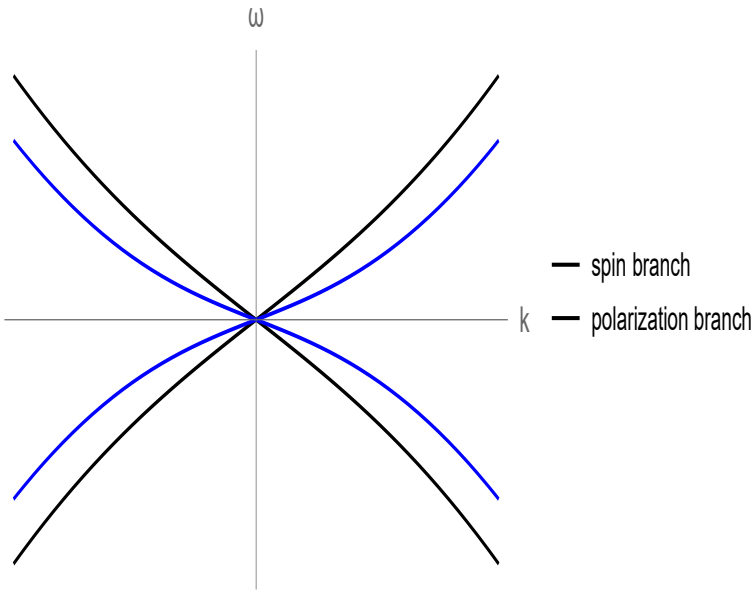

Figure 6.5: Dispersion relation for Rabi-coupled condensates for $\omega_R = 0$ and $\gamma = 0.6$. For no gap, there is no broken $U(1)$ symmetry and the two branches are gapless. Then, there is no distinction between spin and polarization branches. In this figure, however, we insist to this notation just for ease in detecting changes when compared to previous figures, 6.2, 6.3 and 6.4.

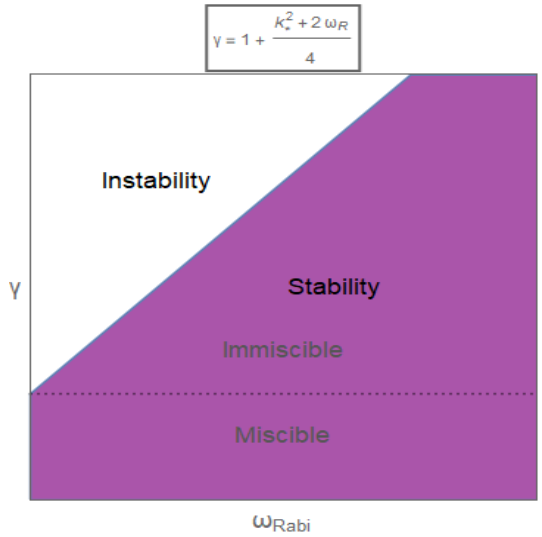

Figure 6.6: The phase diagram of Rabi-coupled condensates with no background flow. Regions in white indicate instability.

polarization branch exist.

- For the density branch,

$$\omega_{1,2}^2 = k^2\left(k^2 + 4(1+\gamma)\right) \Rightarrow k^2 = -2(1+\gamma) \pm \sqrt{4(1+\gamma)^2 + \omega^2}, \tag{6.48}$$

  - $\oplus$, $k^2 > 0 \Rightarrow k \in \mathbb{R}$
  - $\ominus$, $k^2 < 0 \Rightarrow k \in i\mathbb{R}$

  and, then, two real modes and two imaginary ones exist.

- For the polarization branch,

$$\omega_{3,4}^2 = k^2\left(k^2 + 4\omega_R + 4(1-\gamma)\right) + 2\omega_R\left(2\omega_R + 4(1-\gamma)\right) \Rightarrow$$
$$k^2 = -2(\omega_R + 1 + \gamma) \pm \frac{\sqrt{4(1-\gamma)^2 + \omega^2}}{2}, \tag{6.49}$$

  - $\oplus$, $k^2 > 0 \Rightarrow k \in \mathbb{R}$, if

$$\gamma > \frac{\omega_R^2 + 2\omega_R - \omega^2}{2\omega_R} \tag{6.50}$$

    and $k^2 < 0 \Rightarrow k \in i\mathbb{R}$, if

$$\gamma < \frac{\omega_R^2 + 2\omega_R - \omega^2}{2\omega_R} \tag{6.51}$$

  - $\ominus$, $k^2 < 0 \Rightarrow k \in i\mathbb{R}$

    To conclude, the polarization branch can have two real and two imaginary modes or zero real and four imaginary ones for different parameter ranges.

For the case of Equation 6.50, there exist four k solutions that are $k \in \mathbb{R}$ and four that are $k \in i\mathbb{R}$ modes. There exist two modes that have a positive group velocity and two with a negative one[5]. These are the propagating k_{u_1}, k_{u_2}, k_{v_1} ,k_{v_2} modes and the decaying k_{+_1}, k_{+_2}, k_{-_1}, k_{-_2}. The modes with positive imaginary part decay towards $+\infty$. The final picture includes all modes in the respective regions as shown in Table 6.2 or in Table 6.3, according to Equations 6.50 or 6.51.

[5]There are no negative-norm modes with positive frequencies or positive-norm modes with negative frequencies. As a result, it is expected that the Rabi-coupled regions play successfully the role of the subsonic regimes for the prospective black-hole laser of next chapter. What are the modes in the subsonic regions of a black-hole laser consisting of a two-component Bose gas with the subsonic regions being substituted by the Rabi-coupled condensates of this section? These modes are depicted in Table 6.2 or 6.3.

k modes		→	I region	III region
$k = \sqrt{-2(1+\gamma) + \sqrt{4(1+\gamma)^2+\omega^2}}$	$\Big\}\in\mathbb{R}$		$k_{I_{u_1}}$	$k_{III_{u_1}}$
$k = -\sqrt{-2(1+\gamma) + \sqrt{4(1+\gamma)^2+\omega^2}}$			$k_{I_{v_1}}$	$k_{III_{v_1}}$
$k = i\sqrt{2(1+\gamma) + \sqrt{4(1+\gamma)^2+\omega^2}}$	$\Big\}\in i\mathbb{R}$		$k_{I_{+_1}} \overset{x\to-\infty}{\to} \infty$	$k_{III_{+_1}} \overset{x\to+\infty}{\to} 0$
$k = -i\sqrt{2(1+\gamma) + \sqrt{4(1+\gamma)^2+\omega^2}}$			$k_{I_{-_1}} \overset{x\to-\infty}{\to} 0$	$k_{III_{-_1}} \overset{x\to+\infty}{\to} \infty$
$k = \sqrt{-2(\omega_R+1-\gamma) + \sqrt{4(1-\gamma)^2+\omega^2}}$	$\Big\}\in\mathbb{R}$		$k_{I_{u_2}}$	$k_{III_{u_2}}$
$k = -\sqrt{-2(\omega_R+1-\gamma) + \sqrt{4(1-\gamma)^2+\omega^2}}$			$k_{I_{v_2}}$	$k_{III_{v_2}}$
$k = i\sqrt{2(\omega_R+1-\gamma) + \sqrt{4(1-\gamma)^2+\omega^2}}$	$\Big\}\in i\mathbb{R}$		$k_{I_{+_3}} \overset{x\to-\infty}{\to} \infty$	$k_{III_{+_3}} \overset{x\to+\infty}{\to} 0$
$k = -i\sqrt{2(\omega_R+1-\gamma) + \sqrt{4(1-\gamma)^2+\omega^2}}$			$k_{I_{-_3}} \overset{x\to-\infty}{\to} 0$	$k_{III_{-_3}} \overset{x\to+\infty}{\to} \infty$

Table 6.2: Modes for the Rabi-coupled two-component system in the miscible regime, emerging from the Bogoliubov-de Gennes system of 6.36 and 6.37.

† The description of the details of the system will be postponed until Chapter 7.

6.3 The Sine-Gordon domain wall

In this section, the existence of domain wall solutions as solutions of an effective low-energy theory for the countersuperflow of a Rabi-coupled two-component BEC will be demonstrated. We introduce a counterflow between the BECs, when compared to the analysis of Section 6.2, with $V_1 = -V_2 = V$.

Then, the field is decomposed as

$$\psi_1 = \sqrt{n_1 + \delta n_1} e^{i\theta_1} \tag{6.52}$$

$$\psi_2 = \sqrt{n_2 + \delta n_2} e^{i\theta_2}. \tag{6.53}$$

It is assumed that a regime where only fluctuations at length scales larger than the largest healing length, ξ_i, is reached. In this regime, the densities n_1 and n_2 can be regarded as frozen and, then, an effective theory for the phases θ_1 and θ_2 can be attained. The effective energy of the system will be a functional of the two phases. In this section, dimensionful variables are gain used, but with $\hbar = 1$. In this analysis, the densities will be considered as constant in a first low-energy approximation. Then,

$$E[\theta_1, \theta_2] = \int \mathrm{d}x \left(\frac{1}{2m} \left(n_1 (\partial_x \theta_1)^2 + n_2 (\partial_x \theta_2)^2 \right) - 2\Omega \sqrt{n_1 n_2} cos(\theta_1 - \theta_2) \right). \tag{6.54}$$

The potential term $-2\Omega\sqrt{n_1 n_2} cos(\theta_1 - \theta_2)$ has its minimum for $\theta_A = \theta_1 - \theta_2 = 0$. This same configuration is also the global minimum of the energy, Equation 6.54, and hence its ground state. The domain wall solution, another solution (apart from the homogeneous one) of the same equation, Equation 6.54, is a solution with

$$\frac{1}{m} n_1 \partial_x^2 \theta_1 = -\frac{1}{m} n_2 \partial_x^2 \theta_2 = 2\Omega \sqrt{n_1 n_2} \sin(\theta_1 - \theta_2). \tag{6.55}$$

k modes	→	I region	III region
$k = \sqrt{-2(1+\gamma) + \sqrt{4(1+\gamma)^2+\omega^2}}$	$\in \mathbb{R}$	$k_{I_{u_1}}$	$k_{III_{u_1}}$
$k = -\sqrt{-2(1+\gamma) + \sqrt{4(1+\gamma)^2+\omega^2}}$		$k_{I_{v_1}}$	$k_{III_{v_1}}$
$k = i\sqrt{2(1+\gamma) + \sqrt{4(1+\gamma)^2+\omega^2}}$	$\in i\mathbb{R}$	$k_{I_{+_1}} \overset{x\to-\infty}{\to} \infty$	$k_{III_{+_1}} \overset{x\to+\infty}{\to} 0$
$k = -i\sqrt{2(1+\gamma) + \sqrt{4(1+\gamma)^2+\omega^2}}$		$k_{I_{+_1}} \overset{x\to-\infty}{\to} 0$	$k_{III_{+_1}} \overset{x\to+\infty}{\to} 0$
$k = \sqrt{-2(\omega_R+1-\gamma) + \sqrt{4(1-\gamma)^2+\omega^2}}$	$\in i\mathbb{R}$	$k_{I_{+_2}} \overset{x\to-\infty}{\to} \infty$	$k_{III_{+_2}} \overset{x\to+\infty}{\to} 0$
$k = -\sqrt{-2(\omega_R+1-\gamma) + \sqrt{4(1-\gamma)^2+\omega^2}}$		$k_{I_{v_2}} \overset{x\to-\infty}{\to} 0$	$k_{III_{v_2}} \overset{x\to+\infty}{\to} \infty$
$k = i\sqrt{2(\omega_R+1-\gamma) + \sqrt{4(1-\gamma)^2+\omega^2}}$	$\in i\mathbb{R}$	$k_{I_{+_3}} \overset{x\to-\infty}{\to} \infty$	$k_{III_{+_3}} \overset{x\to+\infty}{\to} 0$
$k = -i\sqrt{2(\omega_R+1-\gamma) + \sqrt{4(1-\gamma)^2+\omega^2}}$		$k_{I_{-_3}} \overset{x\to-\infty}{\to} 0$	$k_{III_{-_3}} \overset{x\to+\infty}{\to} \infty$

Table 6.3: The same set of modes for the parameters of the system satisfying 6.51.

This equation admits solutions of the form

$$\theta_1 = \frac{n_2}{n}\phi_A \tag{6.56}$$

$$\theta_2 = -\frac{n_1}{n}\phi_A \tag{6.57}$$

with

$$\theta_A = 4\arctan(e^{qx}) \tag{6.58}$$

and

$$q^2 = 2m\Omega\frac{n}{\sqrt{n_1 n_2}}, \tag{6.59}$$

by assuming that the phases θ_1 and θ_2 approach some constant values as $x \to \pm\infty$.

The relative phase changes from 0 to 2π as the coordinate x runs from $-\infty$ to $+\infty$. By observing that the domain wall solution remains unchanged through $\theta_A = \theta_A + 2\nu\pi$, with $\nu \in \mathbb{Z}$, it can be proven that the domain wall solution of the low-energy effective theory 6.54 has minimal energy among those configurations where θ_A changes by 2π from $-\infty$ to $+\infty$ and cannot be continuously deformed into the configuration with $\theta_A = 0$. This equation, Equation 6.58, resembles the soliton solutions of the Sine-Gordon model (see for example [120, 121]), with the difference that the states at each side of the domain wall are intrinsically different, on contrary to the real Sine-Gordon soliton which sustains a 'single' state across its domain. For this specific case the ground state values are different across the domain wall and take values

$$\theta_1 = \theta_2 = 0, \qquad as\ x \to -\infty \tag{6.60}$$

$$\theta_1 = \frac{2\pi n_2}{n} = -\frac{n_2}{n_1}\theta_2, \qquad as\ x \to +\infty, \tag{6.61}$$

something that due to their $(\mathrm{mod}\ 2\pi)$ definition is equivalent to

$$\theta_1 = \theta_2 = 0, \qquad as\ \ x \to -\infty \tag{6.62}$$

$$\theta_1 = \frac{2\pi n_2}{n} = \theta_2, \qquad as\ \ x \to +\infty. \tag{6.63}$$

Of course, this analysis of the effective theory didn't take into account that it emerges as a model of restricted validity for a specific low-energy range. In full generality, by also including the fluctuations of the densities, it can be concluded that this approximate solution can indeed decay to the global minimum configuration of $\theta_A = 0$. The configuration of the Sine-Gordon domain wall is not strictly topological by taking into account the whole picture through the initial system 6.1. But again, its solution corresponds to a local minimum of the configuration, which assures its metastability.

The domain wall can be described by the velocities of the superfluid components

$$v_1 = \frac{\hbar}{m}\partial_x\theta_1 = \ \frac{n_2}{n}\frac{2q}{\cosh(qx)} \tag{6.64}$$

$$v_2 = \frac{\hbar}{m}\partial_x\theta_2 = -\frac{n_1}{n}\frac{2q}{\cosh(qx)}. \tag{6.65}$$

The rates of conversion for the two components are

$$\partial_x j_1 = -\partial_x j_2 = 2\Omega\sqrt{n_1 n_2}\sin\phi_A = -2\Omega\sqrt{n_1 n_2}\frac{\sinh qx}{\cosh^2(qx)}. \tag{6.66}$$

The velocity of the flow is maximal near the domain wall and decays as the flow departs from the near-to-wall region. From Figure 6.7, it can be seen that the flow changes sign across the domain wall; on one side of the domain wall (negative x-axis), particles from the first component jump to component two, while following the opposite path for positive x values. Different species correspond to different energy levels and therefore energy is absorbed on one side of the domain wall and released to the other.

In conclusion, let us briefly consider the case for the instability of interacting two-component BECs with or without Rabi coupling with relative background motion between the two components. In this case, instabilities emerge in the system for some specific range of its parameters. Note, however, that the reason behind the emerging 'energetic instabilities' in this system is not traced back to the Landau instability, normally experienced by a Galilei invariant superfluid flow. The Landau instability is concerned with the superfluid decay due to friction with the 'rigid' environment, for example the container wall or the normal fluid component. This normal component's velocity is frozen at the boundaries (the wall). The countersuperflow instability for two-component BECs is an internal instability; it has nothing to do with the environment. Therefore, the energy of the system is still conserved, as does the total momentum. In this countersuperflow system it is apparent that the instability by itself cannot cause a reduction of the relative motion of the superfluids. The gradual appearance of (internal) excitations of the superfluids is at the bottom of the momentum exchange. Further results concerning counterflowing two-component BEC systems will be discussed in next chapter or can be found in [105, 106, 113].

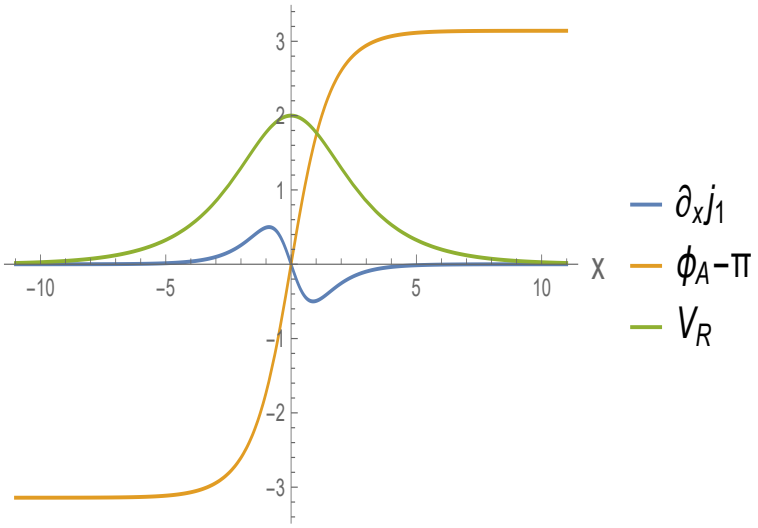

Figure 6.7: The relative phase, the relative velocity and the conversion rate characterizing the domain wall solution for $\Omega = 1$, $n_1 = n_2 = 1$, $q = 1$.

7 A black-hole laser from a two-component Bose gas

7.1 Description of the system. Modes of the two-component system

In this chapter, the two component Rabi-coupled BEC system discussed in Chapter 6 will be considered and a black-hole laser will be analysed based on it. The resulting configuration is shown in Figure 7.1. The supersonic region (Region II) is composed of two BECs with no linear or quadratic interactions between them, meaning a supersonic cavity having a two-component system with $\Omega = 0$ and $\gamma = 0$. In the supersonic regime the two condensates decouple and propagate from Region I to Region III or from Region III to Region I (for component 1 and component 2, respectively).

The Rabi-coupled countersuperflow, as found in [105] or similar treatises, is unstable for a relative velocity between the components, $V_R = V_2 - V_1$, that is $|V_R| > |V_{cr}|$. This critical velocity is always smaller than the speed of sound, c. In this section we want to address the linear stability or instability of the system against perturbations, as also done in Chapter 5. As a result, when constructing the general form of the configuration, a velocity with $|V_R| > |V_{cr}|$ will not be taken into account for the countersuperflow in regions I and III. The corresponding system with $|V_R| > |V_{cr}|$ has been discussed in [105]. In that work, the stability of nonlinear solutions for $|V_R| > |V_{cr}|$ was tested and the system was found to relax to a state with the kink configuration of the relative phase between the two components being broken gradually for increasing relative velocity. Finally, the relative velocity of the two components was found to decrease and the two components exhibited a flow with the same velocity.

Based on the afore-mentioned arguments, an intermediate region between the Rabi-coupled condensates and the supersonic Region II is needed in order to obtain a continuous profile for the background parameters. The phases ϕ_1 and ϕ_2 in the outer Rabi-coupled regions I and III follow from the analysis of the Sine-Gordon soliton, Section 6.3. In the intermediate region, no Rabi coupling is assumed, as shown from the last inlaid figure in Figure 7.1. This is indeed true, as the conversion rate is identically vanishing between the two condensates only when their linear (Rabi) coupling vanishes. Across the horizon, a waterfall profile for both the background velocities of the two components is assumed. Across the horizons the relative velocity, $V_R = V_2 - V_1 = 2V$, of the two components decreases and, in the asymptotic regions, it vanishes . This is the part of the subsonic regions that will be taken into account (near-horizon effects will be disregarded)[1]. There

[1]Note that, even thought this graphical representation seems more than one-dimensional, the analysis

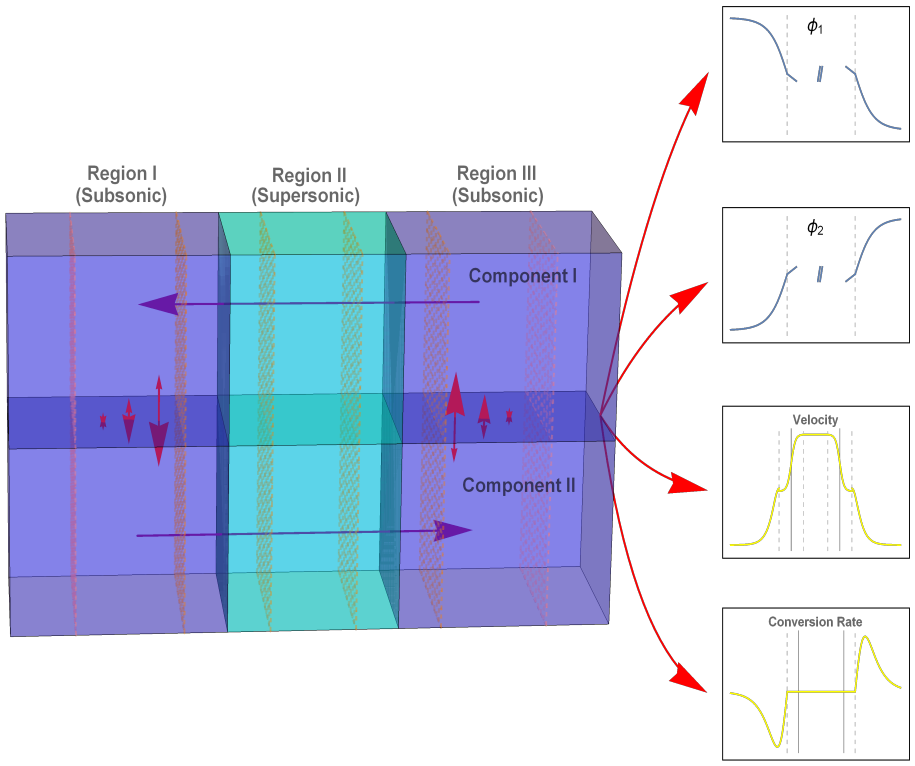

Figure 7.1: The most general form of the black-hole laser with its Regions I and III consisting of two-component BECs. In the inlaid figures the phase of the two components is shown, the relative velocity and the conversion rate between the two components. Resulting figures are based on the analysis of Chapter 6. Phases ϕ_1 and ϕ_2 vary from 0 to $-\pi$ and from 0 to π, respectively. The velocity profile, V, is asymptotically $V \to 0$. The two solid dark lines in the inlaid figures of the velocity and conversion-rate represent the two horizons. The two symmetric dashed lines in the supersonic regime indicate the intermediate regime where the velocity V can be considered in a good approximation constant. The two symmetric dashed lines in Regions I and III indicate the onset of Rabi coupling between the condensates. The quadratic coupling between is (ideally) gradually increased between the horizons and the dashed lines, as in the last two inlaid figures. In the rest of Regions I and III, the Rabi coupling has acquired its final value, Ω. As approaching the two respective asymptotic regions the outer two dashed lines in central figure represent the outer regions of Regions I and III where asymptotic analysis can be used for their description. In these regions, particles have effectively zero velocity, but a constant and nonzero Rabi coupling.

are two intermediate dashed 'surfaces' (in fact, just dashed lines in 1D) in Region II. The regions between them and the two horizons indicate regions where near-horizon effects need to be considered and will be disregarded in the subsequent analysis. Between these two dashed lines in the supersonic region, the two components acquire a constant background velocity, which is assumed to be $V_1 = -V_2$. In each region, Regions I and III, two dashed lines are also included. Coming from Region II and entering symmetrically regions I and III, the first dashed lines encountered indicate the points in space where the linear coupling between the components becomes nonzero. The last two symmetrically placed lines (far left and far right) indicate the regions where the conversion rate has significantly decreased, as approaching $\pm\infty$. In this analysis infinite condensates are assumed, another simplification of the model. These two regions can be safely reproduce asymptotic results based on Region's I and III description. In these regions, there exists a linear and a quadratic coupling between the two BEC components, but the conversion rate asymptotes to zero. By squeezing all the other intermediate regimes, only these last asymptotic regions in this analysis are going to be taken into consideration for the analysis of linear instabilities of the black-hole laser from the two-component BEC.

For the Rabi-coupled condensates in the context of the black-hole laser configuration in the asymptotic analysis, only the state where the Sine-Gordon soliton has obtained its asymptotic form will be retained, meaning that $V_1 = V_2 = 0$. In the supersonic cavity, it will be assumed to leading order that only effects from a constant velocity profile will be considered and all other effects will be subleading, thus, only slightly affecting the stable form of the system. This way near-horizon effects are avoided and the velocity of the two components changes between regions I-III in 'steps', as for the speed of sound in the analysis of Chapter 3 and 5.

7.1.1 Discussion regarding regions I, II and III

The central region will consist of two counterpropagating superfluids with no intraspecies interaction. They are described each by a corresponding one-component BEC model, as that in Chapter 3. The first component will initially encounter the analogue black hole's horizon , starting from the far asymptotic Region III, and then propagate across the analogue white hole's horizon, entering Region I. At the same time, the flow will couple with component two and particles from component one will be transferred to component two. Then, the flow will follow exactly the opposite direction, first across the analogue black hole's horizon, entering Region II and then across the analogue white hole's horizon, before entering Region III.

The real frequency dispersion relation in the supersonic Region II is depicted in Figure 7.2. It incorporates the effects of the supersonic regime for a flow with negative background velocity, as of Figure 3.8, and a relevant with a counterflowing component with positive background velocity, as of Figure 3.9, combined[2].

followed will be restricted to just one dimension, as shown by the big purple arrows. Furthermore, note that the two components seem to be well separated from each other. This is not necessarily true and can vary depending on the experimental set-up chosen for the realization of the system, see discussion in 6.

[2]The dispersion profiles are symmetric under $V \to -V$ and $k \to -k$.

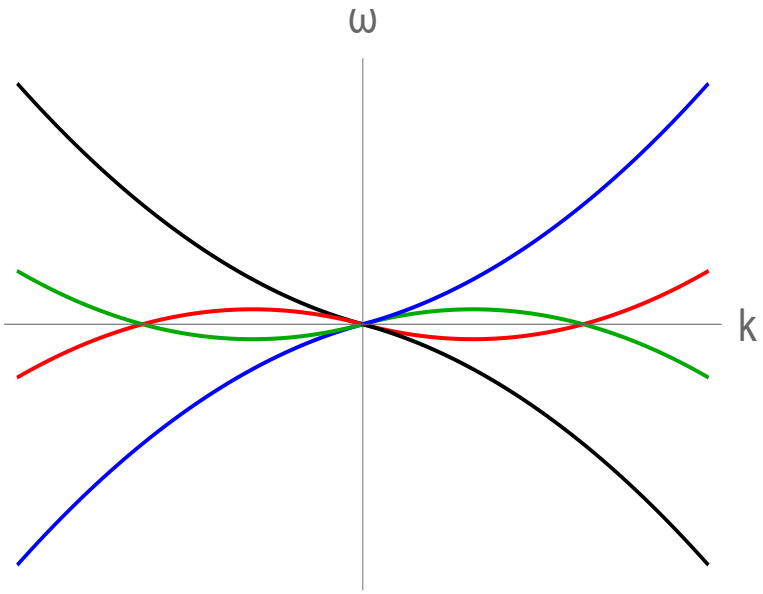

Figure 7.2: The dispersion profile for the central regime with two independent components one flowing with $V < 0$ and the other with $V > 0$.

Regarding the modes for the asymptotic regions I and III, for any positive or negative frequency four real k-modes in Region I (corresponding to the 'asymptotic' countersuperflow of a Rabi-coupled two-component Bose gas, with $V_1 = V_2 = 0$) and four more possessing complex wavevectors exist. In the supersonic regime there exist eight real k-modes. In the symmetric Region III there exist four real k-modes and another four complex ones, as seen from Figures 6.2 or 6.3.

7.2 Discussion on a steplike configuration for a black-hole laser from a two-component BEC system

The two-component BEC configuration of Figure 7.1 gives rise to similar effects regarding real and complex modes, when compared to the one-component case. The real modes of this configuration will be described by a respective set of sixty equations, which fully characterize the system and stem from the analysis of Section 5.2.1, but with the difference that

$$\Phi = \begin{pmatrix} \phi^{u}_{\omega} \\ \phi^{tr*}_{-\omega} \end{pmatrix} \rightarrow \begin{pmatrix} \phi^{u_1}_{\omega} \\ \phi^{tr_1*}_{-\omega} \\ \phi^{u_2}_{\omega} \\ \phi^{tr_2*}_{-\omega} \end{pmatrix} \tag{7.1}$$

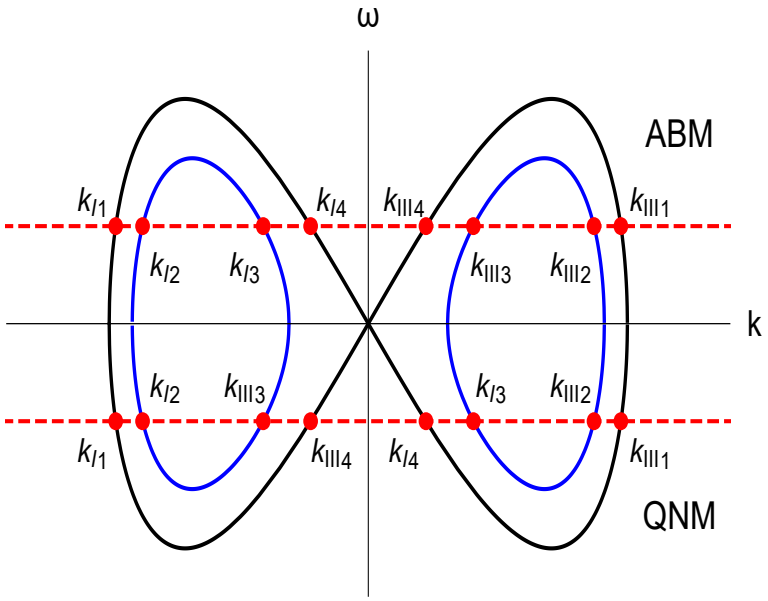

Figure 7.3: Dispersion relation for $\omega \to i\omega$ and $k \to ik$ for the outer symmetric regions I and III for the asymptotic analysis of the two-component BEC of Figure 7.1.

for no u-v mixing and

$$\Phi = \begin{pmatrix} \phi^{u}_{\omega} \\ \phi^{v}_{\omega} \\ \phi^{tr*}_{-\omega} \end{pmatrix} \to \begin{pmatrix} \phi^{u_1}_{\omega} \\ \phi^{v_1}_{\omega} \\ \phi^{tr_1*}_{-\omega} \\ \phi^{u_2}_{\omega} \\ \phi^{v_2}_{\omega} \\ \phi^{tr_2*}_{-\omega} \end{pmatrix} \tag{7.2}$$

by including u-v mixing.

The scattering across the analogue white and black hole's horizons will be comprised of 6×6 matrices for the u-v mixed case. The number of equations in Equations 5.60 and 5.61 will thus be doubled in number.

For the complex frequency modes of the system, the matching-matrix technique will be used. The modes found in each region of the two-component black-hole laser can be found in Figures 7.3 and 7.4. The matching matrix is defined through the same process, as in Chapter 5.

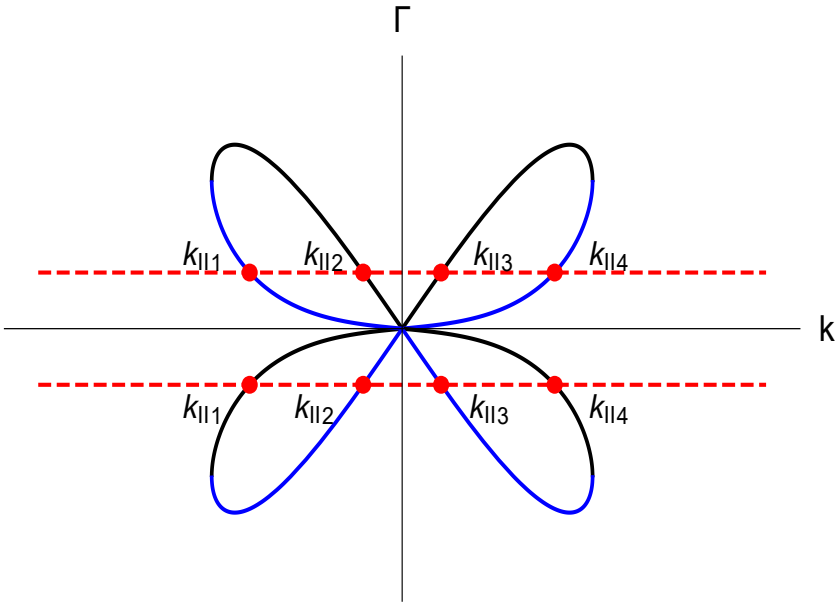

Figure 7.4: Dispersion relation for $\omega \rightarrow i\omega$ and $k \rightarrow ik$ for Region II.

The first four columns of the matching matrix are here presented

$$M = \begin{pmatrix}
e^{-ik_{I_1}L}P(k_{I_1}) & e^{-ik_{I_2}L}P(k_{I_2}) & e^{-ik_{I_3}L}P(k_{I_3}) & e^{-ik_{I_4}L}P(k_{I_4}) \\
e^{-ik_{I_1}L}k_{I_1}P(k_{I_1}) & e^{-ik_{I_2}L}k_{I_2}P(k_{I_2}) & e^{-ik_{I_3}L}k_{I_3}P(k_{I_3}) & e^{-ik_{I_4}L}k_{I_4}P(k_{I_4}) \\
e^{-ik_{I_1}L}R(k_{I_1}) & e^{-ik_{I_2}L}R(k_{I_2}) & e^{-ik_{I_3}L}R(k_{I_3}) & e^{-ik_{I_4}L}R(k_{I_4}) \\
e^{-ik_{I_1}L}k_{I_1}R(k_{I_1}) & e^{-ik_{I_2}L}k_{I_2}R(k_{I_2}) & e^{-ik_{I_3}L}k_{I_3}R(k_{I_3}) & e^{-ik_{I_4}L}k_{I_4}R(k_{I_4}) \\
e^{-ik_{I_1}L}S(k_{I_1}) & e^{-ik_{I_2}L}S(k_{I_2}) & e^{-ik_{I_3}L}S(k_{I_3}) & e^{-ik_{I_4}L}S(k_{I_4}) \\
e^{-ik_{I_1}L}k_{I_1}S(k_{I_1}) & e^{-ik_{I_2}L}k_{I_2}S(k_{I_2}) & e^{-ik_{I_3}L}k_{I_3}S(k_{I_3}) & e^{-ik_{I_4}L}k_{I_4}S\,k_{I_4}) \\
e^{-ik_{I_1}L}T(k_{I_1}) & e^{-ik_{I_2}L}T(k_{I_2}) & e^{-ik_{I_3}L}T(k_{I_3}) & e^{-ik_{I_4}L}T(k_{I_4}) \\
e^{-ik_{I_1}L}k_{I_1}T(k_{I_1}) & e^{-ik_{I_2}L}k_{I_2}T(k_{I_2}) & e^{-ik_{I_3}L}k_{I_3}T(k_{I_3}) & e^{-ik_{I_4}L}k_{I_4}T(k_{I_4}) \\
0 & 0 & 0 & 0 \\
0 & 0 & 0 & 0 \\
0 & 0 & 0 & 0 \\
0 & 0 & 0 & 0 \\
0 & 0 & 0 & 0 \\
0 & 0 & 0 & 0 \\
0 & 0 & 0 & 0 \\
0 & 0 & 0 & 0
\end{pmatrix} \tag{7.3}$$

with the functions $P(k)$, $R(k)$, $S(k)$ and $T(k)$ obtained through the normalization of Equations 6.34, being defined in the Rabi-coupled symmetric regions I and III, similarly to Equation 5.76. Finally, multiplication by k^2 is again used for all elements for numerical accuracy reasons.

The supersonic cavity ranges from $-L$ to L, by assumption. The matching matrix is solved numerically for different lengths of the supersonic cavity, $2L$, for some specific range of the complex frequency. To ensure convergence, a satisfactory number of iterations for the root-finder algorithm and explicit parallelization are being used. The

resulting figure indicates not only quantitative, but also qualitative differences with the one-component case.

As shown in Figure 7.5, the Rabi coupling plays a major role in changing the character of dynamical instability modes for all length scales, L. In this case, the quasi-normal modes for $\lambda < 0$ have not been included, but only their partner-modes having positive imaginary frequency[3]. As L increases, the real part of each dynamical instability mode saturates to a maximum frequency, as before, while the imaginary parts of the dynamical instability modes decrease and tend to vanish. For $L \to \infty$, Region II will solely and fully characterize the whole system. In this case, dynamical instability modes will have $\Gamma \to 0$. For L roughly $L < L_{cr} \sim 2.5$, effects (and modes) observed do not obey a specific pattern and further analysis of the specific modes needs to be performed (this specific region is not included in Figure 7.5). Another important fact about Figure 7.5 is related to the dynamical instability modes plotted for $\omega < 0$. This is another important consistency control of the existence of the underlying symmetries of the problem. As a result, it is obvious that dynamical instability modes continue to emerge as quartets of modes (the analysis of the symmetries of the Bogoliubov-de Gennes equations from the previous chapters remains valid). The real parts of the dynamical instability modes that are responsible for the lasing effect are, as before, those with $\Gamma > 0$.

Concerning Figure 7.5, yellow, purple, green and gray colours indicate the partners of the quasi-normal modes. Note that each real or imaginary component of the aforementioned modes is indicated close to the respective curve in each plot. Note the symmetry of the imaginary parts of the first and third and, equally, of the second and fourth quasi-normal modes. Regarding dynamical instability modes, their imaginary parts have been plotted using undersized dotted lines. The real parts of the (positive and negative) frequencies have also been plotted. Note the symmetry between the red (first) and cyan (third) and, equally, the blue (second) and dark-red (fourth) dynamical instability modes. Our intuition suggests that this symmetry is due to the two-component nature of the system. Each component is responsible for each set of two modes. When compared to the black-hole laser from a one-component BEC, real parts of the dynamical instability modes never 'cross'. However, here this phenomenon is indeed observed, increasing the validity of our interpretation that these modes belong to the two different components of our configuration. One component is thus assumed responsible for the creation of the red and cyan and the other for the blue and darker-red modes.

Another important aspect of the Rabi-coupled condensates, their massive mode, leads to the alteration of the nature of the creation of dynamical instability modes, when compared to the results of Chapter 5. In this case, each quasi-normal mode gives rise to the corresponding dynamical instability mode for some nonzero imaginary part for the respective mode. This suggests that the Rabi-coupling should be responsible for this phenomenon. Although the Rabi coupling of the condensates in Region I and III is always

[3]Note that due to the symmetry of the underlying equations, there is always going to exist dynamical instability or quasi-normal modes for both positive and negative frequencies. It is also crucial to add that modes with positive imaginary part cannot exhibit the character of quasi-normal modes, as they are not decreasing with time. However, in Figure 7.5, we have plotted exactly these modes, for better presentation reasons.

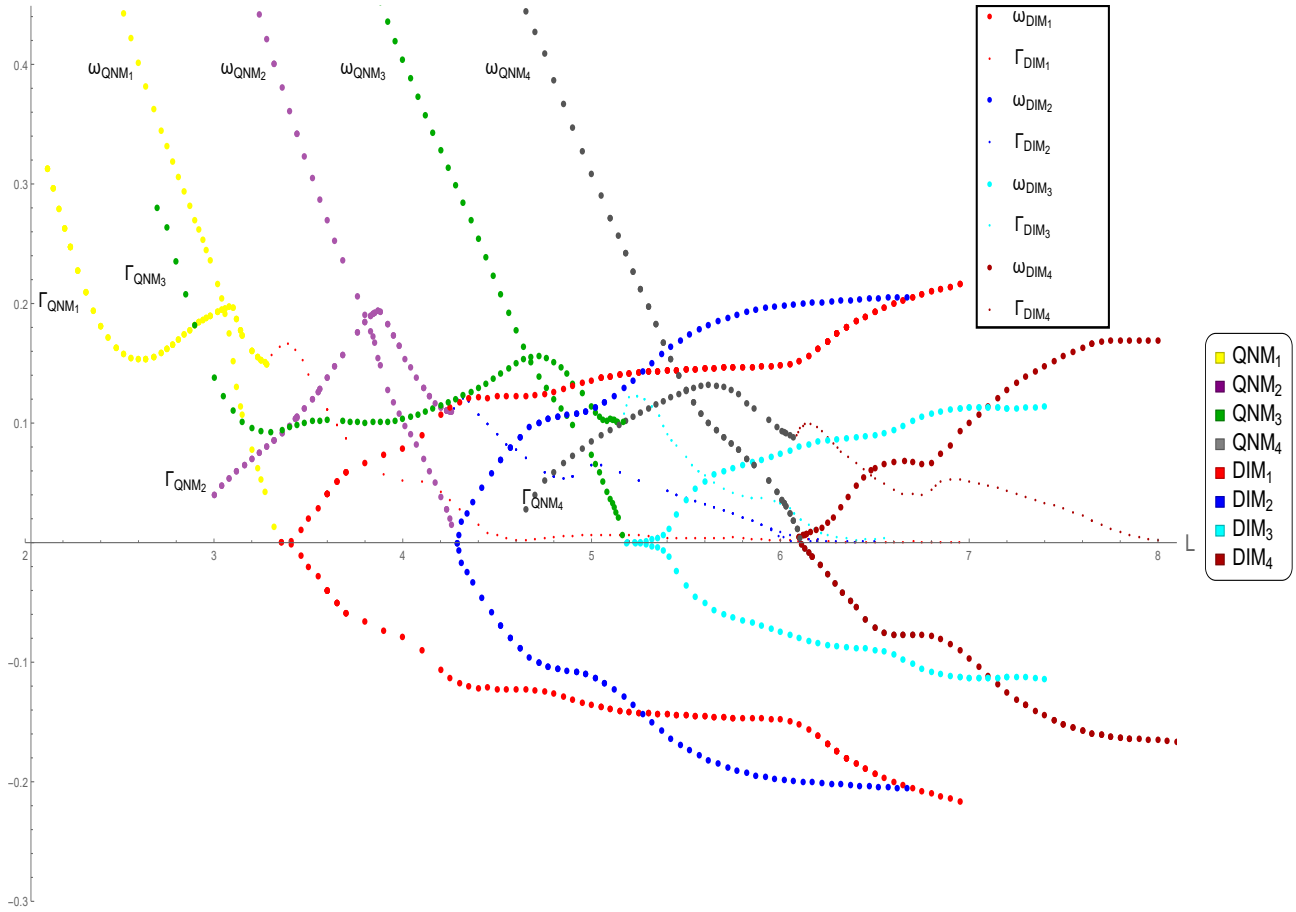

Figure 7.5: The instability character for the black-hole laser of the two-component BEC system depicted in Figure 7.1. As in the black-hole laser analysis of Chapter 4, the values of the parameters used are: $V = -1$ in Region II, $c = 0.5$ across the whole configuration, $\gamma = 0.2$ and $\Omega = 0.1$. Note that for the Rabi-coupled regions, Regions I and III, the speed of sound for the spin excitations is $c_s^2 = c^2(1 + \gamma)$. Only modes for $2 < L < 8$ are depicted.

considered constant, the value of the imaginary part of each dynamical instability mode at the point where it emerges is different for different modes. The interpretation of this phenomenon remains an open question.

Although many effects shown in Figure 7.5 can be explained by the underlying theory governing the instability onset for black-hole lasers, there are important details that are still not clarified by the nature of the specific instability-onset. First of all, the first dynamical instability mode emerging in the system by increasing the length L is probably not depicted in Figure 7.5, and its nature and characteristics are an open question. This causes the problem that the length L for the onset of the first dynamical instability mode in the system cannot be clearly identified. It could be placed in the region where results are still not obtained with the needed accuracy ($L < 2.5$). Furthermore, the emergence of dynamical instability modes does not involve the two- (or generally three-) step process described in Chapter 5. The obvious explanation could include the simultaneous emergence of two imaginary modes when another quasi-normal mode hits the real axis, which then transform to the dynamical instability modes depicted in the corresponding figure. However, these new quasi-normal modes could not be found, as well as the early emergence of degenerate dynamical instability modes. Another possible explanation could involve the emergence of a nondegenerate dynamical instability mode by the corresponding quasi-normal mode, with the two degenerate dynamical instability modes giving instantly rise to the complex mode. However, as well as in the previous case, another quasi-normal mode would be needed for this process to happen, as discussed in Appendix C, due to the conservation of degrees of freedom.

8 Outlook

In this thesis we delved into Analogue Gravity based on Bose-Einstein Condensates [13, 20]. The bosonic nature of the quantized field in the framework of Quantum field theory in Curved Spacetime was presented through the example of the wave equation without dispersion. Basic concepts regarding the different representations of this model were then introduced and the usefulness of ω- and k-representations was demonstrated.

Initially, the theory of BECs was explained and the respective Bogoliubov-de Gennes equations were set. The analogue black hole, the simplest one-horizon analogue model, was analysed, its excitation spectrum found through the respective Bogoliubov-de Gennes analysis and its mode analysis explicitly performed for the simplified picture of flat profiles. By considering, then, flows that cross the speed of sound twice [37–40], a wealth of new phenomena are now present and the relevant description of the model needs to take into account both the continuous and normal real part, but also the discrete and complex part of the spectrum of the system [65, 74, 76, 82]. Flows with a finite supersonic region between two homogeneous and infinite subsonic regions were then considered, under steplike speed of sound and velocity profiles. In this way the calculations were simplified, while retaining most of the essential physical intuition.

As a result, only after the consideration of dynamical instability modes, was the full description of the black-hole laser allowed. These modes belong to the discrete part of the spectrum and emerge through a generally three-step process. Quasi-normal modes are then needed in order to characterize this process. These are modes that, as they are not spatially bound, they are not included in the spectrum. A quasi-normal mode of imaginary (or complex, in general) frequency hits the real axis, by varying an external parameter of the system (in the case considered, the length, L, of the supersonic region). This phenomenon occurs for, say, $L = L_1$ and gives rise to a degenerate dynamical instability mode. Another quasi-normal mode may hit the real axis as well for $L = L_2$, giving rise to a second degenerate dynamical instability for some value of the external parameter, as defined through the Krein theory presented in Appendix C or in Chapter 4. The condition $L = L_2 > L_1$ needs to be satisfied. This second degenerate dynamical instability mode may merge with the previous one for some value $L = L_3$. In the black-hole laser case, it is $L_2 = L_3$ and thus the instability modes emerge in two steps. Then, a quartet of nondegenerate dynamical instability modes is observed, as predicted from the theory of Chapter 4. Conditions for the emergence of dynamical instabilities are formulated in Chapter 4.

The lasing effect originates to the self-amplification of the negative-norm trapped mode in the supersonic region. This is the mode responsible for the Hawking effect and the superradiance observed in analogue black holes [32, 58]. The same three-step picture responsible for the emergence of the nondegenerate dynamical instability modes could

not be fully identified for the case of the two-component one-dimensional Rabi-coupled BECs forming a black-hole laser with the two subsonic regions being asymptotically homogeneous and Rabi-coupled, while the supersonic regime consisting of two identical and counterpropagating one-component BECs with no linear or quadratic couplings.

Further insight is needed for the two-component Rabi-coupled BECs forming the specific idealization of the realistic black-hole laser, presented in Figure 7.1. A more general treatment needs to take into account the full subsonic regions I and III. The system can be described by including the Rabi-coupled countersuperflow of the outer subsonic regions and even by including near horizon effects, as visualized in 7.1. Different velocity and speed of sound profiles could also be examined.

Further results are needed for the nonlinear stability of the configuration. For a black-hole laser formed from a one-component BEC in one dimension, results have shown the stabilization of the black-hole laser with the emission of 'shadow'-soliton or soliton-train solutions at late times, thus suppressing the exponential growth of unstable modes [65, 90]. Further results in the same direction could be obtained for the two-component black-hole laser as well. Another aspect where further results are needed concerns the flat or steplike profile of the background velocity and the speed of sound. In a realistic configuration, smooth variations of the respective parameters need to be taken into account [33, 93] by interchanging the flat profile with, for example, the waterfall configuration which connects closely with experimental implementations [21–23] and analytical soliton solutions for the black-hole laser formed by a one-component BEC [93].

Part I

Appendix

A Black Hole Uniqueness and Properties

It can been proven that all stationary black holes, solutions of the Einstein equations of general relativity, after they achieve a stable condition, can be completely characterized by three external parameters: mass, electric charge (and, if it exists, magnetic as well) and angular momentum. This is stated under the name of *no-hair conjecture* or *no-hair theorem* [5, 7, 8]. As a consequence of this theorem, any two black holes which share the same mass, charge and angular momentum should be exactly the same. These three parameters are the only ones that can be individually detected from observations from outside of the black hole. As the only conserved numbers are the total ones, any falling objects approaching and passing through the horizon lose their ability to maintain their shape, distribution of charge or any other characteristics. This inevitable loss of information in the final stable state that the black hole achieves cannot be reverted by simply the gravitational or the electric field; the matter that created the black hole has fallen into its singularity. The interior of the spacetime and the matter falling there can by no means affect matter in its exterior. Only those characteristics of the field that are connected with globally conserved integrals, such as the mass and angular momentum, survive. The information that can be measured from an observer in the exterior of the black hole is far less than the information of every single object that has fallen inside it, a puzzling fact stated as the *Information Loss Paradox*.

On contrary, a newly born black hole is not stationary. This can be seen from the radiation of its excitation modes. Part of this radiation escapes to infinity and part of it is absorbed. It is crucial to mention that the gravitational field close to the horizon is infinitely strong, but the spacetime remains regular.

Setting $G = c = 1$, there exists a unique solution for the existence of a black hole, if it satisfies

$$M^2 - \left(\frac{J}{M}\right)^2 - Q^2 \geq 0 \tag{A.1}$$

for any set of parameters M, J and Q [7, 8]. Black holes having the minimal possible mass that satisfies this equation are called extremal. This condition is being violated by solutions of the Einstein's equations defined as *naked singularities*. These solutions are unphysical, as they don't possess a horizon and cannot be observed from the black hole's exterior.

The analogue of the black-hole laser effect thoroughly discussed in Chapters 5-7 is similar to the gravitational analogue of a rotating star with ergoregion, but without horizon, as then the radiation would be absorbed and not amplified[1]. Rotating black holes twist spacetime in the direction of the rotation at a speed that decreases with the distance from

[1]For more details, see [72, 73, 94].

the event horizon (as shown from the Lense-Thirring effect). In this case, their spherical symmetry is being completely lost [5]. Rotating black holes are described by the Kerr metric [122]. In the ergosphere, a particle or an observer cannot be regarded as stationary with respect to an outside observer satisfactorily far from the black hole. This could be true only when the observer could move with a speed faster than the speed of light with respect to the local spacetime. When moving away from the event horizon, an observer can appear stationary for some velocity greater than the speed of light. An distancing further from the event horizon, this velocity decreases and, at some point, it becomes equal to the speed, c, of light. This surface of points defines the ergosphere [123].

B Some calculations on Unruh radiation

We are now going to show what does a right Rindler observer see in the Minkowski vacuum and prove that this is a Planck spectrum for bosons with temperature

$$T = \frac{\alpha}{2\pi}. \tag{B.1}$$

Equally,it can be said that the Rindler observer is immersed in a thermal bath of particles [12, 124–127]. For the following calculation arguments based on [128] will be mainly used.

Any solution in Minkowski space can be equally well decomposed in the right Rindler wedge into the plane wave basis. For this, the set g_k^r, g_k^{r*} is considered, which is the eigenvector of the Killing field ∂_η in the respective wedge and the set f_k, f_k^* for the flat spacetime. Then, each field can be decomposed as

$$\phi = \sum_k \left(\alpha_k f_k + h.c.\right) = \sum_k \left(b_k g_k^r + c_k g_k^l + h.c.\right). \tag{B.2}$$

What will an observer see in Minkowski vacuum? The matrix element needed to answer this question is

$$_M\langle 0|N_k^r|0\rangle_M\,, \tag{B.3}$$

where N_k^r needs to be transformed in Minkowski space. This is easily done by a *Bogoliubov transform*. By writing it in continuous fashion, we get

$$g_\omega^r = \int \mathrm{d}\omega' \left(A_{\omega\omega'} f_{\omega'} + B_{\omega\omega'} f_{\omega'}^*\right). \tag{B.4}$$

Then

$$f_{\omega'} = \frac{1}{\sqrt{4\pi\omega'}} e^{-ik_\mu x^\mu} = \frac{1}{\sqrt{4\pi\omega'}} e^{-i\omega'(t-x)} = \frac{1}{\sqrt{4\pi\omega'}} e^{-i\omega' u} \tag{B.5}$$

and Equation B.4 can be written as

$$g_\omega^r(u) = \int \mathrm{d}\omega' \left(A_{\omega\omega'} \frac{1}{2\pi}\sqrt{\frac{\pi}{\omega'}} e^{-i\omega' u} + B_{\omega\omega'} \frac{1}{2\pi}\sqrt{\frac{\pi}{\omega'}} e^{i\omega' u}\right). \tag{B.6}$$

Equally, $g_\omega^r(u)$ can be written as

$$\begin{aligned} g_\omega^R(u) &= \frac{1}{2\pi}\int_{-\infty}^{+\infty} \mathrm{d}\omega'\, e^{-i\omega' u}\tilde{g}_\omega(\omega') \\ &= \frac{1}{2\pi}\int_0^{+\infty} \mathrm{d}\omega'\, e^{-i\omega' u}\tilde{g}_\omega(\omega') + \frac{1}{2\pi}\int_0^{+\infty} \mathrm{d}\omega'\, e^{i\omega' u}\tilde{g}_\omega(-\omega'). \end{aligned} \tag{B.7}$$

Comparing the last two equations, the form of $A_{\omega\omega'}$ and $B_{\omega\omega'}$ can be inferred

$$A_{\omega\omega'} = \sqrt{\frac{\omega'}{\pi}}\tilde{g}_\omega(\omega') \tag{B.8}$$

$$B_{\omega\omega'} = \sqrt{\frac{\omega'}{\pi}}\tilde{g}_\omega(-\omega'). \tag{B.9}$$

The next step is to relate $\tilde{g}_\omega(\omega')$ with $\tilde{g}_\omega(-\omega')$. In order to do this, Equations 2.80 and 2.81 are used, with

$$\tilde{g}_\omega(\omega') = \int_{-\infty}^{+\infty} \mathrm{d}u\, e^{i\omega' u}\tilde{g}^r_\omega(u) = \int_{-\infty}^{+\infty} \mathrm{d}u\, e^{i\omega' u}\frac{1}{\sqrt{4\pi\omega}}e^{ik_\mu x^\mu} \tag{B.10}$$

and, then, by making the coordinate transformation

$$t - x = u = -\frac{1}{\alpha}e^{-\alpha(\eta-\xi)} \Rightarrow \eta - \xi = -\frac{1}{\alpha}\ln(-\alpha u), \tag{B.11}$$

the Fourier transform in Equation B.10 becomes

$$\begin{aligned}
\tilde{g}_\omega(\omega') &= \int_{-\infty}^{0} \mathrm{d}u\, e^{i\omega' u}\frac{1}{\sqrt{4\pi\omega}}e^{\frac{i\omega}{\alpha}\ln(-\alpha u)} \\
&= \frac{1}{\sqrt{4\pi\omega}}\int_{-\infty}^{0} \mathrm{d}u\, e^{i\omega' u}(-\alpha u)^{\frac{i\omega}{\alpha}} \\
&= \frac{1}{\sqrt{4\pi\omega}}\alpha^{\frac{i\omega}{\alpha}}\int_{0}^{\infty} \mathrm{d}u\, e^{-i\omega' u}u^{\frac{i\omega}{\alpha}} \\
&= \frac{1}{\sqrt{4\pi\omega}}\alpha^{\frac{i\omega}{\alpha}}\frac{\omega}{\alpha\omega'}\int_{0}^{\infty} \mathrm{d}u\, e^{-i\omega' u}u^{\frac{i\omega}{\alpha}-1}.
\end{aligned} \tag{B.12}$$

Some general identities and some based on Γ-functions will now be stated. Γ-functions are also analytically continued in the complex plane with

- $$\int_0^\infty \mathrm{d}y\, e^{-y}y^{s-1} = \Gamma(s) \tag{B.13}$$

- $$\int_0^\infty \frac{\mathrm{d}by}{b}e^{-by}\frac{(by)^{s-1}}{b^{s-1}} = b^{-s}\int_0^\infty \mathrm{d}y\, e^{-y}y^{s-1} = e^{-s\ln b}\Gamma(s) \tag{B.14}$$

- $$\begin{aligned}
\ln b = \ln(A + iB) &= \ln r + i\theta = \ln\Big(\sqrt{A^2+B^2}\Big) + i\arctan\left(\frac{B}{A}\right) \\
&= \ln\Big(\sqrt{A^2+B^2}\Big) + i\arctan\left|\frac{B}{A}\right|\mathrm{sign}\left(\frac{B}{A}\right) \\
&\xrightarrow[s=\frac{i\omega}{\alpha}+\epsilon]{b=i\omega'+\epsilon} \ln\Big(\sqrt{\omega'^2+\epsilon^2}\Big) + i\arctan\left|\frac{\omega'}{\epsilon}\right|\mathrm{sign}\left(\frac{\omega'}{\epsilon}\right) \qquad \text{(B.15)} \\
&\xrightarrow{\lim_{\epsilon\to 0^+}} \ln|\omega'| + i\frac{\pi}{2}\,\mathrm{sign}(\omega'). \qquad \text{(B.16)}
\end{aligned}$$

By using this mathematical machinery, the form of the Fourier transformed $\tilde{g}_\omega$ can be obtained,

$$\tilde{g}_\omega(\omega') = \frac{1}{\sqrt{4\pi\omega}}\alpha^{\frac{i\omega}{\alpha}}\left(\frac{\omega}{\alpha|\omega'|}\operatorname{sign}(\omega')\right)e^{-\frac{i\omega}{\alpha}\ln|\omega'|+\frac{\omega\pi}{2\alpha}\operatorname{sign}(\omega')}\Gamma\left(\frac{i\omega}{\alpha}\right). \tag{B.17}$$

It is now obvious that the two solutions for $\tilde{g}_\omega(\omega')$ and $\tilde{g}_\omega(-\omega')$ for $\omega > 0$ are

$$\tilde{g}_\omega(\omega') = \frac{1}{\sqrt{4\pi\omega}}\alpha^{\frac{i\omega}{\alpha}}\left(\frac{\omega}{\alpha|\omega'|}\right)e^{-\frac{i\omega}{\alpha}\ln|\omega'|+\frac{\omega\pi}{2\alpha}}\Gamma\left(\frac{i\omega}{\alpha}\right) \tag{B.18}$$

$$\tilde{g}_\omega(-\omega') = \frac{1}{\sqrt{4\pi\omega}}\alpha^{\frac{i\omega}{\alpha}}\left(-\frac{\omega}{\alpha|\omega'|}\right)e^{-\frac{i\omega}{\alpha}\ln|\omega'|-\frac{\omega\pi}{2\alpha}}\Gamma\left(\frac{i\omega}{\alpha}\right), \tag{B.19}$$

which relates the two coefficients as

$$\tilde{g}_\omega(-\omega') = -e^{-\pi\omega/\alpha}\tilde{g}_\omega(\omega'). \tag{B.20}$$

By returning to the Bogoliubov coefficients, their relation can then be calculated as

$$A_{\omega\omega'} = \sqrt{\frac{\omega'}{\pi}}\tilde{g}_\omega(\omega') = -\sqrt{\frac{\omega'}{\pi}}\tilde{g}_\omega(-\omega')\,e^{\pi\omega/\alpha} = -e^{\pi\omega/\alpha}B_{\omega\omega'}. \tag{B.21}$$

In the last step Equation B.20 is being used. From their definition, it can be seen that they satisfy the relation

$$AA^\dagger - BB^\dagger = 1. \tag{B.22}$$

The final result can then be deduced for the Bogoliubov coefficient B,

$$|B|^2 = \frac{1}{e^{2\pi\omega/\alpha-1}}, \tag{B.23}$$

which is indeed a Planckian spectrum with temperature (after restoring units)

$$k_B T = \frac{\hbar\alpha}{2\pi c}. \tag{B.24}$$

C Krein Theory

This section will introduce some basic notions of Krein theory, based on the Schrödinger equation. The linear perturbations introduced in the context of Bogoliubov-de Gennes equations define the eigenvalue spectrum (by using the notation of Chapter 4)

$$\sigma_3 \mathcal{L} x_n = \lambda_n x_n \tag{C.1}$$

with $\mathcal{L}$ a self-adjoint unbounded operator in the space of square-integrable functions $L^2(\mathbb{R})$ with a dense domain $L^2(\mathbb{R})$ and σ_3 the respective skew-adjoint,
bounded in $L^2(\mathbb{R})$, Pauli spin matrix. We remind that, due to the Hamiltonian symmetry, it follows that

$$\sigma_3 \mathcal{L} + \mathcal{L}^\dagger \sigma_3^\dagger = 0. \tag{C.2}$$

If $\lambda_n \in \mathbb{C}$ is an eigenvalue, then it is neutrally stable if $\mathrm{Im}\{\lambda_n\} = 0$ and unstable for $\mathrm{Im}\{\lambda_n\} < 0$.

For a nonzero eigenvalue $\lambda_n \in \mathbb{C}$, the Krein quantity is defined as[1]

$$K(\lambda_n) := (\mathcal{L} x_n, x_n) \tag{C.3}$$

with $(\cdot, \cdot)$ the inner product defined in Chapter 4. Then,

- for $\lambda_n \in \mathbb{R}$, $K(\lambda_n)$ is real
- for $\lambda_n \in \mathbb{R} \setminus \{0\}$, $K(\lambda_n)$ is simple
- for $\lambda_n \in \mathrm{Im}$, $K(\lambda_n)$ is zero.

The Krein signature is defined as the sign of the Krein quantity $K(\lambda_n)$ for a simple neutrally stable eigenvalue $\lambda_n \in \mathbb{R} \setminus \{0\}$ [97]. The eigenvalues that are simple, as defined through the definition above, even when the parameters of the Gross-Pitaevskii system change, remain on the real axis ($\mathrm{Im}\{\lambda_n\}) = 0$), unless when they coalesce with another eigenvalue or a part of the continuous spectrum, due to the preservation of their multiplicity and the Hamiltonian symmetry of the eigenvalues. In this last case, the eigenvalue λ_n and the Krein quantity remain at least continuous functions of the parameters of the Gross-Pitaevskii equation. Through the stability analysis of this system (but also any other Hamiltonian system with the same symmetries), it is common to find points in parameter space where real eigenvalues (of $\mathcal{L}$ or imaginary ones of K) coalesce at a bifurcation point, followed by a splitting of them into the complex plane as unstable eigenvalues past the bifurcation point. Let us now formulate a necessary condition for the occurrence of instability bifurcations [97]

[1] Note that there also exist other definitions for the Krein quantity, see for example [69].

Theorem 9. *Under some nondegeneracy constraints, the double eigenvalue $\lambda_n = \lambda'_n \in \mathbb{R}$ of the spectral problem, Equation C.1, with a bifurcation parameter $\epsilon \in \mathbb{R}$ splits into a pair of complex eigenvalues symmetric relative to* $\mathrm{Im}\{\lambda_n\} = 0$ *for $\epsilon > 0$, only if there exist two simple eigenvalues $\lambda_n, \lambda'_n \in \mathbb{R}$ with the opposite Krein signature for $\epsilon < 0$.*

For the completeness of the respective spectrum of the problem the following theorem can also be formulated

Theorem 10. *If $\mathcal{L}$ has no kernel, has finitely many negative eigenvalues $n(\mathcal{L}) < \infty$ and the rest of its spectrum is strictly positive, then eigenvalues of the spectral problem C.1 satisfy the completeness relation*

$$n(\mathcal{L}) = N_{real} + N_{comp} + N^{-}_{imag}, \tag{C.4}$$

where N_{real} is the number of real positive eigenvalues, N_{comp} the number of complex eigenvalues and N^{-}_{imag} the number of purely real eigenvalues of negative Krein signature.

Note that this equation, Equation C.4, needs to take into account the algebraic multiplicity of the respective eigenvalues as well. These relations where also formulated in the context of black-hole laser analysis, conducted in Chapters 4 and 5. For more results towards the significance of Krein signature in the identification of stability of Hermitian or nonhermitian Hamiltonian eigenvalue problems and the related concept of Evans function, see [66, 69, 96, 97].

D Lists

D.1 List of Figures

D.2 List of Tables

E Bibliography

[1] J. Sokol. Physicists Argue That Black Holes From the Big Bang Could Be the Dark Matter. *Quanta Magazine*, 2020.

[2] E. Curiel. The many definitions of a black hole. *Nature Astronomy*, 3(1):27–34, January 2019. ISSN 2397-3366. doi:10.1038/s41550-018-0602-1.

[3] L. Parker and D. Toms. *Quantum Field Theory in Curved Spacetime: Quantized Fields and Gravity*. Cambridge Monographs on Mathematical Physics. Cambridge University Press, 2009. doi:10.1017/CBO9780511813924.

[4] N. D. Birrell and P. C. W. Davies. *Quantum Fields in Curved Space*. Cambridge Monographs on Mathematical Physics. Cambridge University Press, 1982. doi:10.1017/CBO9780511622632.

[5] C. Misner, K. Thorne, and J. Wheeler. *Gravitation*. W. H. Freeman, 2017. ISBN 9780691177793.

[6] D. Raine and E. Thomas. *Black Holes: A Student Text (3rd Edition)*. Imperial College Press, 3rd edition, 2014. ISBN 9781783264841. doi:10.1142/p947.

[7] V. Frolov and I. Novikov. *Black Hole Physics: Basic Concepts and New Developments*. Fundamental Theories of Physics. Springer Netherlands, 1998. ISBN 9780792351450. doi:10.1007/978-94-011-5139-9.

[8] V. P. Frolov and A. Zelnikov. *Introduction to Black Hole Physics*. Oxford University Press, 2011. ISBN 9780191731860.

[9] D. Finkelstein. Past-Future Asymmetry of the Gravitational Field of a Point Particle. *Physical Review*, 110(4):965–967, May 1958. doi:10.1103/PhysRev.110.965.

[10] R. M. Wald. Gravitational Collapse and Cosmic Censorship. In B. R. Iyer and B. Bhawal, editors, *Black Holes, Gravitational Radiation and the Universe: Essays in Honor of C.V. Vishveshwara*, Fundamental Theories of Physics, pages 69–86. Springer Netherlands, Dordrecht, 1999. ISBN 9789401709347. doi:10.1007/978-94-017-0934-7_5.

[11] S. W. Hawking and G. F. R. Ellis. *The Large Scale Structure of Space-Time*. Cambridge Monographs on Mathematical Physics. Cambridge University Press, 1973. doi:10.1017/CBO9780511524646.

[12] S. W. Hawking. Black hole explosions? *Nature*, 248(5443):30–31, March 1974. ISSN 1476-4687. doi:10.1038/248030a0.

[13] C. Barceló, S. Liberati, and M. Visser. Analogue Gravity. *Living Reviews in Relativity*, 14(1):3, May 2011. ISSN 1433-8351. doi:10.12942/lrr-2011-3.

[14] K. Crowther, N. S. Linnemann, and C. Wüthrich. What we cannot learn from analogue experiments. *Synthese*, May 2019. ISSN 1573-0964. doi:10.1007/s11229-019-02190-0.

[15] M. Novello, M. Visser, and G. Volovik. *Artificial Black Holes*. World Scientific, October 2002. ISBN 9789810248079 9789812778178. doi:10.1142/4861.

[16] W. G. Unruh. Experimental Black-Hole Evaporation? *Phys. Rev. Lett.*, 46:1351–1353, May 1981. doi:10.1103/PhysRevLett.46.1351.

[17] M. Visser. Acoustic propagation in fluids: an unexpected example of Lorentzian geometry. *arXiv:gr-qc/9311028*, November 1993.

[18] M. Visser. Acoustic black holes: horizons, ergospheres and Hawking radiation. *Classical and Quantum Gravity*, 15(6):1767–1791, jun 1998. doi:10.1088/0264-9381/15/6/024.

[19] M. Visser, C. Barceló, and S. Liberati. Analogue Models of and for Gravity. *General Relativity and Gravitation*, 34(10):1719–1734, October 2002. ISSN 0001-7701, 1572-9532. doi:10.1023/A:1020180409214.

[20] J. Macher and R. Parentani. Black-hole radiation in Bose-Einstein condensates. *Phys. Rev. A*, 80:043601, October 2009. doi:10.1103/PhysRevA.80.043601.

[21] O. Lahav, A. Itah, A. Blumkin, C. Gordon, S. Rinott, A. Zayats, and J. Steinhauer. Realization of a Sonic Black Hole Analog in a Bose-Einstein condensate. *Phys. Rev. Lett.*, 105:240401, December 2010. doi:10.1103/PhysRevLett.105.240401.

[22] J. Steinhauer. Observation of self-amplifying Hawking radiation in an analogue black-hole laser. *Nature Physics*, 10(11):864–869, November 2014. ISSN 1745-2481. doi:10.1038/nphys3104.

[23] J. Steinhauer. Observation of quantum Hawking radiation and its entanglement in an analogue black hole. *Nature Physics*, 12(10):959–965, October 2016. ISSN 1745-2481. doi:10.1038/nphys3863.

[24] V. I. Kolobov, K. Golubkov, J. R. M. de Nova, and J. Steinhauer. Spontaneous hawking radiation and beyond: Observing the time evolution of an analogue black hole. *arXiv:1910.09363*, 2019.

[25] J. R. Muñoz de Nova, K. Golubkov, V. I. Kolobov, and J. Steinhauer. Observation of thermal Hawking radiation and its temperature in an analogue black hole. *Nature*, 569(7758):688–691, May 2019. ISSN 1476-4687. doi:10.1038/s41586-019-1241-0.

[26] U. Leonhardt and S. Robertson. Analytical theory of Hawking radiation in dispersive media. *New Journal of Physics*, 14(5):053003, May 2012. doi:10.1088/1367-2630/14/5/053003.

[27] R. Brout, S. Massar, R. Parentani, and P. Spindel. Hawking radiation without trans-planckian frequencies. *Phys. Rev. D*, 52:4559–4568, October 1995. doi:10.1103/PhysRevD.52.4559.

[28] T. Jacobson. Black-hole evaporation and ultrashort distances. *Phys. Rev. D*, 44: 1731–1739, Sep 1991. doi:10.1103/PhysRevD.44.1731.

[29] C. Barceló, S. Liberati, and M. Visser. Analogue gravity from Bose-Einstein condensates. *Classical and Quantum Gravity*, 18(6):1137–1156, mar 2001. doi:10.1088/0264-9381/18/6/312.

[30] C. Barceló, L. C. Barbado, L. J. Garay, and G. Jannes. Avoiding the Trans-Planckian Problem in Black Hole Physics. In A. García-Parrado, F. C. Mena, F. Moura, and E. Vaz, editors, *Progress in Mathematical Relativity, Gravitation and Cosmology*, Springer Proceedings in Mathematics & Statistics, pages 129–133, Berlin, Heidelberg, 2014. Springer. ISBN 9783642401572. doi:10.1007/978-3-642-40157-2_10.

[31] J. Macher and R. Parentani. Black/white hole radiation from dispersive theories. *Phys. Rev. D*, 79:124008, June 2009. doi:10.1103/PhysRevD.79.124008.

[32] A. Recati, N. Pavloff, and I. Carusotto. Bogoliubov theory of acoustic Hawking radiation in Bose-Einstein condensates. *Phys. Rev. A*, 80:043603, October 2009. doi:10.1103/PhysRevA.80.043603.

[33] P.-E. Larré, A. Recati, I. Carusotto, and N. Pavloff. Quantum fluctuations around black hole horizons in Bose-Einstein condensates. *Phys. Rev. A*, 85:013621, January 2012. doi:10.1103/PhysRevA.85.013621.

[34] C. J. Pethick and H. Smith. *Bose–Einstein Condensation in Dilute Gases*. Cambridge University Press, 2 edition, 2008. doi:10.1017/CBO9780511802850.

[35] L. Pitaevskii and S. Stringari. *Bose-Einstein Condensation and Superfluidity*. International Series of Monographs on Physics. Oxford University Press, 2016. ISBN 9780191818721. doi:10.1093/acprof:oso/9780198758884.001.0001.

[36] A. G. J. MacFarlane, J. P. Dowling, and G. J. Milburn. Quantum technology: the second quantum revolution. *Philosophical Transactions of the Royal Society of London. Series A: Mathematical, Physical and Engineering Sciences*, 361(1809): 1655–1674, 2003. doi:10.1098/rsta.2003.1227.

[37] S. Corley and T. Jacobson. Black hole lasers. *Phys. Rev. D*, 59:124011, May 1999. doi:10.1103/PhysRevD.59.124011.

[38] U. Leonhardt and T. G. Philbin. Black Hole Lasers Revisited. In W. G. Unruh and R. Schützhold, editors, *Quantum Analogues: From Phase Transitions to Black Holes and Cosmology*, Lecture Notes in Physics, pages 229–245. Springer, Berlin, Heidelberg, 2007. ISBN 9783540708599. doi:10.1007/3-540-70859-6_9.

[39] A. Coutant and R. Parentani. Black hole lasers, a mode analysis. *Phys. Rev. D*, 81: 084042, April 2010. doi:10.1103/PhysRevD.81.084042.

[40] S. Finazzi and R. Parentani. Black hole lasers in Bose-Einstein condensates. *New Journal of Physics*, 12(9):095015, September 2010. doi:10.1088/1367-2630/12/9/095015.

[41] C. Barceló. Analogue black-hole horizons. *Nature Physics*, 15(3):210–213, March 2019. ISSN 1745-2481. doi:10.1038/s41567-018-0367-6.

[42] C. Mayoral, A. Recati, A. Fabbri, R. Parentani, R. Balbinot, and I. Carusotto. Acoustic white holes in flowing atomic Bose-Einstein condensates. *New Journal of Physics*, 13(2):025007, February 2011. doi:10.1088/1367-2630/13/2/025007.

[43] L. Susskind. Black Holes and the Information Paradox. *Scientific American*, 276 (4):52–57, 1997. ISSN 00368733, 19467087.

[44] A. Cho. Test of Hawking's Prediction on the Horizon With Mock 'White Hole'. *Science*, 319(5868):1321–1321, March 2008. ISSN 0036-8075, 1095-9203. doi:10.1126/science.319.5868.1321a.

[45] S. A. Fulling. *Aspects of Quantum Field Theory in Curved Spacetime*. London Mathematical Society Student Texts. Cambridge University Press, 1989. doi:10.1017/CBO9781139172073.

[46] R. Brout, S. Massar, R. Parentani, and P. Spindel. A primer for black hole quantum physics. *Physics Reports*, 260(6):329 – 446, 1995. ISSN 0370-1573. doi:https://doi.org/10.1016/0370-1573(95)00008-5.

[47] W. G. Unruh and R. Schützhold. Universality of the hawking effect. *Phys. Rev. D*, 71:024028, Jan 2005. doi:10.1103/PhysRevD.71.024028.

[48] S. Corley. Computing the spectrum of black hole radiation in the presence of high frequency dispersion: An analytical approach. *Phys. Rev. D*, 57:6280–6291, May 1998. doi:10.1103/PhysRevD.57.6280.

[49] S. J. Robertson. *Hawking Radiation in Dispersive Media*. PhD thesis, St. Andrews U., Phys. Astron., 2011.

[50] U. Leonhardt. *Essential Quantum Optics: From Quantum Measurements to Black Holes*. Cambridge University Press, 2010. doi:10.1017/CBO9780511806117.

[51] W. Rindler. *Essential Relativity*. Springer New York, New York, NY, 1969. ISBN 9780387902012 9781475711356. doi:10.1007/978-1-4757-1135-6.

[52] L. C. B. Crispino, A. Higuchi, and G. E. A. Matsas. The Unruh effect and its applications. *Rev. Mod. Phys.*, 80:787–838, July 2008. doi:10.1103/RevModPhys.80.787.

[53] S. Corley and T. Jacobson. Hawking spectrum and high frequency dispersion. *Phys. Rev. D*, 54:1568–1586, July 1996. doi:10.1103/PhysRevD.54.1568.

[54] T. Jacobson. On the origin of the outgoing black hole modes. *Phys. Rev. D*, 53: 7082–7088, June 1996. doi:10.1103/PhysRevD.53.7082.

[55] X.-G. Wen. *Quantum Field Theory of Many-Body Systems: From the Origin of Sound to an Origin of Light and Electrons*. Oxford University Press, 2007. ISBN 9780191713019. doi:10.1093/acprof:oso/9780199227259.001.0001.

[56] A. Fabbri and C. Mayoral. Steplike discontinuities in Bose-Einstein condensates and Hawking radiation: The hydrodynamic limit. *Phys. Rev. D*, 83:124016, June 2011. doi:10.1103/PhysRevD.83.124016.

[57] C. Mayoral, A. Fabbri, and M. Rinaldi. Steplike discontinuities in Bose-Einstein condensates and Hawking radiation: Dispersion effects. *Phys. Rev. D*, 83:124047, June 2011. doi:10.1103/PhysRevD.83.124047.

[58] R. Balbinot, I. Carusotto, A. Fabbri, C. Mayoral, and A. Recati. *Understanding Hawking Radiation from Simple Models of Atomic Bose-Einstein Condensates*, pages 181–219. Springer International Publishing, Cham, 2013. ISBN 978-3-319-00266-8. doi:10.1007/978-3-319-00266-8_9.

[59] E. J. Hinch. *Perturbation Methods*. Cambridge Texts in Applied Mathematics. Cambridge University Press, 1991. doi:10.1017/CBO9781139172189.

[60] A. Nayfeh. *Introduction to Perturbation Techniques*. Wiley Classics Library. Wiley, 2011. ISBN 9783527618453.

[61] I. Carusotto, S. Fagnocchi, A. Recati, R. Balbinot, and A. Fabbri. Numerical observation of Hawking radiation from acoustic black holes in atomic Bose-Einstein condensates. *New Journal of Physics*, 10(10):103001, October 2008. doi:10.1088/1367-2630/10/10/103001.

[62] R. Balbinot, A. Fabbri, S. Fagnocchi, A. Recati, and I. Carusotto. Nonlocal density correlations as a signature of Hawking radiation from acoustic black holes. *Phys. Rev. A*, 78:021603, August 2008. doi:10.1103/PhysRevA.78.021603.

[63] S. Finazzi and R. Parentani. Hawking radiation in dispersive theories, the two regimes. *Phys. Rev. D*, 85:124027, June 2012. doi:10.1103/PhysRevD.85.124027.

[64] I. Zapata, M. Albert, R. Parentani, and F. Sols. Resonant Hawking radiation in Bose-Einstein condensates. *New Journal of Physics*, 13(6):063048, June 2011. doi:10.1088/1367-2630/13/6/063048.

[65] A. Coutant, F. Michel, and R. Parentani. Dynamical instabilities and quasi-normal modes, a spectral analysis with applications to black-hole physics. *Classical and Quantum Gravity*, 33(12):125032, May 2016. doi:10.1088/0264-9381/33/12/125032.

[66] T. Kapitula and K. Promislow. *Spectral and Dynamical Stability of Nonlinear Waves*. Applied Mathematical Sciences. Springer-Verlag, New York, 2013. ISBN 9781461469940. doi:10.1007/978-1-4614-6995-7.

[67] B. Helffer. *Spectral Theory and its Applications*. Cambridge Studies in Advanced Mathematics. Cambridge University Press, 2013. doi:10.1017/CBO9781139505727.

[68] D. E. Pelinovsky. *Localization in Periodic Potentials: From Schrödinger Operators to the Gross–Pitaevskii Equation*. London Mathematical Society Lecture Note Series. Cambridge University Press, 2011. doi:10.1017/CBO9780511997754.

[69] R. Kollár and P. Miller. Graphical Krein Signature Theory and Evans-Krein Functions. *SIAM Rev.*, 56:73–123, 2014. doi:10.1137/120891423.

[70] A. Bachelot. Superradiance and scattering of the charged Klein–Gordon field by a step-like electrostatic potential. *Journal de Mathématiques Pures et Appliquées*, 83(10):1179 – 1239, 2004. ISSN 0021-7824. doi:https://doi.org/10.1016/j.matpur.2004.03.007.

[71] K. D. Kokkotas and B. G. Schmidt. Quasi-Normal Modes of Stars and Black Holes. *Living Reviews in Relativity*, 2(1):2, September 1999. ISSN 1433-8351. doi:10.12942/lrr-1999-2.

[72] G. Kang. Quantum aspects of ergoregion instability. *Phys. Rev. D*, 55:7563–7573, June 1997. doi:10.1103/PhysRevD.55.7563.

[73] G. Kang. *Quantum Ergoregion Instability*, pages 390–399. 1997. doi:10.1142/9789814447287_0014.

[74] E. Fukuyama, M. Mine, M. Okumura, T. Sunaga, and Y. Yamanaka. Condition for the existence of complex modes in a trapped Bose-Einstein condensate with a highly quantized vortex. *Phys. Rev. A*, 76:043608, October 2007. doi:10.1103/PhysRevA.76.043608.

[75] K. Kobayashi, M. Mine, M. Okumura, and Y. Yamanaka. Quantum field theoretical analysis on unstable behavior of Bose–Einstein condensates in optical lattices. *Annals of Physics*, 323(5):1247 – 1270, 2008. ISSN 0003-4916. doi:10.1016/j.aop.2007.09.002.

[76] Y. Nakamura, M. Mine, M. Okumura, and Y. Yamanaka. Condition for emergence of complex eigenvalues in the Bogoliubov–de Gennes equations. *Phys. Rev. A*, 77: 043601, April 2008. doi:10.1103/PhysRevA.77.043601.

[77] Q.-Z. Zhu and B. Wu. Superfluidity of Bose-Einstein condensates in ultracold atomic gases. *Chinese Physics B*, 24(5):050507, April 2015. doi:10.1088/1674-1056/24/5/050507.

[78] Y. Kawaguchi and T. Ohmi. Splitting instability of a multiply charged vortex in a Bose-Einstein condensate. *Phys. Rev. A*, 70:043610, October 2004. doi:10.1103/PhysRevA.70.043610.

[79] D. V. Skryabin. Instabilities of vortices in a binary mixture of trapped Bose-Einstein condensates: Role of collective excitations with positive and negative energies. *Phys. Rev. A*, 63:013602, December 2000. doi:10.1103/PhysRevA.63.013602.

[80] A. D. Jackson, G. M. Kavoulakis, and E. Lundh. Stability of the solutions of the Gross-Pitaevskii equation. *Phys. Rev. A*, 72:053617, November 2005. doi:10.1103/PhysRevA.72.053617.

[81] B. Wu and Q. Niu. Superfluidity of Bose-Einstein condensate in an optical lattice: Landau-Zener tunnelling and dynamical instability. *New Journal of Physics*, 5: 104–104, July 2003. doi:10.1088/1367-2630/5/1/104.

[82] M. Mine, M. Okumura, T. Sunaga, and Y. Yamanaka. Quantum field theoretical description of unstable behavior of trapped Bose–Einstein condensates with complex eigenvalues of Bogoliubov–de Gennes equations. *Annals of Physics*, 322(10):2327 – 2349, 2007. ISSN 0003-4916. doi:https://doi.org/10.1016/j.aop.2007.01.008.

[83] H. Matsumoto and S. Sakamoto. Quantum Phase Coordinate as a Zero-Mode in Bose-Einstein Condensed States. *Progress of Theoretical Physics*, 107(4):679–688, April 2002. ISSN 0033-068X. doi:10.1143/PTP.107.679.

[84] Y. Nakamura, J. Takahashi, and Y. Yamanaka. Formulation for the zero mode of a Bose-Einstein condensate beyond the bogoliubov approximation. *Phys. Rev. A*, 89:013613, January 2014. doi:10.1103/PhysRevA.89.013613.

[85] M. Lewenstein and L. You. Quantum phase diffusion of a Bose-Einstein condensate. *Phys. Rev. Lett.*, 77:3489–3493, October 1996. doi:10.1103/PhysRevLett.77.3489.

[86] L. J. Garay, J. R. Anglin, J. I. Cirac, and P. Zoller. Sonic analog of gravitational black holes in bose-einstein condensates. *Phys. Rev. Lett.*, 85:4643–4647, November 2000. doi:10.1103/PhysRevLett.85.4643.

[87] L. J. Garay, J. R. Anglin, J. I. Cirac, and P. Zoller. Sonic black holes in dilute Bose-Einstein condensates. *Phys. Rev. A*, 63:023611, January 2001. doi:10.1103/PhysRevA.63.023611.

[88] R. Rossignoli and A. M. Kowalski. Complex modes in unstable quadratic bosonic forms. *Phys. Rev. A*, 72:032101, September 2005. doi:10.1103/PhysRevA.72.032101.

[89] R. Carretero-González, D. J. Frantzeskakis, and P. G. Kevrekidis. Nonlinear waves in Bose-Einstein condensates: physical relevance and mathematical techniques. *Nonlinearity*, 21(7):R139–R202, June 2008. doi:10.1088/0951-7715/21/7/r01.

[90] F. Michel and R. Parentani. Saturation of black hole lasers in Bose-Einstein condensates. *Phys. Rev. D*, 88:125012, December 2013. doi:10.1103/PhysRevD.88.125012.

[91] Y. Shen. *The Principles of Nonlinear Optics*. Wiley classics library. Wiley, 2003. ISBN 9780471430803.

[92] A. Coutant, R. Parentani, and S. Finazzi. Black hole radiation with short distance dispersion, an analytical S-matrix approach. *Phys. Rev. D*, 85:024021, January 2012. doi:10.1103/PhysRevD.85.024021.

[93] J. R. Muñoz de Nova. Non-linear stationary solutions in realistic models for analog black-hole lasers. *Universe*, 3(3), 2017. ISSN 2218-1997. doi:10.3390/universe3030054.

[94] G. Kang. Quantization of Scalar Field in the Presence of Imaginary Frequency Modes. *arXiv:hep-th/9603166*, March 1996.

[95] C. M. Bender. Making sense of non-Hermitian Hamiltonians. *Reports on Progress in Physics*, 70(6):947–1018, may 2007. doi:10.1088/0034-4885/70/6/r03.

[96] A. Chernyavsky and D. E. Pelinovsky. Krein signature for instability of PT-symmetric states. *Physica D: Nonlinear Phenomena*, 371:48 – 59, 2018. ISSN 0167-2789. doi:10.1016/j.physd.2018.01.009.

[97] A. Chernyavsky, P. G. Kevrekidis, and D. E. Pelinovsky. *Krein Signature in Hamiltonian and $\mathbb{PT}$-Symmetric Systems*, pages 465–491. Springer Singapore, Singapore, 2018. ISBN 978-981-13-1247-2. doi:10.1007/978-981-13-1247-2_16.

[98] V. V. Konotop. *Coupled Nonlinear Schrödinger Equations with Gain and Loss: Modeling $\mathbb{PT}$-Symmetry*, pages 407–441. Springer Singapore, Singapore, 2018. ISBN 978-981-13-1247-2. doi:10.1007/978-981-13-1247-2_14.

[99] B. Malomed. Multi-Component Bose-Einstein Condensates: Theory. In P. G. Kevrekidis, D. J. Frantzeskakis, and R. Carretero-González, editors, *Emergent Nonlinear Phenomena in Bose-Einstein Condensates: Theory and Experiment*,

Atomic, Optical, and Plasma Physics, pages 287–305. Springer, Berlin, Heidelberg, 2008. ISBN 9783540735915. doi:10.1007/978-3-540-73591-5_15.

[100] A. Aftalion and P. Mason. Rabi-coupled two-component Bose-Einstein condensates: Classification of the ground states, defects, and energy estimates. *Phys. Rev. A*, 94:023616, Aug 2016. doi:10.1103/PhysRevA.94.023616.

[101] D. M. Stamper-Kurn, H.-J. Miesner, A. P. Chikkatur, S. Inouye, J. Stenger, and W. Ketterle. Quantum Tunneling across Spin Domains in a Bose-Einstein Condensate. *Phys. Rev. Lett.*, 83:661–665, Jul 1999. doi:10.1103/PhysRevLett.83.661.

[102] D. M. Stamper-Kurn and M. Ueda. Spinor Bose gases: Symmetries, magnetism, and quantum dynamics. *Rev. Mod. Phys.*, 85:1191–1244, Jul 2013. doi:10.1103/RevModPhys.85.1191.

[103] W. Bao. Ground States and Dynamics of Multicomponent Bose–Einstein Condensates. *Multiscale Modeling & Simulation*, 2(2):210–236, January 2004. ISSN 1540-3459, 1540-3467. doi:10.1137/030600209.

[104] K. Kasamatsu, M. Tsubota, and M. Ueda. Vortices in Multicomponent Bose–Einstein Condensates. *International Journal of Modern Physics B*, 19(11):1835–1904, April 2005. ISSN 0217-9792, 1793-6578. doi:10.1142/S0217979205029602.

[105] A. Usui and H. Takeuchi. Rabi-coupled countersuperflow in binary Bose-Einstein condensates. *Phys. Rev. A*, 91:063635, June 2015. doi:10.1103/PhysRevA.91.063635.

[106] K. Ihara and K. Kasamatsu. Transverse instability and disintegration of a domain wall of a relative phase in coherently coupled two-component Bose-Einstein condensates. *Phys. Rev. A*, 100:013630, July 2019. doi:10.1103/PhysRevA.100.013630.

[107] I. Khalatnikov. Sound propagation in solutions of two superfluid liquids. *Soviet Journal of Experimental and Theoretical Physics Letters*, 17:386, 1973.

[108] A. Andreev and E. Bashkin. Three-velocity hydrodynamics of superfluid solutions. *Soviet Journal of Experimental and Theoretical Physics*, 42:164, 1976.

[109] V. Mineev. The theory of the solution of two near-ideal bose gases. *Zh. Eksp. Teor. Fiz*, 67:263, 1974.

[110] B. D. Esry, C. H. Greene, J. P. Burke, Jr., and J. L. Bohn. Hartree-Fock Theory for Double Condensates. *Phys. Rev. Lett.*, 78:3594–3597, May 1997. doi:10.1103/PhysRevLett.78.3594.

[111] V. E. Zakharov and S. V. Manakov. On the complete integrability of a nonlinear Schrödinger equation. *Theoretical and Mathematical Physics*, 19(3):551–559, June 1974. ISSN 1573-9333. doi:10.1007/BF01035568.

[112] A. Smerzi, A. Trombettoni, T. Lopez-Arias, C. Fort, P. Maddaloni, F. Minardi, and M. Inguscio. Macroscopic oscillations between two weakly coupled Bose-Einstein condensates. *The European Physical Journal B - Condensed Matter and Complex Systems*, 31(4):457–461, February 2003. ISSN 1434-6036. doi:10.1140/epjb/e2003-00055-1.

[113] S. Ishino, M. Tsubota, and H. Takeuchi. Countersuperflow instability in miscible two-component Bose-Einstein condensates. *Phys. Rev. A*, 83:063602, June 2011. doi:10.1103/PhysRevA.83.063602.

[114] J. I. Cirac, M. Lewenstein, K. Mølmer, and P. Zoller. Quantum superposition states of Bose-Einstein condensates. *Phys. Rev. A*, 57:1208–1218, Feb 1998. doi:10.1103/PhysRevA.57.1208.

[115] C. P. Search, A. G. Rojo, and P. R. Berman. Ground state and quasiparticle spectrum of a two-component Bose-Einstein condensate. *Phys. Rev. A*, 64:013615, Jun 2001. doi:10.1103/PhysRevA.64.013615.

[116] E. V. Goldstein and P. Meystre. Quasiparticle instabilities in multicomponent atomic condensates. *Phys. Rev. A*, 55:2935–2940, Apr 1997. doi:10.1103/PhysRevA.55.2935.

[117] C. Lee, W. Hai, L. Shi, and K. Gao. Phase-dependent spontaneous spin polarization and bifurcation delay in coupled two-component Bose-Einstein condensates. *Phys. Rev. A*, 69:033611, Mar 2004. doi:10.1103/PhysRevA.69.033611.

[118] T. Zibold, E. Nicklas, C. Gross, and M. K. Oberthaler. Classical Bifurcation at the Transition from Rabi to Josephson Dynamics. *Phys. Rev. Lett.*, 105:204101, Nov 2010. doi:10.1103/PhysRevLett.105.204101.

[119] I. Kourakis, P. K. Shukla, M. Marklund, and L. Stenflo. Modulational instability criteria for two-component Bose-Einstein condensates. *The European Physical Journal B - Condensed Matter and Complex Systems*, 46(3):381–384, Aug 2005. ISSN 1434-6036. doi:10.1140/epjb/e2005-00271-7.

[120] E. J. Weinberg. *Classical Solutions in Quantum Field Theory: Solitons and Instantons in High Energy Physics*. Cambridge Monographs on Mathematical Physics. Cambridge University Press, 2012. doi:10.1017/CBO9781139017787.

[121] P. G. Drazin and R. S. Johnson. *Solitons: An Introduction*. Cambridge Texts in Applied Mathematics. Cambridge University Press, 2 edition, 1989. doi:10.1017/CBO9781139172059.

[122] M. Visser. The Kerr spacetime: A brief introduction. *arXiv:0706.0622*, January 2008.

[123] Ergosphere, September 2020. Page Version ID: 978407194.

[124] S. A. Fulling. Nonuniqueness of Canonical Field Quantization in Riemannian Space-Time. *Phys. Rev. D*, 7:2850–2862, May 1973. doi:10.1103/PhysRevD.7.2850.

[125] W. G. Unruh. Notes on black-hole evaporation. *Phys. Rev. D*, 14:870–892, Aug 1976. doi:10.1103/PhysRevD.14.870.

[126] W. G. Unruh. *Black holes, dumb holes, and entropy*, page 152–174. Cambridge University Press, 2001. doi:10.1017/CBO9780511612909.008.

[127] S. A. Fulling and G. E. A. Matsas. Unruh effect. *Scholarpedia*, 9(10):31789, October 2014. ISSN 1941-6016. doi:10.4249/scholarpedia.31789.

[128] M. Tettamanti. *Analogue Hawking radiation in Bose-Einstein condensates*. PhD thesis, 2019.

Erklärung:

Ich versichere, dass ich diese Arbeit selbstständig verfasst habe und keine anderen als die angegebenen Quellen und Hilfsmittel benutzt habe.

Heidelberg, den 05.02.2021 .....